Taphonomic studies of fossil preservation in coarse-grained siliciclastic environments

by

Sharon Audrey Newman

B.A. Earth and Environmental Science, Wesleyan University (2008)

M.A. Ecology, Evolution and Environmental Biology, Columbia University (2010)

Submitted to the Department of Earth, Atmospheric and Planetary Sciences

in partial fulfillment of the requirements for the degree of

Doctor of Philosophy

at the

MASSACHUSETTS INSTITUTE OF TECHNOLOGY

November 2017 [February 2018]

Author.. Signature redacted .....
Department of Earth, Atmospheric and Planetary Sciences
November 30th, 2017

Certified by..... Signature redacted .....
Tanja Bosak
Associate Professor, Department of Earth, Atmospheric and Planetary Sciences
Thesis Supervisor

Accepted by..... Signature redacted .....
Robert D. van der Hilst
Schlumberger Professor of Earth and Planetary Sciences
Head, Department of Earth, Atmospheric and Planetary Sciences

THIS PAGE IS INTENTIONALLY LEFT BLANK

Taphonomic studies of fossil preservation in coarse-grained siliciclastic environments

by

Sharon Audrey Newman

Submitted to the Department of Earth, Atmospheric and Planetary Sciences on November 30th, 2017 in partial fulfillment of the requirements for the Degree of

Doctor of Philosophy

Abstract

Ediacaran and early Cambrian sandy and silty sediments commonly preserve microbial fossils and textures as well as the fossils of soft-bodied organisms. The rarity of similar fossils and textures in coarse-grained siliciclastic strata of the later Phanerozoic suggests that a taphonomic window facilitated this mode of fossil preservation. However, environmental and biological factors that promoted fossilization remain unclear. To experimentally identify mechanisms of preservation in siliciclastic sediments, cyanobacteria and soft tissues (scallop adductor muscles) were incubated in silica sand or clay minerals for up to two months. Clay mineral veneers coated both cyanobacterial filaments and the surfaces of soft tissues and were formed by two main processes: 1) the adhesion of fine particles from the sediment and 2) the precipitation of authigenic minerals. Photosynthetic, sheathed microorganisms were best preserved in the presence of high concentrations of dissolved silica ($\geq$0.1 mM) and suspended fine particles (>5.6 mg/L) in solution. We showed that these organisms could be preserved in oxic environments and that the degradation of cyanobacteria by heterotrophic microorganisms was not necessary for fossilization. In contrast, soft tissues buried in sand/clay were preserved under anaerobic

conditions and mineral veneers around them contained reduced iron. All scallops decayed in the presence of endogenous bacteria and the redox cycling of iron that included the microbial reduction of iron(III). We showed that the early precipitation of silica and the formation of microbial death masks is not critical for preservation. Additionally, when the degradation of soft tissues advanced within the first 15 to 30 days, all soft tissues decayed completely and left no morphological imprint. Taken together, these results show that the early microbial reduction of iron(III) present in sedimentary minerals and the formation of mineral veneers are critical for the preservation of organic material. The same processes may have facilitated the formation of exceptionally preserved fossils and textures throughout the Ediacaran and early Cambrian. Future studies should focus on the roles of iron redox cycling, sediment composition and microbial metabolisms in the preservation of soft tissues to better understand mechanisms for Ediacaran-style preservation in siliciclastic environments.

Thesis Supervisor: Tanja Bosak

Associate Professor

Department of Earth, Atmospheric and Planetary Sciences

Acknowledgements

I am grateful to all the wonderful people who have supported me throughout my Ph.D. Below, I list those individuals who deserve my sincerest gratitude and appreciation.

Firstly, I would like to thank my adviser, Tanja Bosak. Tanja has provided me with unwavering support over the past several years. In fact, Tanja was the first person who I ever met at MIT; back in 2011, before the start of my Ph.D., Tanja kindly met with me to discuss opportunities in the field of geobiology. Although neither of us knew it then, I would become her graduate student just a short time later. Her passion for and dedication to geobiology inspires my own. She has taught me many important lessons and has always been there to answer my questions, help brainstorm ideas and provide overwhelming encouragement.

Secondly, I would like to thank the members of my Thesis committee. From 2011 to 2012, I worked as a research technician in Roger Summons' laboratory. It was because of Roger's mentorship that I was able to make the transition from the field of ecology (my Master's field of study) to geobiology and it was with his encouragement that I applied to the Ph.D. program at MIT. Roger continues to mentor me to this very day and I have enjoyed our scientific conversations. Both Sara Pruss and Colleen Hansel have provided me with much guidance throughout my Ph.D. Their insightful suggestions, comments and general advice have been most appreciated.

I would also like to thank several collaborators including Giulio Mariotti, Vanja Klepac-Ceraj, Nicki Watson and Sirine Fakra. Each has supported the work represented in this Thesis and I am grateful for their thoughtful contributions.

Additionally, I would like to thank the wonderful community of E25, both past and current members. Specifically, I would like to thank Christopher Kinsley, Christine Chen, Kelsey Moore, Jeemin Rhim, Alex Evans, David Wang, Ross Williams and Mirna Daye who have been the kindest, most supportive peers and friends. I would also like to thank Melody Abedinejad for her administrative help as well as her friendship and support.

Additionally, I would like to thank my parents who have always supported my dreams and aspirations.

This work was funded by the NASA Astrobiology Institute Foundations of Complex Life, Evolution, Preservation and Detection of Earth and Beyond (NNA13AA90A) as well as the donors of the American Chemical Society Petroleum Research Fund (PRF# 54498-ND8) and was partially supported by grants from the Simons Foundation (327126 and 344707 to TB).

Contents

List of Figs.

List of Tables

Chapter 1. Introduction

Photosynthetic microbial mats and soft-bodied organisms were commonly preserved in Ediacaran (~635-541 Ma) and early Cambrian (~541-520 Ma) siliciclastic sediments. Fossil impressions of macrofauna and sedimentary patterns/textures attributed to microbial mats are considered temporally unique because few examples exist outside of intertidal and subtidal siliciclastic environments of the terminal Proterozoic and early Phanerozoic. Thus, a taphonomic window must have opened and closed during this interval of time to facilitate their preservation. Previous studies have attempted to identify key factors in Ediacaran-style preservation through investigations of the fossil record (e.g., Gehling, 1999; Gaines et al., 2008; Callow and Brasier, 2009; Tarhan et al., 2016) and taphonomic experimentation (e.g., Darroch et al., 2012; Naimark et al., 2016; Sagemann et al., 1999; Wilson and Butterfield, 2014). Despite significant advances in our understanding of fossilization processes in siliciclastic settings, the specific mechanisms of preservation in these settings remain largely unconstrained.

Unique environmental conditions during the Ediacaran Period likely contributed to the exceptional preservation of both soft-bodied organisms and microbial fossils/textures in siliciclastic sediments. For example, high concentrations of dissolved silica in Ediacaran porewaters may have facilitated preservation (Callow and Brasier, 2009; Tarhan et al., 2016); the early precipitation of amorphous silica has been shown to permineralize microbial mats, trees and other organisms (Schultze-Lam et al., 1995; Mustoe, 2008) and similar mechanisms are thought to have facilitated the precipitation of amorphous silica on the surfaces of organic material during the Precambrian. Callow and Brasier (2009) proposed a model of preservation that invoked a steep redox gradient and high porewater concentrations of dissolved silica. Tarhan

et al. (2016) proposed a similar model in which supersaturated oceans promoted the formation of siliceous cements around soft tissues. However, the formation of cherts in peritidal environments of the Precambrian suggests that most marine waters were not supersaturated with respect to amorphous silica (Maliva et al., 2005). Thus, additional environmental and biological factors must be considered when explaining exceptional preservation in siliciclastic sediments.

Additionally, microbial mats were widespread on the Precambrian seafloor due to the effective absence of grazing and bioturbating metazoans (Seilacher and Pflüger, 1994). This contrasts with modern environments, where microbial mats are restricted to settings that are hostile to macrofaunal predators (e.g., highly alkaline, anoxic, saline). The existence of widespread microbial mats during the Precambrian would have, in itself, increased the likelihood of microbial preservation in the rock record, due to the sheer increase in the diversity and extent of microbial biofilms. Moreover, several studies have noted the frequent association of microbial patterns, textures and fossils with well-preserved macrofossil impressions and hypothesized that microbial mats may have played a role in the fossilization of soft-bodied organisms (Gehling, 1999; Callow and Brasier, 2009). Several modes of preservation were proposed, including the development of sealing photosynthetic mats over the surface of sediments and soft tissues. The mats are thought to have created an anoxic microenvironment around decaying soft tissues and facilitated the formation of protective minerals (e.g., pyrite) around tissue surfaces (Gehling, 1999).

The precipitation of authigenic minerals is critical to the preservation of organic material and its eventual incorporation into the siliciclastic rock record. There has been extensive investigation into the mechanisms involved in the precipitation of such minerals, especially related to the formation of authigenic clay minerals on bacterial surfaces (Ferris et al., 1987;

Konhauser, 1997; Konhauser et al., 1998; Konhauser and Urrutia, 1999). Microbial surfaces are negatively charged due to the presence of various functional groups (e.g., carboxyl and phosphate groups within the cell wall of Gram-positive bacteria, Mera and Beveridge, 1993). Therefore, positively charged ions in natural aquatic systems (e.g., iron(II), iron(III), aluminum(III)) can bind to microbial surfaces and promote the nucleation of clay minerals (Konhauser et al., 1998; Konhauser and Urrutia, 1999; Newman et al., 2016, 2017) and other mineral phases such as calcium carbonate (Bosak and Newman, 2003; Bosak et al., 2004). Konhauser et al. (1998, 1999) reported the formation of iron-rich clay minerals on bacterial surfaces in culture and natural riverine settings. Similarly, Michalopoulos and Aller (2004, 1995) investigated the formation of clay minerals on diatoms in the clay- and iron-rich subsurface sediments of the Amazon delta, demonstrating the occurrence of authigenic mineral precipitation within months to years in this environment.

The formation of mineral veneers around soft tissues likely involves similar processes as well as heterotrophic decay (Briggs and Kear, 1994; Briggs, 2003). The metabolic activities of heterotrophic microorganisms such as iron- and sulfate-reducing bacteria may create microenvironments that favor the formation of authigenic minerals (Petrovich, 2001; Briggs, 2003). In fact, the products of these metabolic reactions are the very ions that facilitate mineral formation (e.g., iron(II) is produced during dissimilatory iron(III) reduction). Thus, the activities of microorganisms can promote the fossilization of soft tissues by facilitating the formation of authigenic mineral veneers or prevent it by degrading the tissues before authigenic minerals can form.

In this Thesis we use experimental taphonomy to reconstruct macrofaunal and microbial preservation in shallow marine, coarse-grained siliciclastic settings. We suggest that the

formation of clay mineral veneers on organic material may have promoted the preservation of fossils and sedimentary textures in some Ediacaran and early Cambrian coarse-grained siliciclastic sediments (Gehling, 1999; Mapstone and McIlroy, 2006; Callow and Brasier, 2009). Impressions of soft tissues associated with microbial sedimentary structures have been reported in Ediacaran strata characterized by layers of fine-grained material between fossiliferous sandstones. For example, the Ediacara Member of South Australia (Rawnsley Quartzite, e.g., Gehling, 1999) contains cm-thick horizons of silt and clay as well as thin, aluminosilicate laminae between part and counterpart impressions. Our findings may also have implications for fine-grained sediments composed of silts and clays. Examples of exceptionally preserved carbonaceous compressions associated with clay minerals are found throughout the Ediacaran and early Cambrian rock record (Laflamme et al., 2011; Anderson et al., 2011; Cai et al., 2012). It is likely that these fossils formed by the authigenic mineral replacement of soft tissues (Gaines et al., 2008; see Orr et al., 1998 for similar mechanisms in deepwater settings) in combination with the trapping of fine particles from the sediment. Thus, the preservational models proposed in the current Thesis provide mechanistic explanations for the formation of macrofossil impressions and microbial patterns/textures observed in the siliciclastic rock record.

Thesis foci and layout

This Thesis includes the Introduction (Chapter 1), two chapters describing studies that have been published in *Geology* and *Geobiology* (Chapters 2 and 3, respectively), a chapter that has been prepared for submission to *Nature Geoscience* (Chapter 4), a chapter that has been prepared for submission to *Palaios* and the Conclusion (Chapter 5). Previously published chapters have been reformatted in the current Thesis for internal consistency. All chapters describe the use of

experimental taphonomy to investigate the preservation of photosynthetic microbial mats and soft tissues in siliciclastic substrates.

In Chapter 2, we demonstrated a mechanism for microbial fossilization in siliciclastic settings. This mechanism combines the trapping of fine particles from the sediment onto thick microbial sheaths with the precipitation of clay minerals from ions in solution. To determine environmental conditions conducive to the preservation of cyanobacteria in siliciclastic environments, we incubated cyanobacterial cells in silica sand for one month. Microbial preservation occurred under oxic conditions and the degradation of cyanobacterial cells was minimal. The formation of clay veneers was facilitated by high concentrations of dissolved silica ($\geq$0.1 mM) and fine particles (>5.6 mg/L) that were suspended in solution.

Chapter 3 advances our understanding of microbial preservation in coarse-grained siliciclastic environments by investigating additional environmental and biological factors that affect the formation of mineral veneers around microbial filaments. In this chapter, we constrain fluid energies that lead to the preservation of sheathed cyanobacteria. Agitation generated by waves and currents is required to first suspend and then deposit fine particles onto cyanobacterial mats. Thus, siliciclastic environments that do not suspend sand, but contain suspended silt and clay minerals, preferentially preserve microbial mats and fossils. This process also preferentially preserves microorganisms with thick ($\geq$1 μm) sheaths that can trap suspended particles.

Previous taphonomic studies have shown that kaolinite preserves soft tissues better than other clay minerals such as montmorillonite (Wilson and Butterfield, 2014; Naimark et al., 2016) and that kaolinite may inhibit heterotrophic microbial growth (McMahon et al., 2016). However, mechanisms involved in preservation by clay minerals are not well understood. In Chapter 4 of this Thesis, we investigate the preservation of soft tissues (scallop adductor muscles) that were

buried in kaolinite for 45 days and find that the formation of mineral veneers inhibits the decay of soft tissues. The veneers around soft tissues form by the precipitation of authigenic clay minerals as well as the adhesion of micron-sized clay minerals from the sediment. These mineral coatings provide structural support for the soft tissues and also inhibit interactions between the organic material and heterotrophic microorganisms.

Microbial mats and high concentrations of seawater silica are hypothesized to have played a role in the preservation of soft, labile tissues by facilitating the formation of authigenic minerals such as pyrite or amorphous silica on the surfaces of tissues (Gehling, 1999; Tarhan et al., 2016). To test these hypotheses, Chapter 5 investigates the effects of microbial mats, illite and water chemistry on the preservation of scallop adductor muscles buried in silica sand. In doing this, we determine the relative importance of these environmental and biological factors in the preservation of soft-bodied, macroscopic organisms. Future work will involve using DNA analyses to characterize the microbial communities that grow around soft tissues during incubation. Samples have already been collected and this data will be incorporated into a separate manuscript that is not included in the current Thesis.

Results from taphonomic experiments described by all Thesis chapters are compared to the siliciclastic rock record. We pay particular attention to the Ediacaran Period, when soft tissues and microbial textures were exceptionally preserved in sandy and silty sediments.

References

Anderson, E.P., Schiffbauer, J.D., Xiao, S., 2011. Taphonomic study of Ediacaran organic-walled fossils confirms the importance of clay minerals and pyrite in Burgess Shale-type preservation. Geology 39, 643–646. doi:10.1130/G31969.1.

Bosak, T., Newman, D.K., 2003. Microbial nucleation of calcium carbonate in the Precambrian. Geology 31, 577–580. doi:10.1130/0091-7613(2003)031<0577:MNOCCI>2.0.CO;2.

Bosak, T., Souza-Egipsy, V., Newman, D.K., 2004. A laboratory model of abiotic peloid formation. Geobiology 2, 189–198. doi:10.1111/j.1472-4677.2004.00031.x.

Briggs, D.E.G., 2003. The role of decay and mineralization in the preservation of soft-bodied fossils. Annu Rev. Earth Planet. Sci. 31, 275–301. doi:10.1146/annurev.earth.31.100901.144746.

Briggs, D.E.G., Kear, A.J., 1994. Decay and mineralization of shrimps. Palaios 9, 431-456. doi:10.2307/3515135.

Cai, Y., Schiffbauer, J.D., Hua, H., Xiao, S., 2012. Preservational modes in the Ediacaran Gaojiashan Lagerstätte: Pyritization, aluminosilicification, and carbonaceous compression. Palaeogeogr. Palaeoclimatol. Palaeoecol. 326–328, 109–117. doi:10.1016/j.palaeo.2012.02.009.

Callow, R.H.T., Brasier, M.D., 2009. Remarkable preservation of microbial mats in Neoproterozoic siliciclastic settings: Implications for Ediacaran taphonomic models. Earth-Science Rev. 96, 207–219. doi:10.1016/j.earscirev.2009.07.002.

Darroch, S.A.F., Laflamme, M., Schiffbauer, J.D., Briggs, D.E.G., 2012. Experimental formation of a microbial death mask. Palaios 27, 293–303. doi:10.2110/palo.2011.p11-059r.

Ferris, F.G., Fyfe, W.S., Beveridge, T.J., 1987. Bacteria as nucleation sites for authigenic minerals in a metal-contaminated lake sediment. Chem. Geol. 63, 225–232. doi:10.1016/0009-2541(87)90165-3.

Gaines, R.R., Briggs, D.E.G., Yuanlong, Z., 2008. Cambrian Burgess Shale-type deposits share a common mode of fossilization. Geology 36, 755–758. doi:10.1130/G24961A.1.

Gehling, J.G., 1999. Microbial mats in terminal Proterozoic siliciclastics: Ediacaran death masks. Palaios 14, 40–57. doi:10.2307/3515360.

Konhauser, K., 1997. Bacterial iron biomineralisation in nature. FEMS Microbiol. Rev. 20, 315–326. doi:10.1016/S0168-6445(97)00014-4.

Konhauser, K.O., Fisher, Q.J., Fyfe, W.S., Longstaffe, F.J., Powell, M.A., 1998. Authigenic mineralization and detrital clay binding by freshwater biofilms: The Brahmani river, India. Geomicrobiol. J. 15, 209–222. doi:10.1080/01490459809378077.

Konhauser, K.O., Urrutia, M.M., 1999. Bacterial clay authigenesis: A common biogeochemical process. Chem. Geol. 161, 399–413. doi:10.1016/S0009-2541(99)00118-7.

Laflamme, M., Schiffbauer, J.D., Narbonne, G.M., Briggs, D.E.G., 2011. Microbial biofilms and the preservation of the Ediacara biota. Lethaia 44, 203–213. doi:10.1111/j.1502-3931.2010.00235.x.

Maliva, R.G., Knoll, A.H., Simonson, B.M., 2005. Secular change in the Precambrian silica cycle: Insights from chert petrology. Geol. Soc. Am. Bull. 117, 835–845. doi:10.1130/B25555.1.

Mapstone, N.B., McIlroy, D., 2006. Ediacaran fossil preservation: Taphonomy and diagenesis of a discoid biota from the Amadeus Basin, central Australia. Precambrian Res. 149, 126–148. doi:10.1016/j.precamres.2006.05.007.

McMahon, S., Anderson, R.P., Saupe, E.E., Briggs, D.E.G., 2016. Experimental evidence that clay inhibits bacterial decomposers: Implications for preservation of organic fossils. Geology 44, 867–870. doi:10.1130/G38454.1.

Mera, M.U., Beveridge, T.J., 1993. Mechanism of silicate binding to the bacterial cell wall in *Bacillus subtilis*. J. Bacteriol. 175, 1936–1945.

Michalopoulos, P., Aller, R.C., 2004. Early diagenesis of biogenic silica in the Amazon delta: Alteration, authigenic clay formation, and storage. Geochim. Cosmochim. Acta 68, 1061–1085. doi:10.1016/j.gca.2003.07.018.

Michalopoulos, P., Aller, R.C., 1995. Rapid clay mineral formation in Amazon delta sediments: Reverse weathering and oceanic elemental cycles. Science 270, 614–617. doi:10.1126/Science.270.5236.614.

Mustoe, G.E., 2008. Mineralogy and geochemistry of the late Eocene silicified wood from Florissant Fossil Beds National Monument, Colorado. Geol. Soc. Am. Spec. Pap. 435, 127–140. doi:10.1080/00357529.1995.992662.

Naimark, E., Kalinina, M., Shokurov, A., Boeva, N., Markov, A., Zaytseva, L., 2016. Decaying in different clays: Implications for soft-tissue preservation. Palaeontology 59, 583–595. doi:10.1111/pala.12246.

Newman, S.A., Klepac-Ceraj, V., Mariotti, G., Pruss, S.B., Watson, N., Bosak, T., 2017. Experimental fossilization of mat-forming cyanobacteria in coarse-grained siliciclastic sediments. Geobiology 15, 484–498. doi:10.1111/gbi.12229.

Newman, S.A., Mariotti, G., Pruss, S., Bosak, T., 2016. Insights into cyanobacterial fossilization in Ediacaran siliciclastic environments. Geology 44, 579–582. doi: 10.1130/G37791.1.

Orr, P.J., 1998. Cambrian Burgess Shale animals replicated in clay minerals. Science 281, 1173–1175. doi:10.1126/science.281.5380.1173.

Petrovich, R., 2001. Mechanisms of fossilization of the soft-bodied and lightly armored faunas of the Burgess Shale and of some other classical localities. Am. J. Sci. 301, 683–726. doi:10.2475/ajs.301.8.683.

Sagemann, J., Bale, S.J., Briggs, D.E.G., Parkes, R.J., 1999. Controls on the formation of authigenic minerals in association with decaying organic matter: An experimental approach. Geochim. Cosmochim. Acta 63, 1083–1095. doi:10.1016/S0016-7037(99)00087-3.

Seilacher, A., Pflüger, F., 1994. From Biomats to Benthic Agriculture: A Biohistoric Revolution, in: Krumbein, W.E., Paterson, D.M., Stal, L.J. (Eds.), Biostabalization of Sediments. Bibliotheks - und Informationssystem der Universitat Oldenburg, Oldenburg, Germany, pp. 97–105.

Schultze-Lam, S., Ferris, F.G., Konhauser, K.O., Wiese, R.G., 1995. In situ silicification of an Icelandic hot spring microbial mat: Implications for microfossil formation. Can. J. Earth Sci. 32, 2021–2026. doi:10.1139/e95-155.

Tarhan, L.G., Hood, A.v.S., Droser, M.L., Gehling, J.G., Briggs, D.E.G., 2016. Exceptional preservation of soft-bodied Ediacara Biota promoted by silica-rich oceans. Geology 44, 951–954. doi:10.1130/G38542.1.

Wilson, L.A., Butterfield, N.J., 2014. Sediment effects on the preservation of Burgess Shale-type compression fossils. Palaios 29, 145–154. doi:10.2110/palo.2013.075.

Chapter 2. Insights into cyanobacterial fossilization in Ediacaran siliciclastic environments

Forward

This chapter has been previously published in *Geology*. Citation:

Newman, S.A., Mariotti, G., Pruss, S., Bosak, T., 2016. Insights into cyanobacterial fossilization in Ediacaran siliciclastic environments. *Geology* 44, 579–582. doi: 10.1130/G37791.1.

2.1 Abstract

Ediacaran sedimentary successions are noted for the preservation of microbes and microbial textures on the surfaces of sandstones and siltstones. Although microorganisms have been preserved in coarse-grained siliciclastic sand throughout geologic history, the exceptional preservation of microbes in Ediacaran sediments suggests the potential for a unique taphonomic window. Here, we identify conditions conducive to the fossilization of filamentous cyanobacteria growing in the presence of siliciclastic sand and demonstrate that the sheaths of filamentous cyanobacteria can become coated by clay minerals within days under oxic conditions. Smooth, extensive mineral coatings develop in the presence of 5.6 to 55.6 mg/L of suspended clay and 0.1 mM or greater concentrations of dissolved silica. Thus, elevated concentrations of seawater silica and the delivery of suspended clays promote microbial preservation on sandy and silty surfaces. These factors likely facilitated microbial fossilization in coarse-grained siliciclastic sand

throughout the Ediacaran Period and may have also contributed to microbial fossilization in siliciclastic deposits at other times throughout Earth's history.

2.2 Introduction

Microbial fossils and textures are commonly found in Ediacaran coarse-grained siliciclastic sand (Vidal and Moczydowska, 1992; Gehling, 1999; Schieber et al., 2007; Moczydlowska, 2008; Callow and Brasier, 2009; Cohen et al., 2009). Although microbially induced sedimentary structures (MISSs; Noffke et al., 2001) occur in a variety of coarse-grained sediments, ranging in age from Archaean to modern (e.g., Noffke, 2000; Noffke et al., 2006; Schieber et al., 2007; Noffke, 2010), abundant and commonly exceptionally preserved microbial fossils and MISSs have been reported in Ediacaran siliciclastic sediments of tidal to shallow marine origin (Hagadorn and Bottjer, 1997; Callow and Brasier, 2009). Therefore, a unique environmental window may have facilitated the exceptional preservation of microorganisms in a range of Ediacaran sediments. Microbial mats were widespread during the Precambrian (Seilacher and Pflüger, 1994; Seilacher, 1999) but became less common in subtidal and intertidal environments after the Cambrian Period. A recent review lists occurrences and environmental distributions of Precambrian and Phanerozoic MISSs (Davies et al., 2016, their table 1) that support a notable shift in the environmental distribution of post-Cambrian MISSs; the vast majority of post-Cambrian MISSs are found in restricted or non-marine settings. This likely reflects an environmental restriction caused by the radiation of grazing and bioturbating metazoans (Bottjer et al., 2000) that destroy microbial mats and overprint microbial signatures in the rock record (Byers, 1983; Hagadorn and Bottjer, 1997; Pflueger, 1999; Gehling, 1999;

Bottjer et al., 2000). Thus, the absence of megafaunal predation and sediment bioturbation may have been an essential condition for microbial preservation in Ediacaran siliciclastics.

Additional hypotheses addressing the Ediacaran-type preservation of microbial textures have invoked differences in Precambrian seawater chemistry and organic decay (Gehling, 1999; Callow and Brasier, 2009). To date, these hypotheses have focused primarily on fossilization during organic decay in the anoxic zone of sediments, below the sediment-water interface. For example, Callow and Brasier (2009) suggested that a shallowing of the Ediacaran seafloor redox boundary reduced the degradation of organic matter and enhanced microbial preservation.

Elevated concentrations of silica in Precambrian oceans (Siever, 1957; Maliva et al., 2005) are also hypothesized to have enhanced early fossilization through the precipitation of authigenic silicate minerals (Gehling, 1999; Callow and Brasier, 2009). Although most studies of modern systems do not specifically address fossilization or the role of silica concentrations in microbial preservation, experimental evidence has indicated the role of iron in the precipitation of clay minerals around cell walls (e.g., Urrutia and Beveridge, 1994; Konhauser et al., 1998; Konhauser and Urrutia, 1999; Fein et al., 2002).

Here, we experimentally identify conditions most conducive to the development of smooth, shape-preserving mineral coatings around cyanobacteria grown on siliciclastic sand. We evaluate the influences of microbial trapping of suspended clay, clay loading and seawater silica concentrations. Our results confirm that both dissolved silica and suspended clay promote the formation of mineral coatings around actively growing, photosynthetic organisms under oxic conditions. We also suggest that optimal conditions existed during the terminal Proterozoic

(i.e., high concentrations of dissolved silica and suspended sediment in combination with the relative absence of grazing metazoans) which resulted in the exceptional preservation of microbes and microbial textures in Ediacaran sandy environments.

2.3 Methods

Mixed communities of filamentous cyanobacteria were grown in plastic culture jars (190 mL; BioExpress, Kaysville, Utah, USA) containing artificial seawater (Supplementary Table 2.1). The seawater contained either high (0.1 or 0.4 mM) or low (0 mM) initial concentrations of added silica (reagent-grade sodium silicate solution: $[Na_2O(SiO_2)x \cdot H_2O]$; Sigma-Aldrich, St. Louis, Missouri, USA). Microbes were grown on (1) autoclaved siliciclastic beach sand (purchased from the Ottawa Silica Company, Ottawa, Illinois, USA) composed of quartz and 0.03 wt% clays (iron-, calcium-, potassium-, magnesium- and sodium-rich aluminosilicates) or (2) powdered illite (purchased from Time Laboratories, Pocatello, Idaho, USA; 100% clay fraction, similarly composed of iron-, calcium-, potassium-, magnesium- and sodium-rich aluminosilicates). Continuous agitation on orbital shakers (VWR Mini Shakers; VWR International, Radnor, Pennsylvania, USA) suspended finer silt and clay but did not move larger quartz grains (Supplementary Fig. 2.1), thus mimicking the conditions at seafloors below the fair-weather wave base. Cyanobacterial filaments clustered into aggregates (1 to 5 mm in diameter) that were gently agitated by the fluid motion. To separate cyanobacteria from the substrate and allow ions to pass freely between the sediment and the solution, we packed the sand into dialysis membranes (Standard RC, pore size 12–14 kilodaltons [atomic mass unit]; Spectrum Labs, Rancho Dominguez, California, USA). This prevented the suspension of fine sediment from the sand (Supplementary Fig. 2.1). To determine if any clay nuclei passed through

the dialysis membrane into the surrounding solution, a sterile medium was incubated for two months in the presence of membrane-enclosed sand and then filtered using a 0.22 mm Millipore filter. All samples were imaged using a Zeiss Supra Scanning Electron Microscope with an energy dispersive X-ray spectrometer at 10 kV (Center for Nanoscale Systems, Harvard University, Massachusetts, USA). Experimental conditions are given in Supplementary Table 2.2.

2.4 Results

Cyanobacteria sampled immediately before inoculation were not covered in minerals (Fig. 2.1). After only 5 d of growth on siliciclastic sand or illite powder in continuously agitated media (Supplementary Fig 2.1), most cyanobacterial filaments were coated by clay minerals. Uncoated cyanobacterial filaments were generally thinner than one μm, whereas the thickness of coated filaments ranged from one to 1.5 μm (Fig. 2.2). Mineral coatings around cells were composed of some angular grains with crystalline appearances and smoother, less angular ones (Figs. 2.1 and 2.2). The most extensive coating developed around filaments when the medium contained 0.1 mM or greater concentrations of initial silica (Fig. 2.2). Aluminosilicate minerals were rich in iron, calcium, potassium, magnesium and sodium. Their elemental composition was similar or identical to that of minerals found in the clay fraction of the beach sand or illite (Fig. 2.1, Supplementary Fig. 2.2). These experiments showed that cyanobacterial filaments could be coated within weeks in actively growing, well-aerated cultures and before extensive organic decay.

The compositional similarity between minerals around cells and clay minerals in the siliciclastic sand suggested that cyanobacteria trapped suspended minerals from the solution (Fig.

2.1, Supplementary Fig. 2.2). To test this, we enclosed siliciclastic sand in dialysis bags. The pore size of the dialysis membranes is smaller than the diameter of both cyanobacteria (0.5–40 mm) and sand grains (>62.5 mm) and hinders the release of particles larger than 12–14 kilodaltons into suspension. Cyanobacteria growing under these conditions remained uncoated after 5 d, although the same amount of time was sufficient to generate coating in experiments without dialysis bags. After one month of incubation in the presence of dialysis bags, the filaments contained only rare aluminosilicate grains, which smoothly covered cells (Fig. 2.2, Supplementary Fig. 2.3). The absence of a continuous coating of minerals underscored the importance of suspended minerals in the encrustation of microbial filaments.

Because the pore size of dialysis membranes is larger than the unit cell of various clays (e.g., ~400 daltons for illite), some clay nuclei may have escaped the dialysis barrier. To test this, we incubated 100 mL of sterile media in the presence of sand enclosed within dialysis membranes for two months. The presence of chlorine-, sodium- and potassium-rich clay minerals in the filtrate suggested that some fine-grained clay nuclei may have passed through the dialysis barrier. However, the EDS spectra of these minerals were different from those of small aluminosilicates that formed around filaments during the month-long incubation of cyanobacteria (Supplementary Fig. 2.3), indicating that the latter minerals were precipitated and not trapped from the solution.

The trapping of suspended clay particles by cyanobacterial sheaths played a critical role in the preservation of cyanobacterial filaments in our experiments. Therefore, we sought to investigate the appearance of mineral coating as a function of the quantity of suspended clays (0, 5.6, and 55.6 mg/L). As expected, the smoothest, most extensive coating developed in the

presence of 55.6 mg/L clay (Fig. 2.2). Thus, higher concentrations of suspended fine-grained sediment promote the encrustation of cyanobacterial filaments by clay minerals.

2.5 Discussion

2.5.1 Microbial trapping and precipitation of aluminosilicates

Previous research demonstrated the microbial ability to precipitate clay minerals in cultures and natural environments (Konhauser et al., 1993, 1998; Urrutia and Beveridge, 1994; Konhauser and Urrutia, 1999). However, these studies did not address the contribution of sediment trapping by sticky microbial surfaces, although this process is likely to occur in nature. Here, we show that trapping can preserve the shape of cyanobacterial filaments within days, but fine-grained clay minerals precipitate much more slowly in the absence of abundant clay nuclei. Thus, the trapping of clay minerals from suspension appears to be critical to cyanobacterial preservation because it is the faster and more extensive process.

Precipitation of authigenic clays in modern environments occurs in natural riverine systems and anoxic settings that contain elevated concentrations of iron (Michalopoulos and Aller, 1995; Konhauser and Urrutia, 1999). For example, Michalopoulos and Aller (1995) reported authigenic clay formation in anoxic sediments from the Amazon River delta, where the concentrations of dissolved iron(II) range from 0.3 to 0.7 mM (Aller et al., 1986). Microbes in these environments can bind iron (or other cations, e.g., aluminum) onto cell walls, which subsequently promotes clay formation by lowering the activation energy of aluminosilicate nucleation (Ferris et al., 1987; Konhauser et al., 1994, 1998). In contrast, our experiments demonstrate that cyanobacteria mediate the precipitation of clay minerals at monthly timescales (Fig. 2.2, Supplementary Fig. 2.3) under well-aerated conditions and in the presence of only moderate iron concentrations (<2

mM). Most minerals that precipitated around cyanobacterial filaments under our experimental conditions also lack detectable iron (Supplementary Fig. 2.3). Thus, elevated concentrations of soluble iron and anoxic settings do not appear to be necessary for the preservation of photosynthetic organisms and textures on the surfaces of siliciclastic bedding planes, such as those described by Hagadorn and Bottjer (1997) and Gehling and Droser (2009).

2.5.2 The role of aqueous silica in cyanobacterial fossilization

High concentrations of silica (0.1 mM or greater) enhanced the extent and smoothness of minerals coating cyanobacterial filaments in our experiments. These concentrations are higher than most modern oceanic values but below saturation with respect to amorphous silica (Pilson, 1998, his chapter 8). We tentatively attribute the formation of smoother, more continuous coatings in the presence of 0.1 and 0.4 mM silica to the precipitation of fine-grained aluminosilicates around biologically trapped minerals (Siever and Woodford, 1973). The adsorption of silica onto cationic metals bound to cells (Ferris et al., 1987; Konhauser et al., 1993, 1998; Konhauser and Urrutia, 1999) or the direct adsorption of silica onto cyanobacterial sheaths (Mera and Beveridge, 1993) may also contribute to smooth and continuous mineral coating.

2.5.3 Geological significance

Our experiments show that elevated concentrations of silica and suspended clays may have facilitated the exceptional preservation of microbes and microbial textures throughout the Ediacaran Period (Banerjee and Jeevankumar, 2005; Noffke and Chafetz, 2012). This supports the preservational models proposed by Callow and Brasier (2009) and Hagadorn and Bottjer

(1997); the former authors suggested a relationship between the higher concentrations of silica and Ediacaran preservation, whereas the latter noted abundant clay and mica on the surfaces of bedding planes that preserve wrinkle structures.

The formation of molds around the sheaths of filamentous photosynthetic cyanobacteria depends not only on the ability of these organisms to trap clay minerals, but also on the availability of these minerals. Our experiments suggest that even coarse-grained environments that are characterized by low concentrations of suspended clay (<100 mg/L) would allow for the preservation of exceptional fossils, such as those found in Ediacaran sediments.

2.6 Conclusions

Our findings offer insights into the preservation of photosynthetic microbes and surface textures in coarse siliciclastics. By using the extent and smoothness of mineral coating as indicators of early cyanobacterial fossilization, we identify the following conditions as sufficient for the preservation of mineral-rich microbial fossils and textures in coarse-grained siliciclastics: (1) persistent concentrations of silica ≥0.1 mM and (2) the availability of suspended clays in solution (5.6–55.6 mg/L). We suggest that these factors, in combination with reduced grazing and bioturbation, contributed to the preservation of cyanobacteria and other photosynthetic organisms throughout the Ediacaran Period and at other times in Earth history.

2.7 References

Aller, R.C., Mackin, J.E., Cox, R.T., 1986. Diagenesis of Fe and S in Amazon inner shelf muds: Apparent dominance of Fe reduction and implications for the genesis of ironstones. Cont. Shelf Res. 6, 263–289. doi:10.1016/0278-4343(86)90064-6.

Banerjee, S., Jeevankumar, S., 2005. Microbially originated wrinkle structures on sandstone and their stratigraphic context: Palaeoproterozoic Koldaha Shale, central India. Sediment. Geol. 176, 211–224. doi:10.1016/j.sedgeo.2004.12.013.

Bottjer, D.J., Hagadorn, J.W., Dornbos, S.Q., 2000. The Cambrian substrate revolution. GSA Today 10, 1–7.

Byers, C.W., 1983. Geological significance of marine biogenic sedimentary structures, in: McCall, P.L., Tevesz, M.J.S. (Eds.), Animal-Sediment Relations: The Biogenic Alteration of Sediments. Plenum Press, New York, NY, pp. 221–256.

Callow, R.H.T., Brasier, M.D., 2009. Remarkable preservation of microbial mats in Neoproterozoic siliciclastic settings: Implications for Ediacaran taphonomic models. Earth-Science Rev. 96, 207–219. doi:10.1016/j.earscirev.2009.07.002.

Cohen, P.A., Bradley, A., Knoll, A.H., Grotzinger, J.P., Jensen, S., Abelson, J., Hand, K., Love, G., Metz, J., McLoughlin, N., Meister, P., Shepard, R., Tice, M., Wilson, J.P., 2009. Tubular compression fossils from the Ediacaran Nama Group, Namibia. J. Paleontol. 83, 110–122. doi:10.1666/09-040R.1.

Davies, N.S., Liu, A.G., Gibling, M.R., Miller, R.F., 2016. Resolving MISS conceptions and misconceptions: A geological approach to sedimentary surface textures generated by microbial and abiotic processes. Earth-Science Rev. 154, 210–246. doi:10.1016/j.earscirev.2016.01.005.

Fein, J.B., Scott, S., Rivera, N., 2002. The effect of Fe on Si adsorption by *Bacillus subtilis* cell walls: Insights into non-metabolic bacterial precipitation of silicate minerals. Chem. Geol. 182, 265–273. doi:10.1016/S0009-2541(01)00294-7.

Ferris, F.G., Fyfe, W.S., Beveridge, T.J., 1987. Bacteria as nucleation sites for authigenic minerals in a metal-contaminated lake sediment. Chem. Geol. 63, 225–232. doi:10.1016/0009-2541(87)90165-3.

Gehling, J.G., 1999. Microbial mats in terminal Proterozoic siliciclastics: Ediacaran death masks. Palaios 14, 40–57. doi:10.2307/3515360.

Gehling, J.G., Droser, M.L., 2009. Textured organic surfaces associated with the Ediacara biota in South Australia. Earth-Science Rev. 96, 196–206. doi:10.1016/j.earscirev.2009.03.002.

Hagadorn, J.W., Bottjer, D.J., 1997. Wrinkle structures: Microbially mediated sedimentary structures common in subtidal siliciclastic settings at the Proterozoic-Phanerozoic transition. Geology 25, 1047–1050. doi:10.1130/0091-7613(1997)025<1047.

Konhauser, K.O., Fisher, Q.J., Fyfe, W.S., Longstaffe, F.J., Powell, M.A., 1998. Authigenic mineralization and detrital clay binding by freshwater biofilms: The Brahmani river, India. Geomicrobiol. J. 15, 209–222. doi:10.1080/01490459809378077.

Konhauser, K.O., Fyfe, W.S., Ferris, F.G., Beveridge, T.J., 1993. Metal sorption and mineral precipitation by bacteria in two Amazonian river systems: Rio Solimoes and Rio Negro, Brazil. Geology 21, 1103–1106.

Konhauser, K.O., Schultze-Lam, S., Ferris, F.G., Fyfe, W.S., Longstaffe, F.J., Beveridge, T.J., 1994. Mineral precipitation by epilithic biofilms in the Speed River, Ontario, Canada. Appl. Environ. Microbiol. 60, 549–553.

Konhauser, K.O., Urrutia, M.M., 1999. Bacterial clay authigenesis: A common biogeochemical process. Chem. Geol. 161, 399–413. doi:10.1016/S0009-2541(99)00118-7.

Maliva, R.G., Knoll, A.H., Simonson, B.M., 2005. Secular change in the Precambrian silica cycle: Insights from chert petrology. Geol. Soc. Am. Bull. 117, 835–845. doi:10.1130/B25555.1.

Mera, M.U., Beveridge, T.J., 1993. Mechanism of silicate binding to the bacterial cell wall in *Bacillus subtilis*. J. Bacteriol. 175, 1936–1945.

Michalopoulos, P., Aller, R.C., 1995. Rapid clay mineral formation in Amazon Delta sediments: Reverse weathering and oceanic elemental cycles. Science 270, 614–617. doi:10.1126/Science.270.5236.614.

Moczydłowska, M., 2008. New records of late Ediacaran microbiota from Poland. Precambrian Res. 167, 71–92.

Noffke, N., 2010. Microbial Mats in Sandy Deposits from the Archean Era to Today. Springer-Verlag, Heidelberg, Germany, 194 p.

Noffke, N., 2000. Extensive microbial mats and their influences on the erosional and depositional dynamics of a siliciclastic cold water environment (Lower Arenigian, Montagne Noire, France). Sediment. Geol. 136, 207–215. doi:10.1016/S0037-0738(00)00098-1.

Noffke, N., Chafetz, H., 2012. Microbial Mats in Siliciclastic Depositional Systems Through Time, 1st ed. SEPM Society for Sedimentary Geology, Tulsa, Oklahoma.

Noffke, N., Eriksson, K.A., Hazen, R.M., Simpson, E.L., 2006. A new window into Early Archean life: Microbial mats in Earth's oldest siliciclastic tidal deposits (3.2 Ga Moodies Group, South Africa). Geology 34, 253–256. doi:10.1130/G22246.1.

Noffke, N., Gerdes, G., Klenke, T., Krumbein, W., 2001. Microbially induced sedimentary structures — A new category within the classification of primary sedimentary structures. J. Sediment. Res. 71, 649–656.

Pflueger, F., 1999. Matground structures and redox facies. Palaios 14, 25–39. doi:10.2307/3515359.

Pilson, M.E.Q., 1998. Nutrients, in: An Introduction to the Chemistry of the Sea. Prentice Hall, Upper Saddle River, NJ, pp. 156–206.

Schieber, J., Bose, P., Eriksson, P., Banerjee, S., Sarkar, S., Altermann, W., Catuneau, O., 2007. Atlas of Microbial Mat Features Preserved within the Siliciclastic Rock Record. Elsevier, Amsterdam, 311 p.

Seilacher, A., 1999. Biomat-related lifestyles in the Precambrian. Palaios 14, 86–93. doi:10.2307/3515363.

Seilacher, A., Pflüger, F., 1994. From Biomats to Benthic Agriculture: A Biohistoric Revolution, in: Krumbein, W.E., Paterson, D.M., Stal, L.J. (Eds.), Biostabalization of Sediments. Bibliotheks - und Informationssystem der Universitat Oldenburg, Oldenburg, Germany, pp. 97–105.

Siever, R., 1957. The silica budget in the sedimentary cycle. Am. Mineral. 42, 821–841.

Siever, R., Woodford, N., 1973. Sorption of silica by clay minerals. Geochim. Cosmochim. Acta 37, 1851–1880.

Urrutia, M.M., Beveridge, T.J., 1994. Formation of fine-grained metal and silicate precipitates on a bacterial surface (*Bacillus subtilis*). Chem. Geol. 116, 261–280.

Vidal, G., Moczydowska, M., 1992. Patterns of phytoplankton radiation across the Precambrian-Cambrian boundary. J. Geol. Soc. London. 149, 647–654. doi:10.1144/gsjgs.149.4.0647.

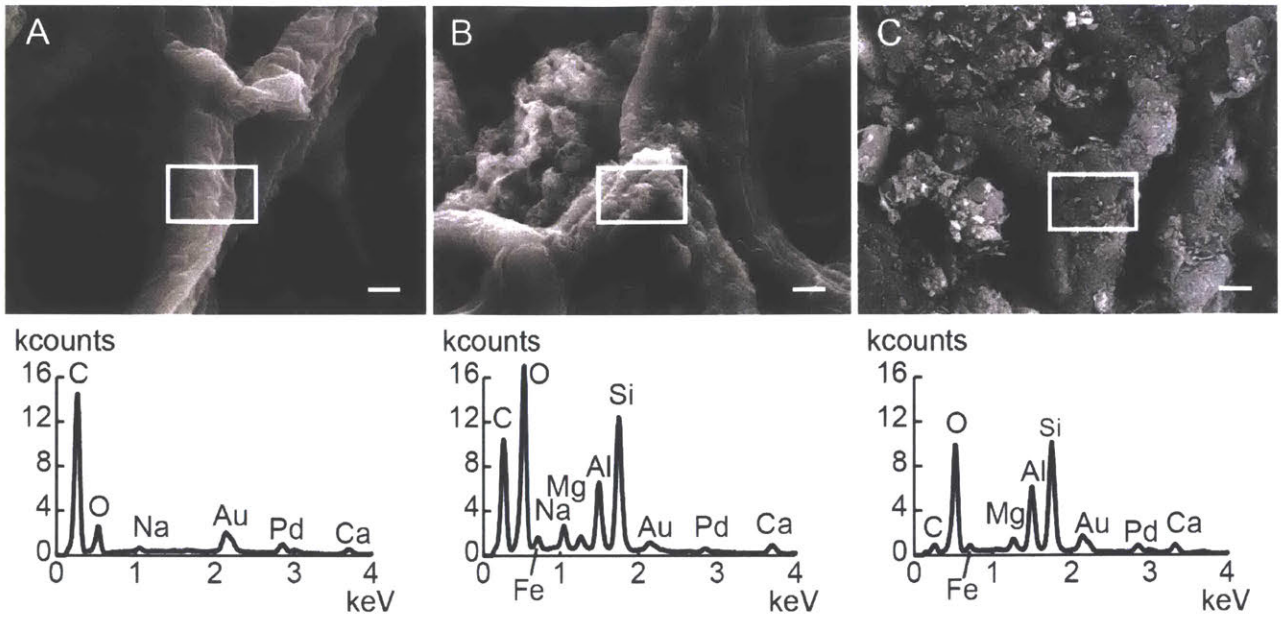

Fig. 2.1. Representative scanning electron microscopy (SEM) images and SEM-EDS (energy-dispersive X-ray spectroscopy) spectra of filamentous cyanobacteria and minerals. A) Inoculum (day 0). B) Cells grown on beach sand for 5 days. C) Cells grown on illite powder for 5 days. White boxes indicate areas analyzed by SEM-EDS. EDS spectra are located directly beneath corresponding SEM images. Scale bars are 1 μm. Samples were coated with gold and palladium.

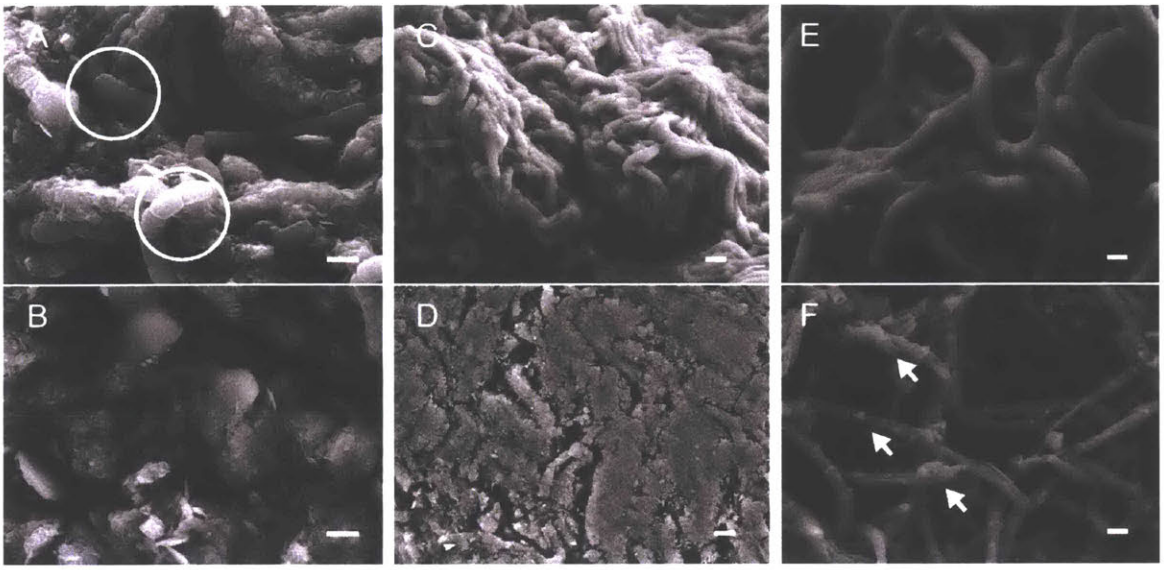

Fig. 2.2. Effects of dissolved silica concentrations and clay loading on fossilization. A-D) Cyanobacteria after 15 d of growth: A) Coated cyanobacterial filaments in solutions with 0 mM initial silica. Circles mark uncoated cells. These cells lack thick sheaths. B) Smoother and more extensive minerals coat cells grown in solution with 0.1 mM dissolved silica. C) Uncoated cyanobacteria grown in solutions that lacked added clays or silica sand. D) Extensive coating in the presence of 55.6 mg/L of clay. E) Sheathed filaments separated from sand by dialysis bags lack any visible minerals after 5 days of growth. F) Sparse minerals (arrows) attached to sheaths of cyanobacteria that had been separated from sand for one month. Scale bars are 1 μm (A, B) and 2 μm (C–F). Samples were coated with gold and palladium.

2.8 Supplementary Information

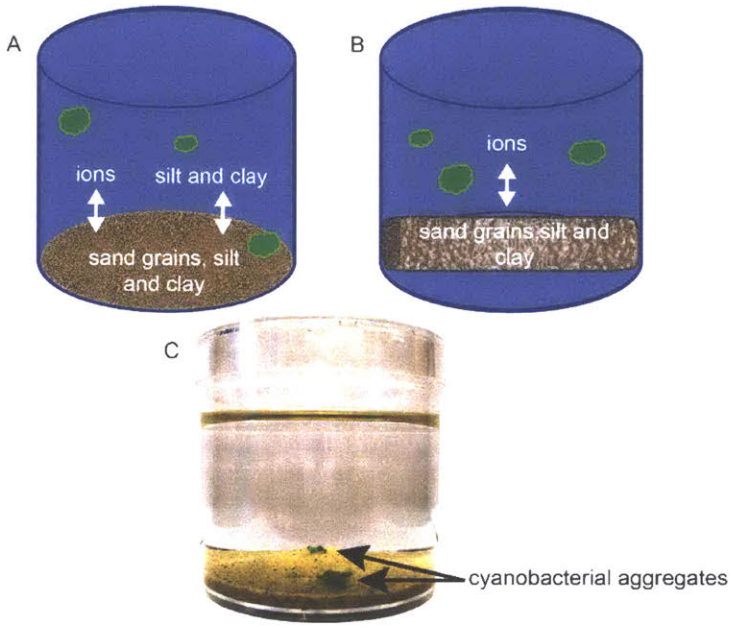

Supplementary Fig. 2.1. Schematic of experimental setup. A) Cyanobacterial aggregates growing directly on siliciclastic sand in the presence of continuous fluid agitation (VWR Minishaker, 190 rpm, 3 mm orbital diameter). Ions, silt and clay minerals can be suspended, but sand grains cannot. B) Cyanobacterial aggregates growing on a dialysis membrane in the presence of continuous fluid agitation (VWR Minishaker, 190 rpm, 3 mm orbital diameter). Ions can pass into solution, but sand grains, silt and clay minerals are trapped inside the dialysis bag. C) Photograph of cyanobacterial aggregates after two weeks of growth. Culture jars are 68 mm (diameter) x 68 mm (height).

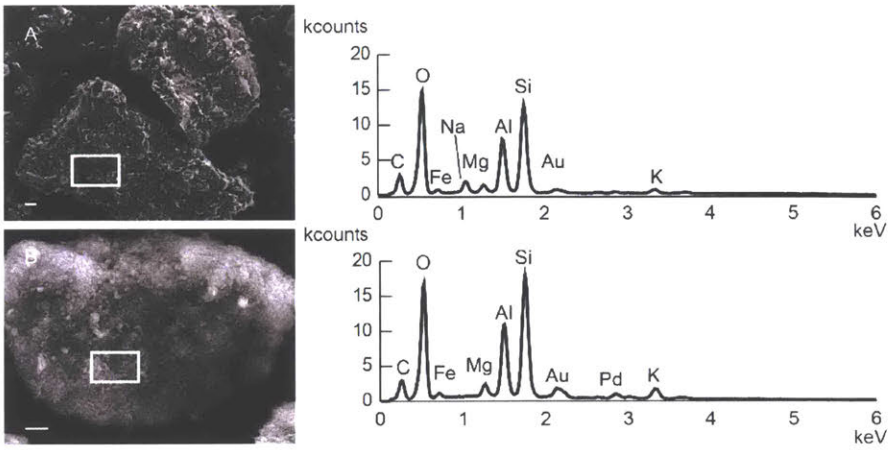

Supplementary Fig. 2.2. Representative SEM images and SEM-EDS spectra of sterile substrates. A) Aggregates of clay minerals filtered from the siliciclastic sand and B) aggregates of illite used in suspended sediment experiments. White boxes indicate analyzed areas. EDS spectra are located to the right of corresponding SEM images. Scale bar: 10 μm (A) and 1 μm (B). Samples were coated with gold and palladium.

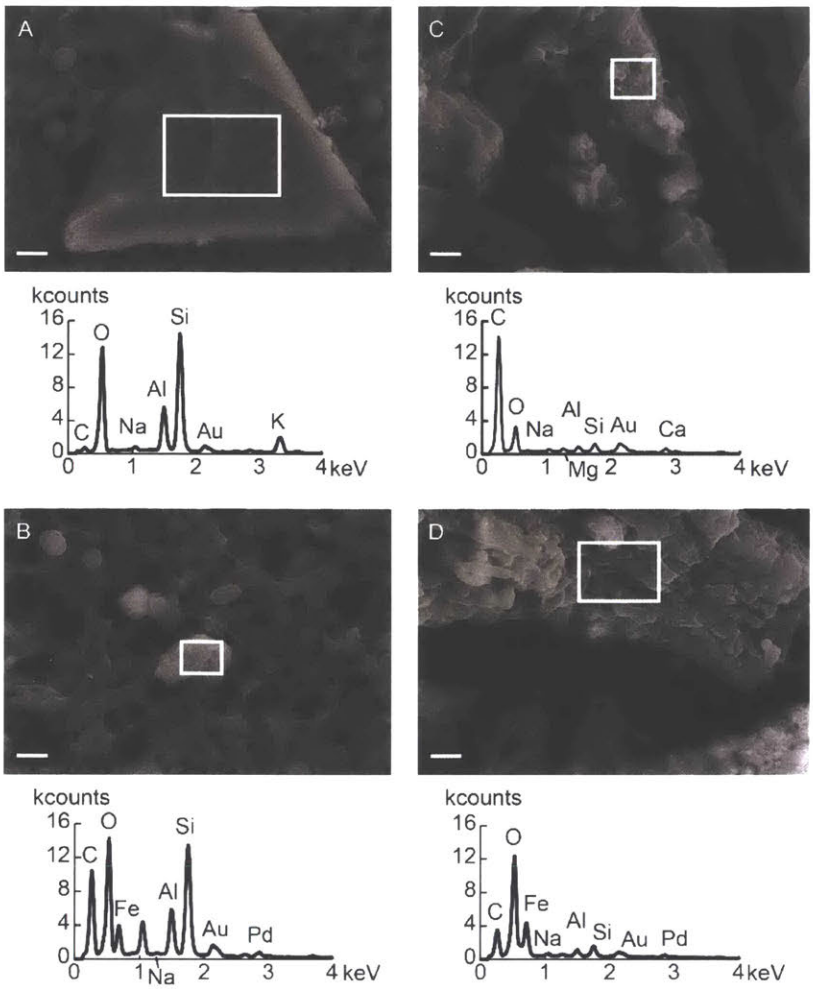

Supplementary Fig. 2.3. Representative SEM images and SEM-EDS spectra of dialysis experiments. A and B) minerals which passed through dialysis bags after less than two months in sterile solutions. The minerals were collected by filtration. C and D) Minerals which formed around cyanobacterial filaments in dialysis experiments after one month of cell growth. White boxes indicate analyzed areas. EDS spectra are located beneath corresponding SEM images. Scale bar: 1 μm. Samples were coated with gold and palladium.

Supplementary Table 2.1. List of ingredients used to make 1 L of artificial seawater.

Ingredient	Amount (g/L)	Volume of stock solution added to 1 L of medium (mL)
Nitrate solution[†]		0.5
KNO_3	5.15	
$NaNO_3$	34.45	
Major "10x" solution[†]		10.0
Nitrilotriacetic Acid	1.00	
NaCl	4.82	
NaH_2PO_4	0.09	
KCl	0.74	
Cast D Trace[†]		1.0
$MnCl_3*4H_2O$	2.67	
$ZnSO_4*7H_2O$	0.50	
$CuSO_4*5H_2O$	0.03	
Na_2MoO_4	0.02	
$Co(NO_3)_2*6H_20$	0.06	
H_3BO_3	0.50	
H_2SO_4 (concentrated)	0.50	
$NiCl_2$	$0.48*10^{-4}$	
$FeCl_3$[†]	3.00	0.1
Mg/Ca solution (5:1)[†]		50.0
$CaCl_2*2H_20$	29.40	
$MgCl_2*6H_20$	203.30	
Sodium silicate solution[†,§]	≤0.09	
NaCl[†]	23.0	
Na_2SO_4[†]	0.71	
KCl[†]	1.48	
$NaHCO_3$[†]	0.34	

Note: Underlined ingredients denote stock solutions. The individual components of each stock solution are given (in g/L). The volume of stock solution (in mL) added to 1L of the basal medium is also given.

[†]Ingredient was added directly to 1L of basal medium.

[§]Reagent grade sodium silicate solution ($Na_2O(SiO_2)_x \cdot xH_2O$) was purchased from Sigma-Aldrich (St. Louis, MO).

Supplementary Table 2.2. List of experimental conditions.

Substrate	Clay (mg/L)	Silica concentration (mM)	Dialysis membranes
Siliciclastic sand	0.03*	0.0	no
Siliciclastic sand	0.03*	0.4	no
None	0.0	0.0	no
None	0.0	0.1	no
Illite	5.6	0.0	no
Illite	5.6	0.1	no
Illite	55.6	0.0	no
Illite	55.6	0.1	no
Siliciclastic sand	0.03*	0.4	yes

Note: Siliciclastic sand was purchased from the Ottawa Silica Co. (Ottawa, IL, USA) and contained quartz, mica and clay minerals. Illite powder was purchased from Time Laboratories (Pocatello, ID, USA) and was 100% clay fraction.

*Given as weight percent of siliciclastic sand.

Chapter 3. Experimental fossilization of mat-forming cyanobacteria in coarse-grained siliciclastic sediments

Forward

This chapter has been previously published in *Geobiology* as Newman et al. (2017). Citation: Newman, S.A., Klepac-Ceraj, V., Mariotti, G., Pruss, S.B., Watson, N., Bosak, T., 2017. Experimental fossilization of mat-forming cyanobacteria in coarse-grained siliciclastic sediments. *Geobiology* 15, 484–498. doi:10.1111/gbi.12229.

3.1 Abstract

Microbial fossils and textures are commonly preserved in Ediacaran and early Cambrian coarse-grained siliciclastic sediments that were deposited in tidal and intertidal marine settings. In contrast, the fossilization of microorganisms in similar marine environments of post-Cambrian age is less frequently reported. Thus, temporal discrepancies in microbial preservation may have resulted from the opening and closing of a unique taphonomic window during the terminal Proterozoic and early Phanerozoic, respectively. Here, we expand upon previous work to identify environmental factors which may have facilitated the preservation of cyanobacteria growing on siliciclastic sand, by experimentally determining the ability of microbial mats to trap small, suspended mineral grains and precipitate minerals from ions in solution. We show that (i) fine grains coat the sheaths of filamentous cyanobacteria (e.g., *Nodosilinea* sp.) residing within the mat, after less than one week of cell growth under aerobic conditions, (ii) clay minerals do not coat sterile cellulose fibers and rarely coat unsheathed cyanobacterial cells (e.g., *Nostoc* sp.), (iii) stronger disturbances (where culture jars were agitated at 170 rpm; 3 mm orbital diameter) produce the smoothest and most extensive mineral veneers around cells, compared with those

agitated at slower rotational speeds (150 and 0 rpm), and (iv) mineral veneers coating cyanobacterial cells are ~1 μm in width. These new findings suggest that sheathed filamentous cyanobacteria may be preferentially preserved under conditions of high fluid energy. We integrate these results into a mechanistic model that explains the preservation of microbial fossils and textures in Ediacaran sandstones and siltstones and in fine-grained siliciclastic deposits that contain exceptionally preserved microbial mats.

3.2. Introduction

Exceptionally preserved microbial fossils and textures (including fossilized tubes and sheaths of photosynthetic microorganisms, as well as microbially induced sedimentary structures, MISS) commonly occur in coarse-grained siliciclastic sediments of the terminal Proterozoic (e.g., Vidal and Moczydowska, 1992; Gehling, 1999; Noffke et al., 2006; Noffke, 2007; Moczydlowska, 2008; Callow and Brasier, 2009; Cohen et al., 2009; Gehling and Droser, 2009). MISS, which are defined as textures formed by interactions between microorganisms and sediment surfaces (Noffke et al., 2001), have been reported in various coarse-grained siliciclastic sediments throughout the sedimentary record (Pruss et al., 2004; Noffke et al., 2003; Noffke, 2007; Schieber et al., 2007). However, their frequent and arguably unique occurrence in subtidal and intertidal marine environments of the Ediacaran and early Cambrian (see Davies et al., 2016, their Table 1 for a compilation) is attributed to flourishing benthic microorganisms in these settings (Seilacher and Pflüger, 1994; Mariotti et al., 2014) in the absence of effective grazing and bioturbating metazoans (Byers, 1983; Pflüger and Gresse, 1996; Hagadorn and Bottjer, 1997; Gehling, 1999).

In addition to organismal activity, seawater chemistry may also have influenced patterns of microbial preservation in siliciclastic sediments through time. Concentrations of oceanic silica were likely much higher during the terminal Proterozoic than today because the radiation of silica-secreting organisms (e.g., siliceous sponges and diatoms) did not occur until the early Phanerozoic (Siever, 1957; Maliva et al., 1989; Knoll and Kotrc, 2015). Thus, high concentrations of dissolved silica are hypothesized to have contributed to the precipitation of authigenic minerals and the subsequent fossilization of microorganisms (Callow and Brasier, 2009).

In a previous study by Newman, Mariotti, Pruss and Bosak (2016), the authors reveal the rapid formation of mineral veneers around microbial cells growing as millimeter-wide microbial aggregates on siliciclastic sand. The most extensive veneers formed in the presence of high concentrations of dissolved silica (0.1 and 0.4 mm) and clay powder (5.5 and 55.6 mg of clay powder/L medium). However, sandstones and siltstones more commonly preserve patterns and textures of ancient microbial mats, rather than fossils of individual cyanobacteria or cyanobacterial aggregates (e.g., Callow and Brasier, 2009). The current study explores the potential of mat-forming cyanobacteria to become extensively coated by clay minerals after only a few days of cell growth. Additionally, for the first time, we quantitatively characterize the thickness of mineral coating that develops around cyanobacterial filaments under fully oxic conditions, compare the fossilization potentials of sheathed and unsheathed cyanobacteria, test the role of non-microbial organic surfaces in fossilization and directly investigate the importance of fluid agitation in the mineral coating of cells. These experiments show that trapped suspended clay minerals and sticky microbial sheaths contribute most critically to the rapid preservation of photosynthetic microbes in sandy sediments. Based on these findings, we propose a mechanism

to explain various occurrences of fossilized microbes and microbial textures in coarser siliciclastics through time.

3.3 Methods

3.3.1 Growth media

We prepared artificial seawater with either low (0 mM) or high (0.1 or 0.4 mM) concentrations of silica (reagent-grade sodium silicate solution ($Na_2O(SiO_2)x \cdot xH_2O$, Sigma-Aldrich, St. Louis, MO). This basal growth medium (see Supplementary Table 2.1 for a complete list of ingredients) was prepared and stored in polypropylene containers (1L Nalgene, Thomas Scientific, Swedesboro, NJ, USA), autoclaved at 121°C for 40 min and then allowed to cool to room temperature. A separate stock solution containing 203.3 g of $MgCl_2*6H_2O$ and 29.4 g of $CaCl_2*2H_2O$/L of double-distilled water (5:1 molar concentration; equivalent to modern seawater concentrations, Pilson, 2013) was filtered through a 0.2 μm membrane (AcroVac Vacuum Filter, Pall Laboratory, Port Washington, NY, USA) and 50 mL of this solution was added to 1L of the autoclaved and cooled basal medium. The pH of the sterile medium was measured with a portable, digital pH meter (WTW, Weilheim, Germany) and adjusted to 7.8 by the addition of 1.0 M HCl/NaOH.

3.3.2 Cyanobacterial cultures

Mixed cyanobacterial communities were enriched from a natural microbial mat collected from the Great Sippewissett Salt Marsh (lower Eastern Buzzards Bay, Cape Cod, MA, USA). The cells were incubated in a 1.9 L plastic container (The Glad Products Co., Oakland, CA, USA) in a silica-free medium in the absence of a solid substrate (e.g., sand or glass beads). This hindered

the precipitation of minerals around cyanobacterial cells before inoculation. At the start of each experiment, cell inoculum was first transferred into a conical tube (5 ml of culture into a 25 ml tube, VWR International, Radnor, PA, USA) and allowed to settle for about 10 min. The liquid was then discarded and replaced with a sterile, silica-free medium three times to wash cells and prevent the transfer of any residual particles to the experimental culture jars (68 × 68 mm diameter and height, BioExpress, Kaysville, UT, USA). Cyanobacteria were then immersed in the experimental medium (see Table 3.1 for a list of experimental conditions), the cells were dispersed by a hand-held mixer (Smart Stick, Cuisinart, East Windsor, NJ, USA) to ensure a homogenous mixture of cells and 5 mL of this suspension was added to the surfaces of autoclaved substrates (e.g., sand, glass beads and illite, see Table 3.1 and the text below) in culture jars. Additional sterile media, containing the desired concentrations of silica, were added to make up a final volume of 90 or 100 mL of medium in each jar. All experiments were performed in duplicate.

Cyanobacteria were submerged in medium and continuously agitated on VWR Minishakers (with a 3 or 15 mm orbital diameter, VWR International, Radnor, PA, USA; see Supplementary Table 3.1 for a calculation of fluid velocity). Agitation was not large enough to mobilize larger sand grains, but did suspend some fine particles in solution and supported the formation of 5 mm-wide cyanobacterial aggregates. The culture medium was replaced every three to four days to maintain a semi-constant pH (7.8–8.6) as well as to provide a fresh supply of ions for cyanobacterial growth. Visual observations and biweekly pH measurements confirmed that cyanobacteria grew from the initial inoculum and photosynthesized throughout the course of all experiments.

3.3.3 Substrate composition and silica concentrations

To gain greater insight into the effects of sediment composition on the mineral coating around cyanobacterial aggregates, cultures were grown on pure quartz sand (purchased from Sigma-Aldrich, St. Louis, MO, USA), glass beads (purchased from Sigma-Aldrich, St. Louis, MO, USA) and no substrate. Results from these experiments were compared with those from Newman et al. (2016), where the authors incubated cyanobacterial cultures on siliciclastic sand and illite powder. Samples were collected for SEM analyses during the first, third and last weeks of cell growth and most experiments were terminated after one month. It is important to note that after 22 days of microbial incubation on glass beads and quartz sand, the pH of the medium rose sharply (>9) and this change in pH may have directly affected the formation of minerals (e.g., $CaCO_3$) around cyanobacterial filaments. Thus, for those experiments we consider data only from the first 22 days of incubation (when the pH of the medium was <9). In a single experiment, cyanobacteria were grown on siliciclastic sand in the presence of high (0.4 mM) and low (0 mM) concentrations of silica for a total of 41 days to investigate changes in the mineral coating of cells over time. Mineral coatings that formed in different experiments were sampled and compared at identical time points, unless otherwise stated.

3.3.4 Organic surfaces

To test the ability of non-microbial organic surfaces to trap and precipitate clay minerals, we incubated sterile cellulose fibers (Kimtech Science Kimwipes, Roswell, GA, USA) in a medium containing high (0.1 mM or 0.4 mM) or low (0 mM) concentrations of silica over 20 g of siliciclastic sand (beach sand, composed of quartz, micas and 0.03% w/w calcium-, iron-, potassium-, magnesium- and/or sodium-rich clay minerals, purchased from the Ottawa Silica

Company, Ottawa, IL, USA). Cellulose fibers were cut into squares (0.5 cm in diameter) and autoclaved at 121°C for 40 min before inoculation. The medium was replaced biweekly and the samples were collected after one month and analyzed by SEM, as described below.

3.3.5 Suspended sediment

We determined the influence of suspended fine particles on the mineral coating of cyanobacterial aggregates during one month of cyanobacterial incubation by altering (i) the amount of clay added to solution and (ii) the fluid agitation in our culture jars. To manipulate clay load, we added varying quantities of illite powder (0, 5.6, and 55.6 mg/L, purchased from Time Laboratories, Pocatello, ID, USA) to the basal medium. In a separate series of experiments, we compared cyanobacteria growing in the absence of mechanical agitation (0 rpm) to those continuously agitated at moderate (150 rpm) and high (170 rpm) rotational speeds using VWR Minishakers with a 15 mm orbital diameter (VWR International, Radnor, PA, USA, Table 3.1; see Supplementary Methods and Supplementary Table 3.1 for fluid velocity calculations). These experiments were performed in the presence of 20 g of siliciclastic sand, in a medium lacking any added silica. This enabled us to focus specifically on the effect of increasing suspended sediment on clay coating, rather than the combined effects of elevated silica concentrations and the increase in suspended clay minerals. In the absence of agitation, microbial aggregates attached to the sediment surface. To facilitate the formation of microbial aggregates and prevent the growth of surface-attached microbial mats, we gently detached cells in these experiments with sterile tweezers. Fluid agitation did not suspend larger sand grains, even though microbial aggregates slowly moved sand grains in more highly agitated cultures by mechanisms described in Mariotti et al. (2014).

The weight of suspended fine particles in each agitation condition was measured by filtering sterile media (90 mL/jar) that had been exposed to 20 g of siliciclastic sand and continuous fluid agitation (0, 150, 170 rpm, VWR Minishakers, 15 mm orbital diameter). These solutions were filtered using pre-weighed, 0.2 μm pore-size PTFE membranes (Millipore, Billerica, MA, USA), and the collected particles were washed with double-distilled water. All membranes were allowed to air-dry at room temperature for one week and weighed to determine the amount of suspended fine particles.

3.3.6 Fossilization of microbial mats

To determine whether clay minerals would coat cyanobacterial filaments forming a microbial mat, we inoculated 5 mL of cells suspended in experimental medium on 450 g of siliciclastic sand in 2 L of sterile medium (3.8 L plastic culture jars, Carolina Biological Supply Company, Burlington, NC, USA). This large volume of medium prevented a rapid increase in pH due to microbial growth. The medium was titrated biweekly (with HCl/NaOH) to maintain a semi-constant pH (ranging from 7 to 9). The cultures were agitated at slow speeds (50 rpm, VWR Minishaker with a 15 mm orbital diameter, VWR International, Radnor PA, USA, Table 3.1) to facilitate the growth of microbial mats and prevent the formation of microbial aggregates (which requires faster agitation, ≥150 rpm). Microbial mats covered the sand surface after 41 days, at which point we added 1 g of illite to the medium. We sampled the cultures on day 0, before the addition of illite (day 41), 5 days after the addition of illite (day 46) and after two months of cell growth (day 60). We did not add any clay to the control and sampled this culture at the same time points.

3.3.7 Concentration of dissolved silica

Concentrations of dissolved silica were measured in 25 mL samples, which were collected at various time points throughout each preservation experiment. The samples were filtered using 60 mL syringes and 0.45 μm filters (VWR, Acrodisc syringe filter) and the filtrates were stored in tightly capped polyethylene containers at −20°C. Silica standards were prepared by diluting a concentrated silica solution (J.T. Baker "DILUT-IT" Silica Standard, original concentration of 16.4 mM) in 0 mM media to create two dilution series: (i) 0.025, 0.05, 0.075, 0.1 and 0.125 mM silica (for 0 and 0.1 mM silica experiments) and (ii) 0.15, 0.3, 0.45, 0.6, 0.75 and 0.9 mM silica (for 0.4 mM silica experiments). The frozen samples were thawed overnight and diluted tenfold in a medium containing 0 mM silica. Concentrations of silica were determined using the methods described in House (1997). Optical densities of standards and samples were measured at 810 nm using a BioTek microplate reader.

3.3.8 Scanning electron microscopy

Cyanobacterial samples were fixed using 2.5% glutaraldehyde in 0.1 M sodium cacodylate buffer with 0.1% $CaCl_2$ at pH 7.4. The fixed samples were incubated overnight at 4°C, washed by three successive, 10 min incubations in 0.2 M sodium cacodylate buffer at 4°C without centrifugation and dehydrated in an ethanol-water drying series (30%, 50%, 70%, 80%, 90%, 100%, 100%) with 20 min steps. Samples were attached to carbon tape and coated by gold and palladium (Keck Facility, Whitehead Institute, MIT, Cambridge, MA, USA) and imaged by a Zeiss Supra Scanning Electron Microscope with an energy-dispersive X-ray spectrometer at 10 kV (Center for Nanoscale Systems, Harvard University, Cambridge, MA, USA) and a secondary electron detector. The elemental compositions of select areas were analyzed using EDS at 10 kV.

3.3.9 Transmission electron microscopy

Samples were fixed in 2.5% glutaraldehyde, 3% paraformaldehyde and 5% sucrose in a 0.1 M sodium cacodylate buffer with a pH of 7.4. Cells were then post-fixed in 1% osmium tetraoxide in a veronal acetate buffer, stained overnight in 0.5% uranyl acetate in veronal acetate buffer (pH = 6.0) and dehydrated in an ethanol–water drying series (50%, 75%, 90%, 95%, 100%, 100%, 100%) with 15 to 20 min steps. Cells were then embedded in Embed 812 resin. Cyanobacterial sections were cut using a diamond knife on a Reichert Ultracut E microtome (with a thickness setting of 50 nm) and were stained with uranyl acetate and lead citrate. Transmission electron microscopy was performed on a FEI Tecnai spirit at 80 KV and images were photographed with an AMT CCD camera (Keck Facility, Whitehead Institute, MIT, Cambridge, MA, USA).

3.3.10 Image processing

We compared the thicknesses of coated and uncoated filamentous cyanobacteria to determine the average thickness of mineral coatings for microbial aggregates and mats (after one month and two months of incubation, respectively). SEM images were imported into Adobe Photoshop CS5 and processed in ImageJ (public domain software program, version 1.41) to determine the relative thicknesses of cyanobacterial filaments (total area divided by width, in μm). Only individual cyanobacterial filaments in the foreground of each image were analyzed because the size and thickness of multifilament masses depended primarily on the total number of filaments, rather than the presence or absence of mineral coatings. Clay minerals were identified (and distinguished from EPS) by their morphology and size (see Results for a description of minerals coating cyanobacteria). Cyanobacterial filaments were extracted from the image using the

polygonal lasso tool and rotated until parallel with the vertical axis. For curved filaments, we divided the entire filament into multiple, rectangular sections and cropped the ends of each filament and/or filament section to ensure a uniform length of analyzed sections. The areas and lengths of these sections were measured in ImageJ. When a single filament was divided into multiple segments, the statistical analyses included only the thickest segment to avoid misrepresenting multiple segments from the same filament as independent samples.

3.3.11 DNA extraction and Illumina sequencing

To characterize the composition of microbial communities, we analyzed four samples: two replicates from cultures used to inoculate fossilization experiments and two samples of experimental cultures grown on siliciclastic sand. Genomic DNA (250 μg per extraction) was extracted using the PowerSoil DNA Isolation Kit (MoBio, Carlsbad, CA, USA) according to the manufacturer's instructions and eluted in 35 μl of elution buffer. Upon extraction, DNA was quantified using NanoDrop (Thermo Scientific, Inc., Wilmington, DE, USA) and sent to Argonne National Laboratories on dry ice. V4 region of the 16S rRNA region (515F-806R) was amplified using the Earth Microbiome Project barcoded primers with Illumina adaptors (Caporaso et al., 2012). PCR products from respective samples were each tagged by a sample-specific 12-base barcode (Caporaso et al., 2012). Briefly, template DNA was amplified using Q5 Hot Start High Fidelity Master Mix (NEB, Ipswich, MA, USA), Forward Primer (200 pM final concentration) and Golay Barcode Tagged Reverse Primer (200 pM final concentration). The conditions for PCR were as follows: denaturing step at 94°C for 3 min, with 35 cycles at 94°C for 45 s, 50°C for 60 s and 72°C for 90 s, with a final extension of 10 min at 72°C. The PCR amplicons were quantified using a plate reader and PicoGreen (Invitrogen, Carlsbad, CA, USA) and pooled in equal concentrations into a single tube. This pool was cleaned up using UltraClean

PCR Cleanup Kit (MoBio, Carlsbad, CA, USA) and quantified using the Qubit (Invitrogen, Carlsbad, CA, USA). Four pM of the pooled samples (with 30% PhiX reference sequences) was sequenced on a MiSeq Illumina sequencer (Illumina, San Diego, CA, USA).

3.4 Results

3.4.1 Microbial diversity

Microscopic observations revealed that sheathed, filamentous cyanobacteria (≥1 μm wide, Fig. 3.1) were abundant in all cultures and under all experimental conditions. Also present were heterocystous cyanobacteria and thinner (<1 μm wide) filamentous cyanobacteria (Fig. 3.1) with thinner or absent sheaths. Cells were surrounded by extracellular polymeric substances (EPS, Fig. 3.1b). The increase in the size of microbial aggregates and the increase in pH after each medium replacement confirmed that cyanobacteria grew and photosynthesized throughout the experiments.

To determine the composition of the bacterial community in microbial aggregates, we sequenced 16S rRNA genes of two samples of the inoculum and two samples harvested from experimental cultures by Illumina sequencing. Cyanobacterial sequences accounted for 50 to 76% of OTUs in all analyzed samples (Fig. 3.2). The remaining OTUs belonged to three additional phyla: *Proteobacteria* (13 to 24%), *Bacteroidetes* (9 to 23%) and *Actinobacteria* (<2%, Fig. 3.2). The most abundant cyanobacterial sequences were those of a single genus, Pseudoanabaenaceae (72 to 75% of all OTUs in the two experimental cultures, Fig. 3.2). These OTUs were most similar to the sequences belonging to the genus *Nodosilinea* characterized as filamentous cyanobacteria with thick sheaths (Perkerson et al., 2011). We attribute these OTUs to the thickly sheathed cyanobacteria observed by microscopy. OTUs from *Leptolyngbya*, *Nostoc*

and two other genera of Pseudoanabaenaceae were present, but much less abundant. *Leptolyngbya*, a filamentous cyanobacterium composed of single, thin trichomes, and generally unsheathed (e.g., Taton et al., 2012) contributed 0.4 to 20% of OTUs. *Nostoc*, a heterocystous cyanobacterium (Potts, 2000), contributed even fewer (0 to 0.2%). The cultures also contained OTUs of Nostocaceae related to *Anabaena*, a cyanobacterium known to form heterocystous cells (Prasanna et al., 2006, 0.1 to 5.9%). Thus, microscopic observations were in general agreement with the molecular diversity of cyanobacteria in the samples.

Alphaproteobacteria related to *Hyphomicrobiaceae, Rhizobiaceae* and *Rhodobacteraceae* and Gammaproteobacteria related to *Chromatiaceae* and HTCC2188 were the major Proteobacteria in the samples. The presence of these OTUs indicated a potential for methylotrophy, nitrogen fixation and anoxygenic photosynthesis in the cultures. The most abundant sequences of *Bacteroidetes* belonged to *Cytophagia* (9 to 22%), supporting the potential for aerobic degradation of polysaccharides and proteins (McBride et al., 2014), including those in cyanobacterial sheaths. Similar proteobacterial communities are also reported in association with some modern marine ooids (O'Reilly et al., 2016), where diatoms are more abundant primary producers than cyanobacteria.

3.4.2 Minerals coating cyanobacterial aggregates

In all experiments, clay minerals coated filamentous cyanobacteria with thick sheaths (likely *Nodosilinea* sp.) and some thin filamentous cyanobacteria (likely *Leptolyngbya* sp.) during the first week of cell growth (Fig. 3.3). Beadlike cyanobacteria, which lacked thick sheaths (likely *Anabaena/Nostoc*), were less frequently coated by minerals (Fig. 3.1f). After 34 days of growth, the coated cyanobacterial filaments were significantly thicker than uncoated filaments (coated:

2.05 ± 0.43 μm, uncoated: 1.63 ± 0.49 μm; *t* test, $t = -3.01$, df = 42, $p < 0.01$), indicating an average coating thickness of 0.42 μm for these experiments. The minerals were present primarily in association with filament sheaths and were typically absent from intercellular spaces (Figs. 3.1f, 3.3b-d), although these spaces contained extracellular polymeric substances (EPS, Fig. 3.1b). Minerals coating cyanobacterial filaments had varying morphologies, ranging from bulky and platy (Fig. 3.1c, d) to smaller and amorphous (Fig. 3.1e). These minerals surrounded the thick filament sheaths, but did not penetrate into the interior of the cells (Fig. 3.4). In fact, some cyanobacterial cells escaped their sheaths, leaving empty, coated sheaths behind (Fig. 3.4c). All these observations support the hypothesis that microbial sheaths play a key role in fossilization.

To further test the role of different organic surfaces in cyanobacterial fossilization on the surfaces of sand and silt, we incubated sterile, hydrophilic cellulose fibers (Kimtech Science Kimwipes, Roswell, GA, USA) on siliciclastic sand in media containing 0, 0.1 or 0.4 mM silica. Although thick coatings developed around cyanobacterial cells after 5 days in the presence of 0.1 mM or 0.4 mM added silica, we did not observe any minerals associated with cellulose fibers even after one month (Fig. 3.5), further emphasizing the importance of microbial surfaces and sheaths in the formation of clay veneers.

To understand the origin of minerals associated with cyanobacterial sheaths, we compared their composition to the composition of the solid substrate. Cyanobacteria in the inoculum contained carbon and oxygen, as well as a few spots with aluminum, sodium and calcium (Fig. 3.6a, b). Cyanobacteria grown on pure quartz were coated extensively by SiO_2 and aluminosilicates, with sporadic spots also containing iron (Fig. 3.6c, d). Cyanobacteria grown on glass beads (composed of sodium, magnesium, silica and calcium) were less extensively coated than in other experiments at similar time points. EDS spectra of cells grown in the presence of

glass beads revealed small peaks of calcium, iron, magnesium, sodium and silica (Fig. 3.6e, f). Together, these elemental analyses reveal a similarity between the composition and morphology of minerals coating cyanobacterial cells and minerals found in the substrates, highlighting the role of sediment trapping. Possible exceptions to this were iron-rich aluminosilicates found in cultures incubated on pure quartz sand and iron-containing minerals coating cells grown on glass beads (Fig. 3.6c, e). These iron-containing minerals lacked equivalents in the solid substrate (Fig. 3.6d, f) and formed by biological precipitation from ions in the medium.

3.4.3 Silica concentrations in solution

We incubated cyanobacteria in solutions containing different concentrations of silica (0 to 0.4 mM) to determine the role of silica in the formation of mineral coatings around cyanobacterial cells. Smoother and more continuous coatings formed around cells grown in media with high concentrations of silica (0.1 and 0.4 mM) compared with cells grown in the silica-free medium (Fig. 3.7, see also Newman et al., 2016 for similar findings). Measurements of dissolved silica concentrations confirmed that these concentrations matched the concentrations of silica in the sterile experimental medium (0, 0.1 or 0.4 mM). Thus, the presence of different solid substrates (e.g., siliciclastic sand, illite powder) did not measurably increase the concentration of silica and experimental media were undersaturated with respect to the precipitation of amorphous silica throughout the experiments.

3.4.4 Suspended sediment

To understand the relationship between suspended fine particles and fossilization, we incubated cyanobacteria in culture jars with different amounts of illite added to the solution (0, 5.6 and 55.6

mg/L) or in the presence of mechanical agitation that can suspend fine sediment (0, 150 or 170 rpm; 15 mm orbital diameter). Smoother, more extensive mineral coating formed in experiments with higher concentrations of fine particles (5.6 and 55.6 mg/L) and faster mechanical agitation (150 and 170 rpm, Fig. 3.7). These experiments also revealed conditions that were able to coat thin filamentous cyanobacteria and heterocystous cells, which lacked thick sheaths (Fig. 3.7). Namely, when 55.6 mg/L of illite was added to the medium or when increased agitation (170 rpm) suspended more clay minerals from the sand, nearly all filaments in the cyanobacterial aggregates had a smooth, thick mineral veneer (~0.5 μm) and minerals were also present in the extracellular spaces between cyanobacterial filaments (Fig. 3.7e, h). Minerals completely enveloped cells within 5 days under these conditions and commonly preserved the shape and texture of individual microbial filaments. Mechanical agitation suspended a measurable quantity of fine particles into solution. As expected, large mechanical disturbances (170 rpm) suspended the greatest amount of fine particles into solution (84 ± 20 mg/L), whereas moderate disturbance (150 rpm) and no motion suspended 14 ± 1 mg/L and 5 ± 3 mg/L of material, respectively. Thus, increased loads of fine particles in suspension promoted the formation of mineral coatings around cyanobacterial cells and the filling of intercellular spaces.

3.4.5 Preservation of microbial mats

Next, we determined whether the same mechanisms were able to preserve surface-attached microbial mats. In the absence of added illite powder, cyanobacterial cells remained effectively uncoated during incubation (60 days, Fig. 3.8a, b, Supplementary Fig. 3.1). In a separate experiment, we added illite powder to the solution above the established mats (after 41 days of microbial growth); the addition of clay mimics conditions expected in natural environments,

where continuous or intermittent waves and currents suspend clay minerals and deliver them to microbial mats. After only 5 days in the presence of added clay (46 days of microbial incubation), we observed that cyanobacterial filaments in mats were covered by a smooth veneer of platy minerals (Fig. 3.8c, d). Minerals were present both around filaments and in intercellular spaces and preserved the shapes of individual cyanobacterial filaments. After 60 days (Fig. 3.8e), cyanobacterial filaments in the mats with added clays were significantly thicker than those in clay-free solutions that were sampled at the same time point (mats with clays: 2.77 ± 1.05 μm, clay-free mats: 1.07 ± 0.26 μm, *t* test, $t = 7.31$, $df = 21$, $p < .01$), indicating that the average coating thickness was 1.70 μm.

3.5 Discussion

3.5.1 Rapid and extensive coating of cyanobacterial filaments by clay minerals

Clay minerals around microbial cells are commonly reported in natural environments and can precipitate in some microbial cultures (e.g., Konhauser et al., 1998; Konhauser and Urrutia, 1999; Phoenix and Konhauser, 2008). These microbe–mineral associations may be beneficial to microbial growth. Firstly, clays have been shown to reduce the negative effects of UV irradiation in bacteria (Bitton et al., 1972) and protect bacteria from environmental toxins by effectively decreasing concentrations of harmful chemical species (Habte and Barrion, 1984; Phoenix and Konhauser, 2008). Additionally, clays and iron-rich phosphates are thought to be important sources of exchangeable nutrients (Stotzky and Rem, 1996; Phoenix and Konhauser, 2008), particularly in nutrient-poor environments (Konhauser and Urrutia, 1999). Cyanobacteria in our study likely experienced similar benefits, but we also note that the complete encrustation of cyanobacteria by minerals (as observed in our suspended sediment experiments, Fig. 3.7) may

have reduced the transport of cellular waste and nutrients and limited the penetration of sunlight. The observed enrichment of thick-sheathed cyanobacteria in our experimental cultures (Fig. 3.2) and the abundance of empty cyanobacterial sheaths (e.g., Fig. 3.4c) suggest that cyanobacteria were able to avoid harmful effects of complete encrustation by escaping from their sheaths into the surrounding medium.

The rapid formation of shape-preserving mineral coating is key to the preservation of microbial fossils in the geologic record. Our experiments demonstrate that clay minerals can coat cyanobacterial cells within weeks, under oxic conditions and without any noticeable interruption to cell growth or photosynthetic abilities. These observations provide additional insight into previous studies which have attributed enhanced microbial preservation to the presence of anoxic conditions where photosynthetic organisms undergo moderate to extreme cell decay (e.g., Callow and Brasier, 2009).

3.5.2 Microbial trapping of sediment and the precipitation of clay minerals

Extracellular polymeric substances (EPS) and sheaths around cyanobacterial filaments have been shown to facilitate the biological flocculation, trapping and precipitation of minerals (e.g., Bar-Or and Shilo, 1988; Phoenix et al., 2000; Chen et al., 2011), especially in carbonate systems (e.g., Merz-Preiß and Riding, 1999; Obst et al., 2009; Zippel and Neu, 2011). EPS are secreted by most cyanobacteria into the surrounding environment (Wingender et al., 1999) and are composed primarily of polysaccharides (Costerton et al., 1981), but also may contain proteins and nucleic acids (Platt et al., 1985; Nielsen et al., 1997; Dignac et al., 1998). In contrast, cyanobacterial sheaths, which are composed of carbohydrates, directly encapsulate microbial cells (Tease and Walker, 1987; Wingender et al., 1999). In our experiments, minerals readily

coated the surfaces of thick cyanobacterial sheaths (e.g., Figs. 3.1 and 3.3), but only filled the intercellular spaces in experiments with the greatest amount of added illite powder and fluid agitation (Fig. 3.7). Minerals may have preferentially coated microbial sheaths due to chemical differences between bacterial sheaths and EPS (e.g., Nicolaus et al., 1999). Alternatively, because the complete encrustation of microbial sheaths occurred over short timescales (i.e., weeks), such rapid and extensive coating may have prevented the subsequent release of EPS into the surrounding environment and thus, hindered the coating of intercellular spaces in most experiments. Regardless, our observations are consistent with reports of commonly and exceptionally preserved cyanobacterial sheaths throughout the geologic record on a wide range of sedimentary surfaces in siliciclastic environments (German and Podkovyrov, 2011; Sergeev et al., 2011; Schopf et al., 2015).

Cyanobacterial sheaths in our experiments are encrusted by aluminum- and iron-rich minerals identical to particles suspended from the underlying siliciclastic sand and illite powder. Previous experiments demonstrated that most of these minerals are trapped from suspension rather than precipitated (Newman et al., 2016). However, similar minerals also occur, albeit less frequently, in the presence of quartz sand and glass beads even though these substrates contain neither iron nor aluminum. This suggests that these iron- and aluminum-rich minerals can also form through precipitation. For this process to occur, sources of aluminum and iron must be present. Although generally considered toxic to cyanobacteria, the accumulation of aluminum has been shown in the cultures of *Anabaena cylindrica* (Pettersson et al., 1986, 1988). Therefore, the accumulation of aluminum and other metals by inoculum cells could have stimulated the subsequent precipitation of minerals in our experiments.

In contrast to aluminum, iron was not detected in cells from the inoculum or in the glass bead and quartz sand substrates. This suggests that iron-rich minerals precipitated around cells from ions present in the medium (Fig. 3.6c, e). Field and laboratory studies of microbe-mineral interactions in iron-rich environments have proposed the essential role of iron in the nucleation and precipitation of aluminosilicates (Ferris et al., 1988; Konhauser et al., 1993; Konhauser, 1997). Although iron-rich aluminosilicates were sometimes present in the coatings around cyanobacteria (Fig. 3.6), these precipitates were not ubiquitous in these experiments, showing that iron is not essential for the formation of mineral coatings around cyanobacterial cells.

3.5.3 A model for microbial preservation and implications for the geologic record

Shales and other rocks composed of fine-grained sediments are typical sources of the best-preserved microbial fossils (e.g., Knoll, 1985; Schieber, 1986; Butterfield et al., 1988). Our experiments investigating the effects of high clay load (e.g., 55.6 mg/L of medium) specifically address conditions that are relevant to fossil preservation in these environments. In contrast, conditions that probe lower clay loads highlight associations between exceptionally preserved microbial fossils and textures, and sandy environments rich in clay and silt (e.g., Hagadorn and Bottjer, 1997; Banerjee and Jeevankumar, 2005; Lan and Chen, 2013; Menon et al., 2015). For example, Banerjee and Jeevankumar (2005) identify a veneer of clay minerals coating the microbially shaped surfaces of a Paleoproterozoic sandstone. Similarly, Hagadorn and Bottjer (1997) report the exceptional preservation of MISS in shallow subtidal to intertidal depositional environments with inferred high concentrations of clay minerals and micas. Our experiments provide a mechanistic explanation for these observations and constrain the amounts of clay and other fine-grained minerals required to preserve microbial textures and fossils. We show that the

trapping and binding of minerals and the microbially mediated mineral precipitation may have promoted the preservation of microbial mats and features on sediment surfaces (e.g., wrinkle structures). The same processes may have also fossilized microbial tubes and sheaths throughout the Proterozoic and early Paleozoic. Moreover, MISS are also expected when microbial particles and mats experience sediment loads larger than 13 mg/L and/or high concentrations of dissolved silica (0.1 to 0.4 mM, Figs. 3.7 and 3.8).

Exceptionally preserved MISS and microbial fossils are frequently preserved in depositional environments characterized by moderate to strong wave and tidal energies (e.g., Gehling, 1999; Noffke et al., 2002; Gehling and Droser, 2009). Tidal currents have been found to play an important role in the formation of modern microbial mats (Cuadrado et al., 2013, 2014), and may also have promoted microbial fossilization in the siliciclastic record. In our study, we find extensive, veneer-forming minerals coating cyanobacteria in cultures exposed to the greatest fluid agitation (170 rpm), which suspended the largest quantity of fine particles (~84 mg/L). However, the positive influence of fluid motion on microbial preservation may be limited; if the wave energy is excessively strong, microbial mats will not be able to grow or can be broken up and completely eroded (Noffke et al., 2002; Bosak et al., 2013; Mariotti et al., 2014). Alternatively, if the environmental disturbances produce and sustain only weak fluid motion, fine particles will not be suspended into solution. Thus, the fossilization of microbial mats on the surfaces of barren, coarse-grained siliciclastic sand may occur as follows: (i) Microbial mats develop in environments characterized by low or moderate wave energies that allow for the initial colonization and growth (approximately one month, Bosak et al., 2013; Mariotti et al., 2014; Fig. 3.9a). (ii) Intermittent storms suspend fine particles in the water column, but do not erode microbial mats. This hydraulic agitation delivers a steady load of fine sediment (Fig. 3.9b).

(iii) Trapped clay minerals promote the coating of microbial filaments and precipitation of authigenic minerals around microbial cells within days to weeks (Fig. 3.9c). Depending on the concentration of suspended clay minerals, this process may take as long as several weeks to completely coat microbial filaments. However, under ideal conditions (e.g., high concentrations of suspended sediment, ~84 mg/L, which is consistent with values for modern shallow water environments, see MacIntyre et al., 1996), microbial mats can become covered by clay minerals in only a few days (Fig. 3.7). This preservation model builds upon previously proposed models (e.g., Noffke et al., 2002), but does not require that mats be buried below layers of light-blocking sediment. Instead, in the presence of moderate and intermittent hydraulic disturbances, the preservation of microbial fossils and mat textures in coarser siliciclastic sediments may merely require the formation of a thin, shape-preserving veneer of clay minerals around living cyanobacteria and growing mats.

3.6 Conclusions

Fossilization of cyanobacteria in coarse-grained siliciclastic sediments requires a synergistic contribution of mineral precipitation and the trapping of fine, suspended particles by filamentous microorganisms. This process can occur within weeks in oxic solutions and creates ~1 μm wide coatings around cyanobacterial sheaths, but does not preserve the interiors of cells. High silica concentrations in solution (0.1 mM), the presence of added clay minerals in the sediment (5.6 to 55.6 mg/L) and fluid agitation (150 to 170 rpm) coat cyanobacteria with the smoothest and most continuous mineral layers. Sticky bacterial sheaths increase the fossilization potential under these conditions and accumulate more minerals than non-microbial organic surfaces, spaces filled with extracellular polymeric substances or unsheathed cyanobacteria. A combination of higher concentrations of oceanic silica, the delivery of clay minerals by waves and currents and the

absence of metazoan grazing and bioturbation may have preserved microbial textures and fossils in subtidal and intertidal siliciclastic environments during the Proterozoic. The same conditions may have been met in more restricted siliciclastic environments after the Cambrian Period.

3.7 References

Banerjee, S., Jeevankumar, S., 2005. Microbially originated wrinkle structures on sandstone and their stratigraphic context: Palaeoproterozoic Koldaha Shale, central India. Sediment. Geol. 176, 211–224. doi:10.1016/j.sedgeo.2004.12.013.

Bar-Or, Y., Shilo, M., 1988. The role of cell-bound flocculants in coflocculation of benthic cyanobacteria with clay particles. FEMS Microbiol. Lett. 53, 169–174. doi:10.1016/0378-1097(88)90439-9.

Bitton, G., Henis, Y., Lahav, N., 1972. Effect of several clay minerals and humic acid on the survival of *Klebsiella aerogenes* exposed to ultraviolet irradiation. Appl. Microbiol. 23, 870-874.

Bosak, T., Knoll, A.H., Petroff, A.P., 2013. The meaning of stromatolites. Annu. Rev. Earth Planet. Sci. 41, 21–44. doi:10.1146/annurev-earth-042711-105327.

Butterfield, N.J., Knoll, A.H., Swett, K., 1988. Exceptional preservation of fossils in an Upper Proterozoic shale. Nature 334, 424–427. doi:10.1038/332141a0.

Byers, C.W., 1983. Geological significance of marine biogenic sedimentary structures, in: McCall, P.L., Tevesz, M.J.S. (Eds.), Animal-Sediment Relations: The Biogenic Alteration of Sediments. Plenum Press, New York, NY, pp. 221–256.

Callow, R.H.T., Brasier, M.D., 2009. Remarkable preservation of microbial mats in Neoproterozoic siliciclastic settings: Implications for Ediacaran taphonomic models. Earth-Science Rev. 96, 207–219. doi:10.1016/j.earscirev.2009.07.002.

Caporaso, J.G., Lauber, C.L., Walters, W.A., Berg-Lyons, D., Huntley, J., Fierer, N., Owens, S.M., Betley, J., Fraser, L., Bauer, M., Gormley, N., Gilbert, J.A., Smith, G., Knight, R., 2012. Ultra-high-throughput microbial community analysis on the Illumina HiSeq and MiSeq platforms. ISME J. 6, 1621–1624. doi:10.1038/ismej.2012.8.

Chen, L., Li, T., Guan, L., Zhou, Y., Li, P., 2011. Flocculating activities of polysaccharides released from the marine mat-forming cyanobacteria *Microcoleus* and *Lyngbya*. Aquat. Biol. 11, 243–248. doi:10.3354/ab00309.

Cohen, P.A., Bradley, A., Knoll, A.H., Grotzinger, J.P., Jensen, S., Abelson, J., Hand, K., Love, G., Metz, J., McLoughlin, N., Meister, P., Shepard, R., Tice, M., Wilson, J.P., 2009. Tubular

compression fossils from the Ediacaran Nama Group, Namibia. J. Paleontol. 83, 110–122. doi:10.1666/09-040R.1.

Costerton, J., Irvin, R., Cheng, K., 1981. The bacterial glycocalyx in nature and disease. Annu. Rev. Microbiol. 35, 299–324. doi:10.1146/annurev.mi.35.100181.001503.

Cuadrado, D.G., Bournod, C.N., Pan, J., Carmona, N.B., 2013. Microbially-induced sedimentary structures (MISS) as record of storm action in supratidal modern estuarine setting. Sediment. Geol. 296, 1–8. doi:10.1016/j.sedgeo.2013.07.006.

Cuadrado, D.G., Perillo, G.M.E., Vitale, A.J., 2014. Modern microbial mats in siliciclastic tidal flats: Evolution, structure and the role of hydrodynamics. Mar. Geol. 352, 367–380. doi:10.1016/j.margeo.2013.10.002.

Davies, N.S., Liu, A.G., Gibling, M.R., Miller, R.F., 2016. Resolving MISS conceptions and misconceptions: A geological approach to sedimentary surface textures generated by microbial and abiotic processes. Earth-Science Rev. 154, 210–246. doi:10.1016/j.earscirev.2016.01.005.

Dignac, M.-F., Urbain, V., Rybacki, D., Bruchet, A., Snidaro, D., Scribe, P., 1998. Chemical description of extracellular polymers: Implication on activated sludge floc structure. Water Sci. Technol. 38, 45–53.

Ferris, F.G., Fyfe, W.S., Beveridge, T.J., 1988. Metallic ion binding by *Bacillus subtilis*: Implications for the fossilization of microorganisms. Geology 16, 149-152. doi:10.1130/0091-7613(1988)016<0149.

Gehling, J.G., 1999. Microbial mats in terminal Proterozoic siliciclastics: Ediacaran death masks. Palaios 14, 40–57. doi:10.2307/3515360.

Gehling, J.G., Droser, M.L., 2009. Textured organic surfaces associated with the Ediacara biota in South Australia. Earth-Science Rev. 96, 196–206. doi:10.1016/j.earscirev.2009.03.002.

German, T.N., Podkovyrov, V.N., 2011. The role of cyanobacteria in the assemblage of the Lakhanda Microbiota. Paleontol. J. 45, 320–332. doi:10.1134/s0031030111020079.

Habte, M., Barrion, M., 1984. Interaction of Rhizobium sp. with toxin-producing fungus in culture medium and in a tropical soil. Appl. Environ. Microbiol. 47, 1080–1083.

Hagadorn, J.W., Bottjer, D.J., 1997. Wrinkle structures: Microbially mediated sedimentary structures common in subtidal siliciclastic settings at the Proterozoic-Phanerozoic transition. Geology 25, 1047–1050.

House, F., 1997. The determination of reactive silica in seawater, in: BATS Methods. Bermuda Biological Station for Research, Inc., pp. 75–79.

Knoll, A.H., Kotrc, B., 2015. Protistan Skeletons: A Geologic History of Evolution and Constraints, in: Hamm, C. (Ed.), Evolution of Lightweight Structures. Springer, New York, NY, pp. 1–16. doi:10.1007/978-94-017-9398-8.

Knoll, A.H., 1985. The distribution and evolution of microbial life in the Late Proterozoic Era. Annu. Rev. Microbiol. 39, 391–417. doi:10.1146/annurev.mi.39.100185.002135.

Konhauser, K., 1997. Bacterial iron biomineralization in nature. FEMS Microbiol. Rev. 20, 315–326. doi:10.1016/S0168-6445(97)00014-4.

Konhauser, K.O., Fisher, Q.J., Fyfe, W.S., Longstaffe, F.J., Powell, M.A., 1998. Authigenic mineralization and detrital clay binding by freshwater biofilms: The Brahmani river, India. Geomicrobiol. J. 15, 209–222. doi:10.1080/01490459809378077.

Konhauser, K.O., Fyfe, W.S., Ferris, F.G., Beveridge, T.J., 1993. Metal sorption and mineral precipitation by bacteria in two Amazonian river systems: Rio Solimoes and Rio Negro, Brazil. Geology 21, 1103–1106.

Konhauser, K.O., Urrutia, M.M., 1999. Bacterial clay authigenesis: A common biogeochemical process. Chem. Geol. 161, 399–413. doi:10.1016/S0009-2541(99)00118-7.

Lan, Z.W., Chen, Z.Q., 2013. Proliferation of MISS-forming microbial mats after the late Neoproterozoic glaciations: Evidence from the Kimberley region, NW Australia. Precambrian Res. 224, 529–550. doi:10.1016/j.precamres.2012.11.008.

MacIntyre, H.L., Geider, R.J., Miller, D.C., 1996. Microphytobenthos: The ecological role of the "secret garden" of unvegetated, shallow-water marine habitats. II. Role in sediment stability and shallow-water food webs. Estuaries 19, 202. doi:10.2307/1352225.

Maliva, R.G., Knoll, A.H., Siever, R., 1989. Secular change in chert distribution: A reflection of evolving biological participation in the silica cycle. Palaios 4, 519–532. doi:10.2307/3514743.

Mariotti, G., Pruss, S.B., Perron, J.T., Bosak, T., 2014. Microbial shaping of sedimentary wrinkle structures. Nat. Geosci. 7, 736–740. doi:10.1038/ngeo2229.

McBride, M.J., Lu, X., Zhu, Y., Zhang, W., 2014. The family Cytophagaceae, in: Rosenberg, E., DeLong, E.F., Lory, S., Stackenbrandt, E., Thompson, F. (Eds.), The Prokaryotes - Other Major Lineages of Bacteria and the Archaea. Springer, Berlin Heidelberg, pp. 577–593. doi:10.1007/0-387-30743-5.

Menon, L.R., McIlroy, D., Liu, A.G., Brasier, M.D., 2015. The dynamic influence of microbial mats on sediments: Fluid escape and pseudofossil formation in the Ediacaran Longmyndian Supergroup, UK. J. Geol. Soc. London. 173, 177–185. doi:10.1144/jgs2015-036.

Merz-Preiß, M., Riding, R., 1999. Cyanobacterial tufa calcification in two freshwater streams: Ambient environment, chemical thresholds and biological processes. Sediment. Geol. 126, 103–124. doi:10.1016/S0037-0738(99)00035-4.

Moczydłowska, M., 2008. New records of late Ediacaran microbiota from Poland. Precambrian Res. 167, 71–92.

Newman, S.A., Mariotti, G., Pruss, S., Bosak, T., 2016. Insights into cyanobacterial fossilization in Ediacaran siliciclastic environments. Geology 44, 579–582. doi: 10.1130/G37791.1.

Nicolaus, B., Panico, A., Lama, L., Romano, I., Manca, M.C., De Giulio, A., Gambacorta, A., 1999. Chemical composition and production of exopolysaccharides from representative members of heterocystous and non-heterocystous cyanobacteria. Phytochemistry 52, 639–647. doi:10.1016/S0031-9422(99)00202-2.

Nielsen, P.H., Jahn, A., Palmgren, R. 1997. Conceptual model for production and composition of exopolymers in biofilms. Water Sci. Technol. 36, 11–19. doi:10.1016/S0273-1223(97)00318-1.

Noffke, N., 2007. Microbially induced sedimentary structures in Archean sandstones: A new window into early life. Gondwana Res. 11, 336–342. doi:10.1016/j.gr.2006.10.004.

Noffke, N., Eriksson, K.A., Hazen, R.M., Simpson, E.L., 2006. A new window into Early Archean life: Microbial mats in Earth's oldest siliciclastic tidal deposits (3.2 Ga Moodies Group, South Africa). Geology 34, 253–256. doi:10.1130/G22246.1.

Noffke, N., Gerdes, G., Klenke, T., Krumbein, W., 2001. Microbially induced sedimentary structures — A new category within the classification of primary sedimentary structures. J. Sediment. Res. 71, 649–656.

Noffke, N., Hazen, R., Nhelko, N., 2003. Earth's earliest microbial mats in a siliciclastic marine environment (2.9 Ga Mozaan Group, South Africa). Geol. Soc. Am. 31, 673–676. doi:10.1130/G19704.1.

Noffke, N., Knoll, A.H., Grotzinger, J.P., 2002. Sedimentary controls on the formation and preservation of microbial mats in siliciclastic deposits: A case study from the upper Neoproterozoic Nama Group, Namibia. Palaios 17, 533–544. doi:10.1669/0883-1351(2002)017<0533:SCOTFA>2.0.CO;2.

O'Reilly, S., Mariotti, G., Winter, A., Newman, S., Matys, E., McDermott, F., Pruss, S., Bosak, T., Summons, R., Klepac-Ceraj, V., 2016. Molecular biosignatures reveal common benthic microbial sources of organic matter in ooids and grapestones from Pigeon Cay, the Bahamas. Geobiology 15, 112–130. doi:10.1111/gbi.12196.

Obst, M., Dynes, J.J., Lawrence, J.R., Swerhone, G.D.W., Benzerara, K., Karunakaran, C., Kaznatcheev, K., Tyliszczak, T., Hitchcock, A.P., 2009. Precipitation of amorphous $CaCO_3$ (aragonite-like) by cyanobacteria: A STXM study of the influence of EPS on the nucleation process. Geochim. Cosmochim. Acta 73, 4180–4198. doi:10.1016/j.gca.2009.04.013.

Perkerson, R.B., Johansen, J.R., Kovácik, L., Brand, J., Kaštovský, J., Casamatta, D.A., 2011. A unique pseudanabaenalean (cyanobacteria) genus *Nodosilinea* gen. nov. based on morphological and molecular data. J. Phycol. 47, 1397–1412. doi:10.1111/j.1529-8817.2011.01077.x.

Pettersson, A., Hällbom, L., Bergman, B., 1988. Aluminum effects on uptake and metabolism of phosphorus by the cyanobacterium *Anabaena cylindrica*. Physiol. Plant. 86, 112–116.

Pettersson, A., Hällbom, L., Bergman, B., 1986. Aluminium uptake by *Anabaena cylindrica*. J. Gen. Microbiol. 132, 1771–1774.

Pflüger, F., Gresse, P.G., 1996. Microbial sand chips—a non-actualistic sedimentary structure. Sediment. Geol. 102, 263–274. doi:10.1016/0037-0738(95)00072-0.

Phoenix, V.R., Adams, D.G., Konhauser, K.O., 2000. Cyanobacterial viability during hydrothermal biomineralization. Chem. Geol. 169, 329–338. doi:10.1016/S0009-2541(00)00212-6.

Phoenix, V.R., Konhauser, K.O., 2008. Benefits of bacterial biomineralization. Geobiology 6, 303–308. doi:10.1111/j.1472-4669.2008.00147.x.

Platt, R.M., Geesey, G.G., Davis, J.D., White, D.C., 1985. Isolation and partial chemical analysis of firmly bound exopolysaccharide from adherent cells of a freshwater sediment bacterium. Can. J. Microbiol. 31, 675–680.

Prasanna, R., Kumar, R., Sood, A., Prasanna, B.M., Singh, P.K., 2006. Morphological, physiochemical and molecular characterization of *Anabaena* strains. Microbiol. Res. 161, 187–202. doi:10.1016/j.micres.2005.08.001.

Pruss, S., Fraiser, M., Bottjer, D.J., 2004. Proliferation of Early Triassic wrinkle structures: Implications for environmental stress following the end-Permian mass extinction. Geology 32, 461. doi:10.1130/G20354.1.

Schieber, J., 1986. The possible role of benthic microbial mats during the formation of carbonaceous shales in shallow Mid-Proterozoic basins. Sedimentology 33, 521–536. doi:10.1111/j.1365-3091.1986.tb00758.x.

Schieber, J., Bose, P., Eriksson, P., Banerjee, S., Sarkar, S., Altermann, W., Catuneau, O., 2007. Atlas of Microbial Mat Features Preserved within the Siliciclastic Rock Record. Elsevier, Amsterdam.

Schopf, J.W., Sergeev, V.N., Kudryavtsev, A.B., 2015. A new approach to ancient microorganisms: Taxonomy, paleoecology, and biostratigraphy of the Lower Cambrian Berkuta and Chulaktau microbiotas of South Kazakhstan. J. Paleontol. 89, 695–729. doi:10.1017/jpa.2015.56.

Seilacher, A., Pflüger, F., 1994. From Biomats to Benthic Agriculture: A Biohistoric Revolution, in: Krumbein, W.E., Paterson, D.M., Stal, L.J. (Eds.), Biostabalization of Sediments. Bibliotheks - und Informationssystem der Universitat Oldenburg, Oldenburg, Germany, pp. 97–105.

Sergeev, V.N., Knoll, A.H., Vorob'Eva, N.G., 2011. Ediacaran microfossils from the Ura Formation, Baikal-Patom Uplift, Siberia: Taxonomy and biostratigraphic significance. J. Paleontol. 85, 987–1011. doi:10.1666/11-022.1.

Siever, R., 1957. The silica budget in the sedimentary cycle. Am. Mineral. 42, 821–841.

Stotzky, G., Rem, L.T., 1996. Influence of clay minerals on microorganisms: I. Montmorillonite and kaolinite on bacteria. Can. J. Microbiol. 12, 547–563.

Taton, A., Lis, E., Adin, D.M., Dong, G., Cookson, S., Kay, S.A., Golden, S.S., Golden, J.W., 2012. Gene transfer in *Leptolyngbya* sp. strain BL0902, a cyanobacterium suitable for production of biomass and bioproducts. PLoS One 7, 1–15. doi:10.1371/journal.pone.0030901.

Tease, B.E., Walker, R.W., 1987. Comparative composition of the sheath of the cyanobacterium *Gloeothece* ATCC 27152 cultured with and without combined nitrogen. J. Gen. Microbiol. 133, 3331–3339. doi:10.1099/00221287-133-12-3331.

Vidal, G., Moczydowska, M., 1992. Patterns of phytoplankton radiation across the Precambrian-Cambrian boundary. J. Geol. Soc. London. 149, 647–654. doi:10.1144/gsjgs.149.4.0647.

Wingender, J., Neu, T.R., Flemming, H.-C., 1999. What are bacterial extracellular polymeric substances?, in: Wingender, J., Neu, T.R., Flemming, H.-C. (Eds.), Microbial Extracellular Polymeric Substances. Springer-Verlag, Berlin Heidelberg, pp. 1–19.

Zippel, B., Neu, T.R., 2011. Characterization of glycoconjugates of extracellular polymeric substances in tufa-associated biofilms by using fluorescence lectin-binding analysis. Appl. Environ. Microbiol. 77, 505–516. doi:10.1128/AEM.01660-10.

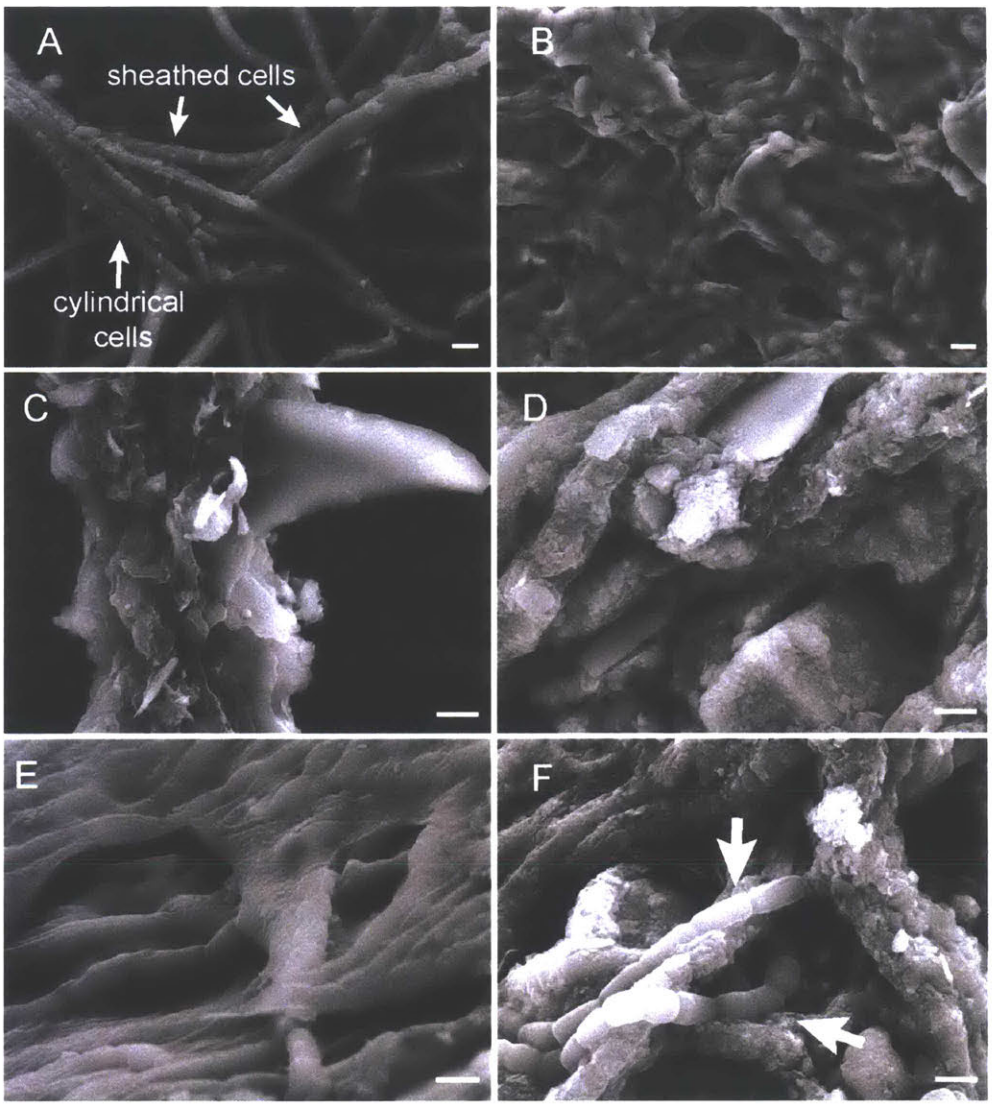

Fig. 3.1. Representative SEM images showing the morphological diversity of cyanobacteria and mineral coatings. A and B) Cyanobacterial cells in the inoculum (day 0). The cells are not coated by clay minerals. A) Thick filamentous cyanobacteria with sheaths (≥1 μm wide, likely *Nodosilinea*), thin filamentous cyanobacteria (<1 μm wide, likely *Leptolyngbya*) and unsheathed or thinly sheathed cyanobacteria with cylindrical cells (likely Nostoc/Anabaena). B) Extracellular polymeric substances (EPS) surround cells in the inoculum. C-E) Thick filaments (≥1 μm wide) are coated by minerals. (c) Bulky minerals coat cyanobacterial filaments incubated on siliciclastic sand and agitated at 150 rpm (41 days of incubation). D) Platy minerals coat filaments incubated on illite powder and agitated at 150 rpm (15 days of incubation). E) Smooth, extensive mineral coating encrusts filaments incubated on siliciclastic sand and agitated at 170 rpm (15 days of incubation). The entire surface is covered by small (<0.2 μm wide) mineral grains. F) Unsheathed filaments with cylindrical cells (white arrows) remain uncoated after 15 days of microbial growth (agitated at 170 rpm on illite powder). All cultures were agitated on VWR Minishakers with 15 mm orbital diameters (VWR International, Radnor, PA, USA). Scale bar: A and B = 2 μm, C–F= 1 μm.

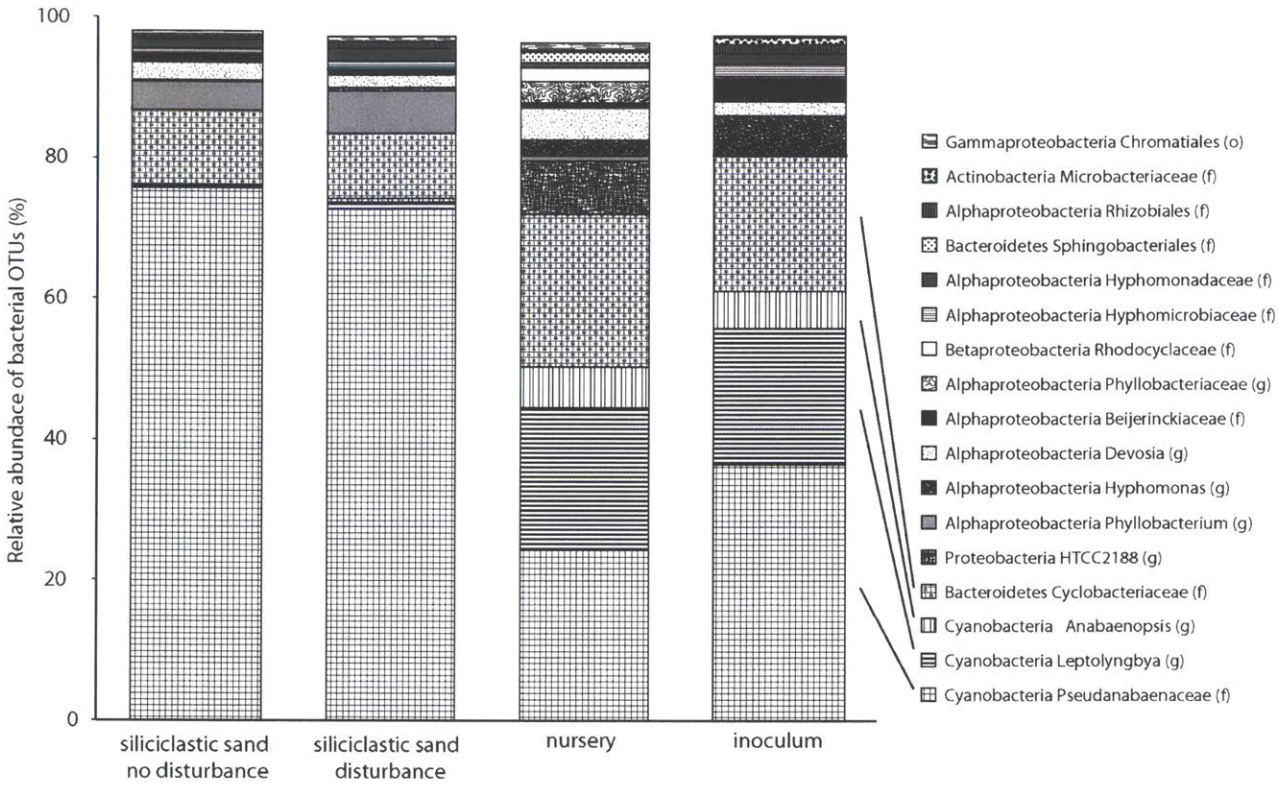

Fig. 3.2. Microbial diversity of bacteria in experimental cultures and inoculum. 16S rRNA genes were sequenced by Illumina sequencing. Experimental cultures incubated in the medium without added silica (1. no agitation and 2. moderate agitation, 150 rpm, 15 mm orbital diameter) are compared to the inoculum (two replicates). *Nodosilinea*, *Leptolyngbya* and *Anabaena* were the most frequently represented cyanobacterial genera by OTU.

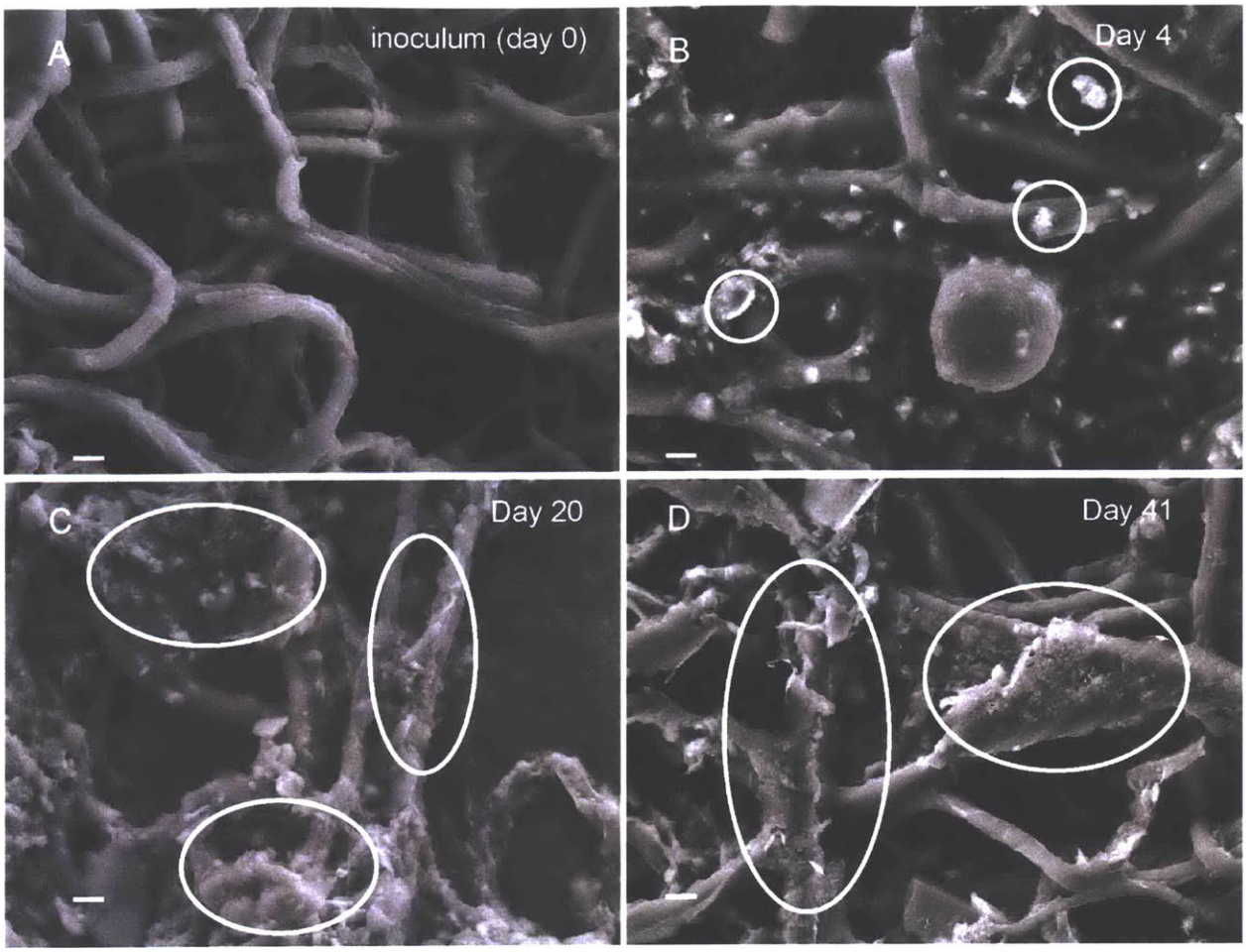

Fig. 3.3. Representative SEM images of cyanobacteria grown on silica sand after A) 0 days, B) 4 days, C) 20 days and D) 41 days. The extent of mineral coverage and smoothness of coatings increases during the first three weeks. Circles denote areas of extensive mineral coverage around cyanobacterial filaments. Scale bar = 2 μm.

.

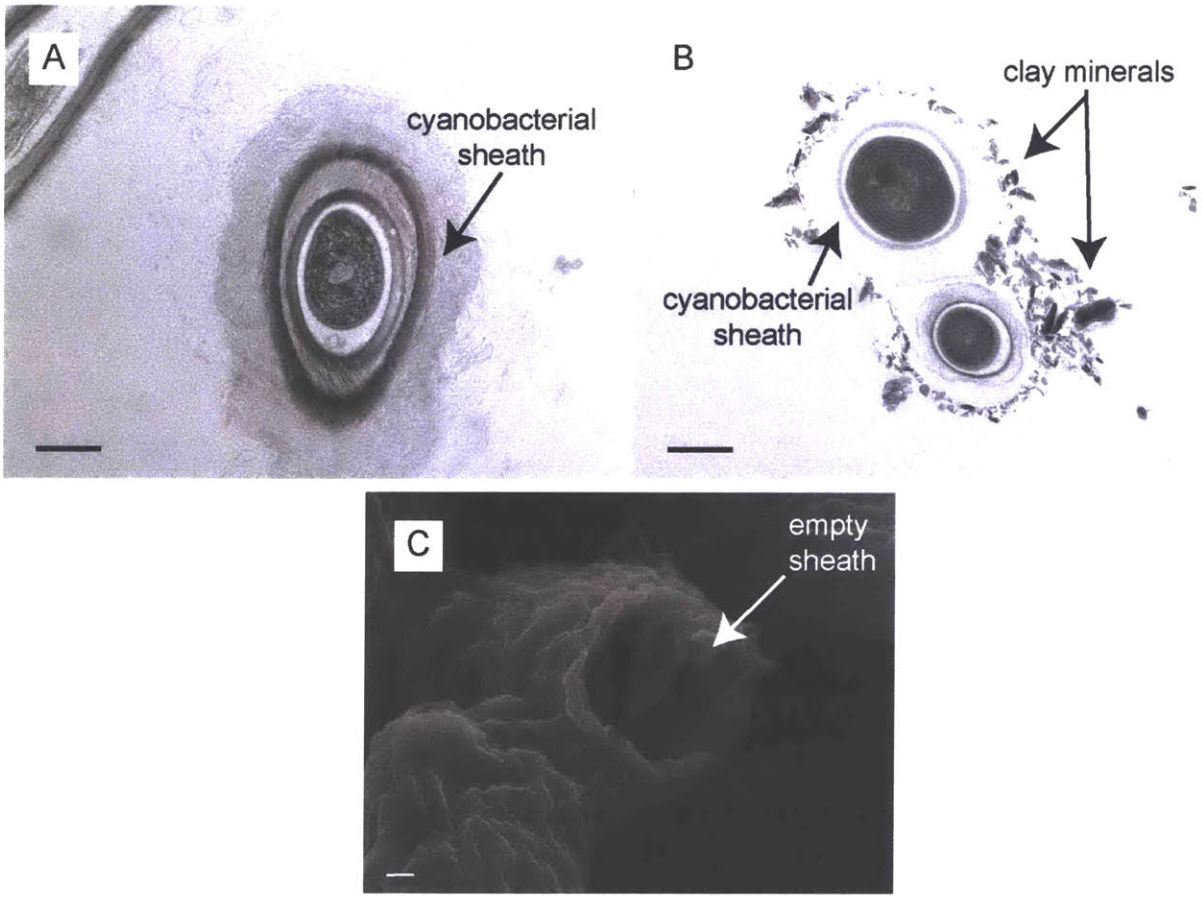

Fig. 3.4. Electron microscopy images of cyanobacterial sheaths. A and B): Transmission electron microscopy (TEM) images of cyanobacterial cells grown in the presence of 5.6 mg of illite powder/L of medium. A) Inoculum cells are not coated in clay minerals (day 0). Fibrous material around the cells is the sheath, which is at least as thick as the cell itself. B) After 15 days of growth on illite powder, cyanobacterial cells are encrusted by small clay grains. Minerals do not penetrate into the interiors of the cells, but instead coat the sheaths. C) SEM image of an empty cyanobacterial sheath (cell culture grown on glass beads for 15 days). Scale bar: A and B = 800 nm, C = 200 nm.

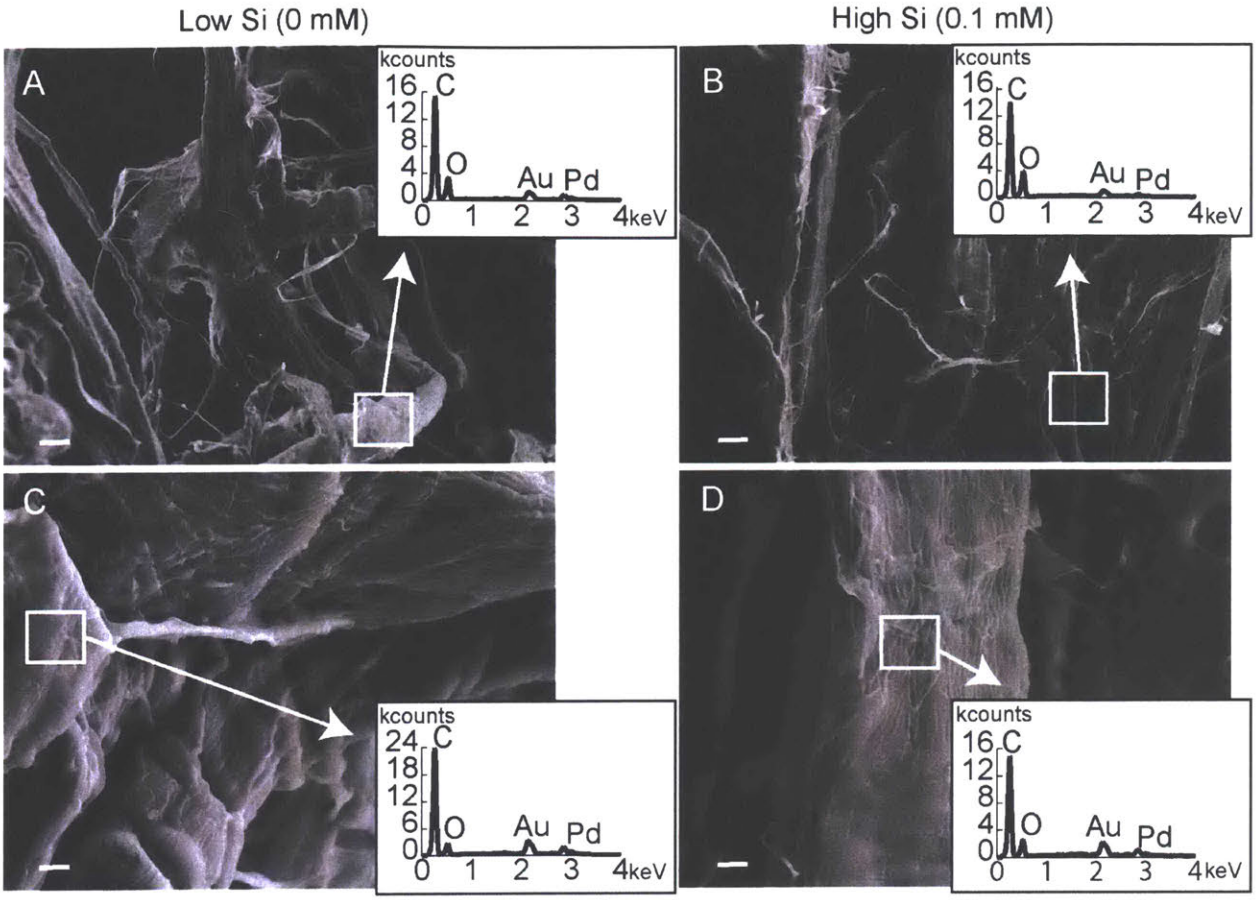

Fig. 3.5. Representative SEM images and EDS spectra showing the absence of mineral coating around cellulose fibers incubated in media with low (0 mM) and high (0.1 mM) silica in the presence of silica sand. A) and C) cellulose fibers in the medium containing 0 mM silica after 15 days. B) and D) cellulose fibers in the medium containing 0.1 mM silica after 15 days. Squares denote areas analyzed by EDS. Scale bar: A and B = 10 μm; C and D = 2 μm.

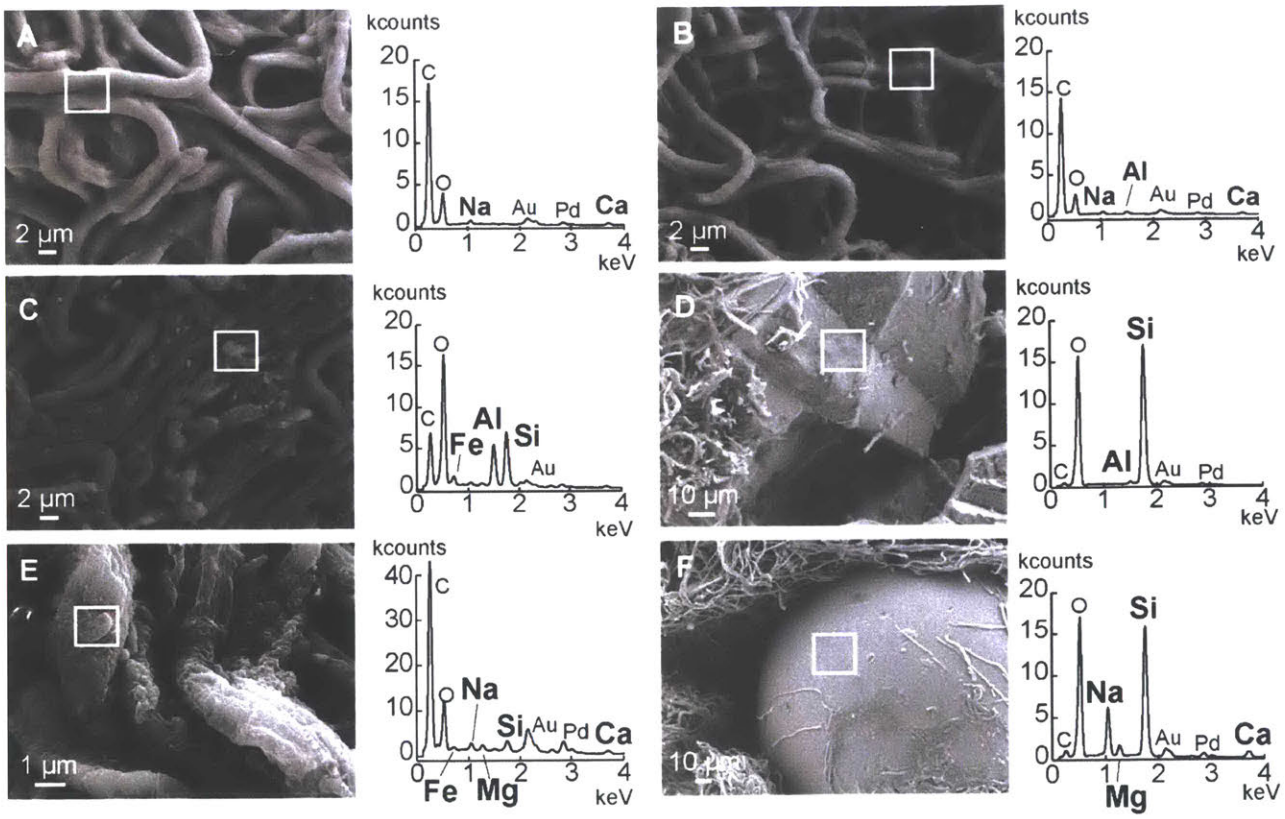

Fig. 3.6. Representative SEM images and EDS spectra of coated cyanobacteria and corresponding solid substrates. A and B) inoculum that was not exposed to any minerals (day 0). C) Cyanobacteria grown on a pure quartz substrate (after 14 days of incubation) and D) close-up of quartz grain. E) Cyanobacteria grown on glass beads (after 14 days of incubation) and F) close-up of a single glass bead. Square boxes indicate areas analyzed by EDS. Quartz substrate and glass beads were purchased from Sigma–Aldrich (St. Louis, MO, USA).

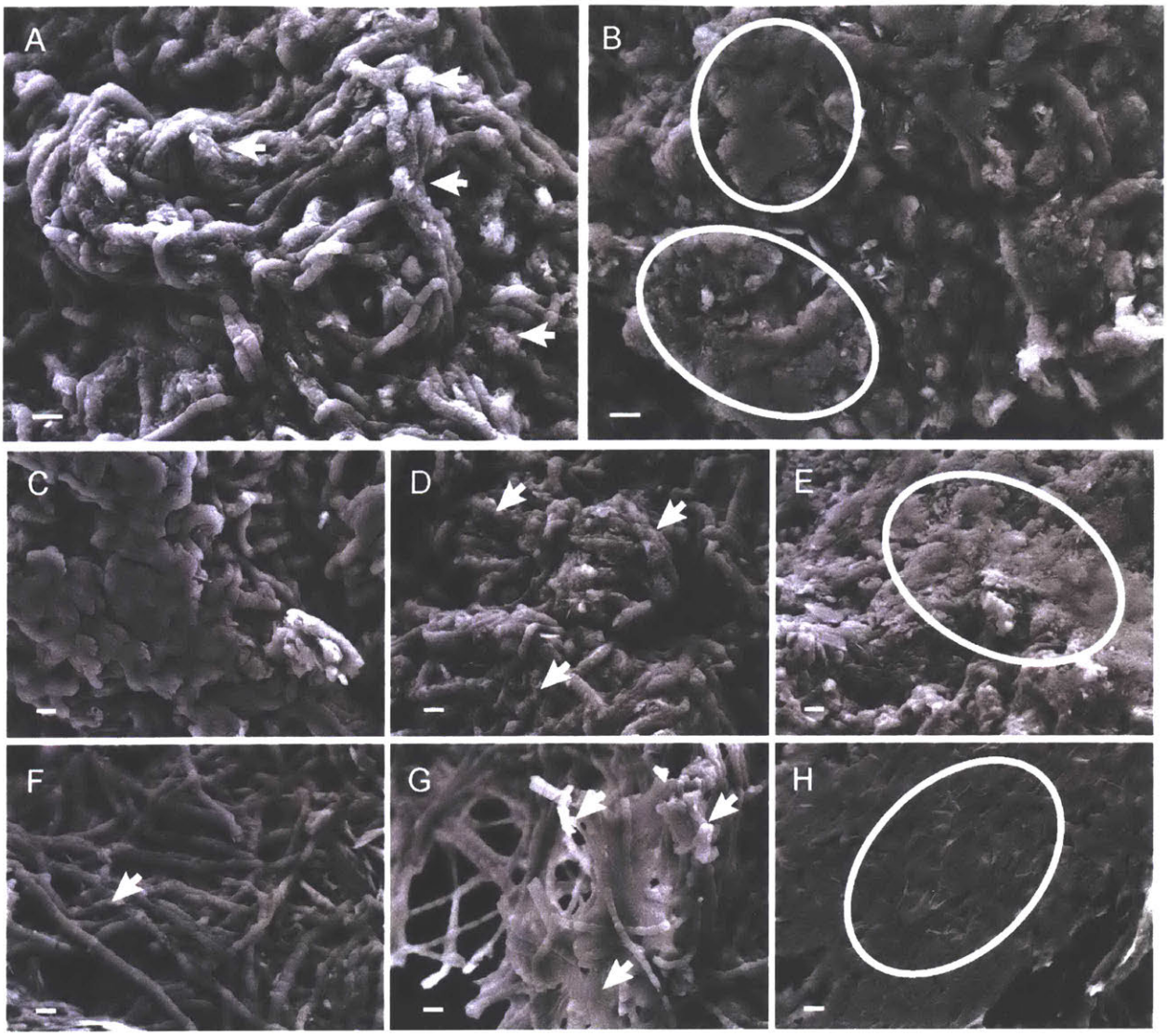

Fig. 3.7. Representative SEM images showing the mineral coating of cyanobacteria with varying concentrations of silica (0–0.1 mM), clay added to solution (0–55.6 mg/L medium), and mechanical disturbance (0–170 rpm, 15 mm orbital diameter) after 15 days of incubation. Variations in silica concentrations: A) cyanobacteria grown in the presence of low silica concentrations (0 mM) on powdered illite and B) cyanobacteria grown in the presence of high silica concentrations (0.1 mM) on powdered illite. Variations in clay added to solution: C) cyanobacteria grown without a solid substrate, D) cyanobacteria grown with 5.6 mg of illite powder/L of medium and E) cyanobacteria grown with 55.6 mg of illite powder/L of medium. Variations in mechanical disturbance: F) cyanobacteria grown without any agitation, G) moderate agitation (150 rpm) and H) high agitation (170 rpm) on silica sand. Circles denote areas of extensive mineral coverage of cyanobacterial filaments; arrows denote minimal and/or localized mineral coverage. Scale bar = 1 μm.

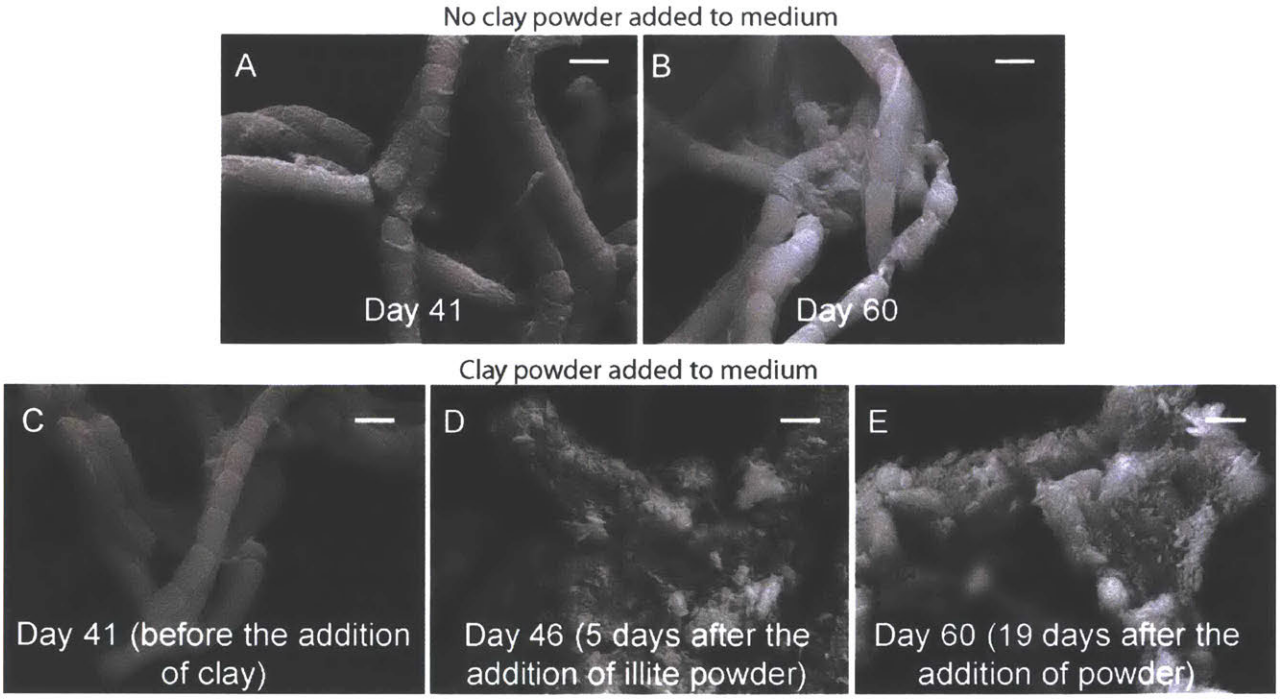

Fig. 3.8. Representative SEM images of cyanobacterial mats grown on silica sand. A) Cells growing without illite remain uncoated after 41 days and B) 60 days of growth. C) Mat growth after 41 days, immediately before the addition of 1 g illite. D) Mats coated in clay minerals 5 days after the addition of illite and E) coated mats after 60 days of microbial growth. Scale bar = 1 μm.

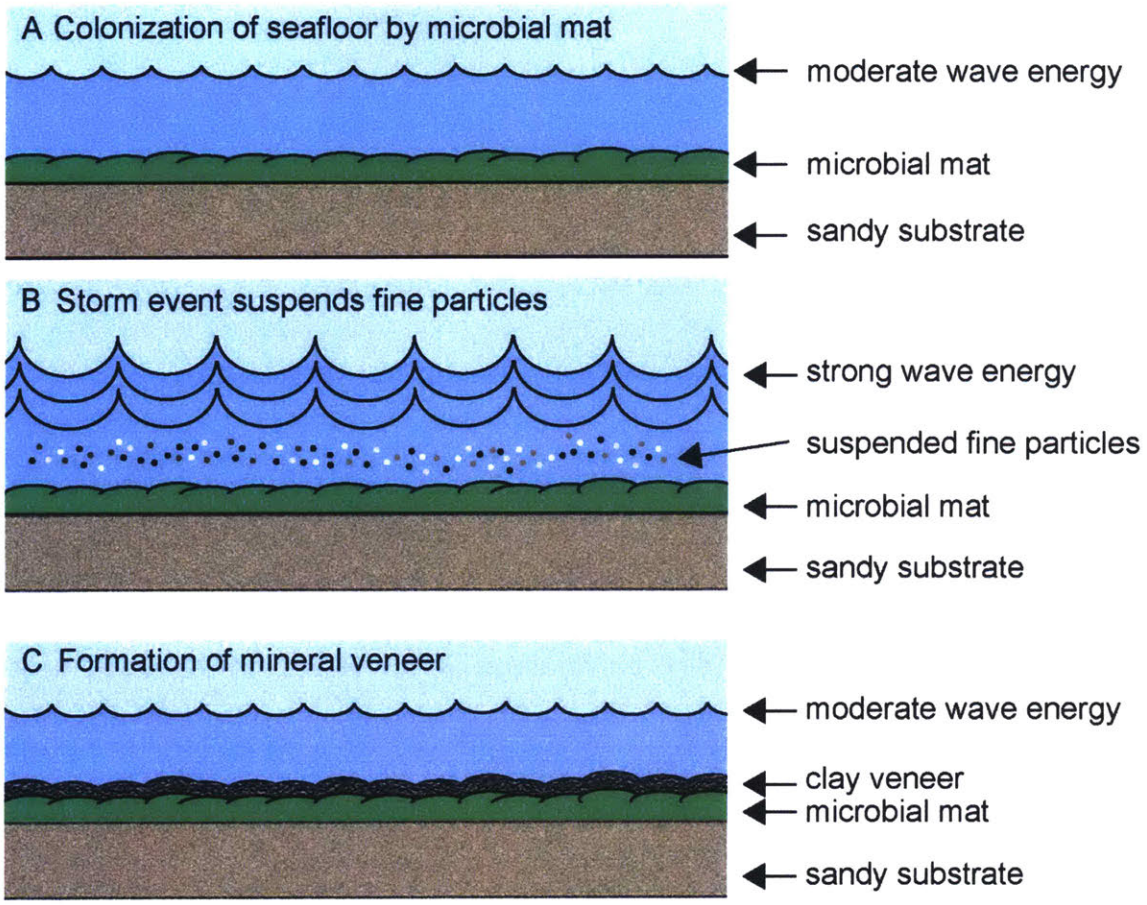

Fig. 3.9. Model of microbial mat preservation in sandy, marine environments. A) Microbial mat colonizes marine environments with low to moderate wave energies. B) Intermittent storms suspend fine particles into solution, but do not erode the microbial mat. C) Fine particles are biologically trapped by the microbial mat, which promotes the precipitation of authigenic minerals. A mineral veneer is formed in days to weeks.

Table 3.1. List of experiments.

Substrate	Amount of substrate added to culture jar (g)	Silica concentration of basal media (mM)	Organic material	Rotations per minute (rpm)
Silica sand	20.0	0.0, 0.1 or 0.4	cyanobacterial aggregates	190*
Silica sand	20.0	0.0, 0.1 or 0.4	cellulose fibers	190*
Quartz sand	~20.0	0.0	cyanobacterial aggregates	190*
Glass beads	~20.0	0.0	cyanobacterial aggregates	190*
Illite	0.0	0.0 or 0.1	cyanobacterial aggregates	190*
Illite	0.0005	0.0 or 0.1	cyanobacterial aggregates	190*
Illite	0.005	0.0 or 0.1	cyanobacterial aggregates	190*
Silica sand	20.0	0.0	cyanobacterial aggregates	0**
Silica sand	20.0	0.0	cyanobacterial aggregates	150**
Silica sand	20.0	0.0	cyanobacterial aggregates	170**
Silica sand	450.0	0.1	cyanobacterial mat	50**

*VWR Minishaker (VWR International, Radnor, PA, USA), 3 mm orbital diameter.
**VWR Minishaker (VWR International, Radnor, PA, USA), 15 mm orbital diameter.

3.8 Supplementary Information

Supplementary Methods: Calculation of fluid velocity for a comparison of agitation across experiments

Cyanobacteria were continuously submerged and agitated on a VWR Minishaker with a 3 or 15 mm orbital diameter (VWR International, Radnor, PA, USA). The orbital motion of the shaker produced a rotating surface wave within the jar, with a highly complex associated flow (Salek *et al.*, 2011). Visual observations suggest that the horizontal motion of the shaker excited the first mode of the wave, which is characterized by the lowest period among all the possible modes (Reclari, 2013; Reclari *et al.* 2014). Assuming that the rotating wave is linear, i.e., the wave height is smaller than the wavelength, and that the orbital motion of the shaker is small compared to the fluid orbital motion associated with the wave, the maximum tangential velocity over a wave cycle calculated near the bed at the most outward position in the jar reads

$$U_m = \frac{gHT}{2\pi D cosh(2\varepsilon_{11}h/D)} \quad ,$$

where g is the gravitational acceleration, T is the oscillation period, calculated from the dispersion relationship as $2\pi / \sqrt{\frac{2g}{D} tanh(2\varepsilon_{11}h/D)}$, h is the still water depth, D is the jar diameter, H is the crest-to-trough wave height, which was directly measured with a ruler on the side of the jar and ε_{11} is the first root of the derivative of the Bessel function of the first kind, which has an approximate value of 1.841 (Reclari, 2013). This formula, despite being approximated, gives a robust prediction that allows for a comparison of the intensity of the near bed flow across different experiments (Supplementary Table 3.1).

References

Reclari, M. 2013. Hydrodynamics of orbital shaken bioreactors. PhD Thesis, Department of Mechanics, École Polytechnique Fédérale de Lausanne, Lausanne, Switzerland.

Reclari, M., Dreyer, M., Tissot, S., Obreschkow, D., Wurm, F.M., Farhat, M., 2014. Surface wave dynamics in orbital shaken cylindrical containers. Phys. Fluids 26, 1–19. doi:10.1063/1.4874612.

Salek, M.M., Sattari, P., Martinuzzi, R.J., 2012. Analysis of fluid flow and wall shear stress patterns inside partially filled agitated culture well plates. Ann. Biomed. Eng. 40, 707–728. doi:10.1007/s10439-011-0444-9.

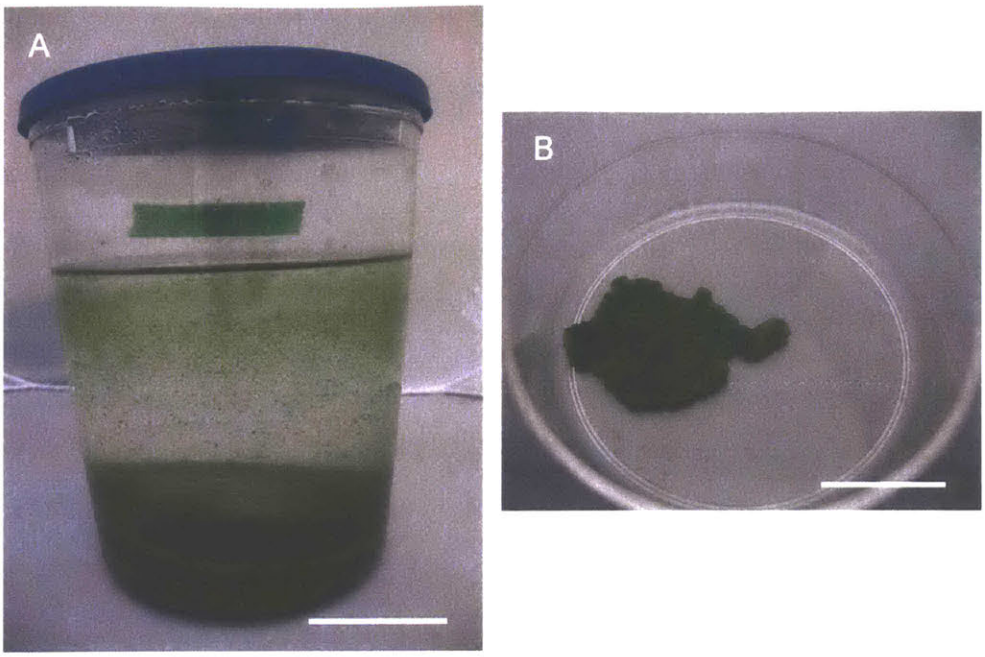

Supplementary Fig. 3.1. Microbial mat grown over silica sand. A) Microbial mat incubated for 60 days. B) Close-up of a piece of microbial mat. Scale bar = 8 cm (A) and 1.4 cm (B).

Supplementary Table 3.1. Calculated fluid velocity for each experiment

Substrate	Silica concentration of basal media (mM)	Organic material	Depth of medium in culture jar (cm)	Wave height due to agitation (cm)	Fluid velocity (cm/s)
Silica sand	0.0, 0.1 or 0.4	cyanobacterial aggregates	2.5	0.7	3.1*
Silica sand	0.0, 0.1 or 0.4	cellulose fibers	2.5	0.7	3.1*
Quartz sand	0.0	cyanobacterial aggregates	2.5	0.7	3.1*
Glass beads	0.0	cyanobacterial aggregates	2.5	0.7	3.1*
Illite	0.0 or 0.1	cyanobacterial aggregates	2.5	0.7	3.1*
Illite	0.0 or 0.1	cyanobacterial aggregates	2.5	0.7	3.1*
Illite	0.0 or 0.1	cyanobacterial aggregates	2.5	0.7	3.1*
Silica sand	0.0	cyanobacterial aggregates	2.8	0.0	0.0**
Silica sand	0.0	cyanobacterial aggregates	2.8	1.1	4.2**
Silica sand	0.0	cyanobacterial aggregates	2.8	2.2	8.4**
Silica sand	0.1	cyanobacterial mat	13.0	0.5	0.2**

Note: Fluid velocity was calculated for all experimental conditions assuming jars to be non-conical cylinders. See Supplemental Methods.

*VWR Minishaker (VWR International, Radnor, PA, USA), 3 mm orbital diameter, 190 RPM.

**VWR Minishaker (VWR International, Radnor, PA, USA), 15 mm orbital diameter, 0, 150 or 170 RPM.

Chapter 4. Rapid formation of clay veneers delays the decay of soft tissues in kaolinite-rich environments

4.1 Abstract

Exceptionally preserved fossils of soft-bodied organisms from the terminal Proterozoic and early Phanerozoic are found in sandstone and siltstone strata characterized by abundant clay-rich layers. Previous taphonomic experiments have shown that clay minerals such as kaolinite can inhibit the decay of soft tissues, but the respective roles of clay minerals and microbial processes in preservation remain to be elucidated. Here we seek to identify some of these mechanisms by incubating scallop muscles for 45 days in kaolinite or silica sand. We find that <0.5 mm thick veneers readily form around soft tissues incubated in kaolinite, but equally thick veneers do not form around tissues incubated in its absence. These veneers are comprised of kaolinite grains from the sediment and newly formed amorphous aluminosilicate phases that precipitated in iron(II)-rich porewaters. The mineral veneers preserve the macroscopic shape of the soft tissues in spite of continued decay. We hypothesize that this process, combined with sediment compaction during diagenesis, may have led to the formation of two-dimensional compression fossils in fine-grained sediments that were not disturbed by bioturbation.

4.2 Introduction

Ediacaran and early Cambrian siliciclastic sediments yield exceptionally preserved fossils of soft-bodied organisms (Narbonne, 2005; Laflamme et al., 2011; Anderson et al., 2011; Cai et al., 2012). These include two-dimensional Burgess Shale-type compressions in shales (Gaines et al., 2008, 2012) and impressions of soft tissues in some Ediacaran sandstones and siltstones

(Narbonne, 2005; Callow and Brasier, 2009; Gehling and Droser, 2009). Because clay minerals are commonly found in fossiliferous sandy sediments and can even form thin laminae between part/counterpart fossil impressions (Gehling, 1999) or aluminosilicate veneers (Orr et al., 1998), they are hypothesized to facilitate the preservation of soft-bodied organisms (Butterfield, 1990). The mechanisms for this are unclear, but may involve the replacement of labile tissues during early diagenesis (Orr et al., 1998) and the inhibition of heterotrophic microbial activity (Butterfield, 1990; McMahon et al., 2016). A role for mat-forming microorganisms is also suggested in the sealing of soft tissues beneath the sediment surface by forming "death masks" which facilitate the precipitation of protective veneers of iron sulfide (Gehling, 1999; Darroch et al., 2012; Liu, 2016). Additionally, microbial processes are hypothesized to have promoted the precipitation of authigenic clays around degraded tissues (Petrovich, 2001). However, most of these mechanisms, as well as the shape-preserving interplay between porewater chemistry, mineral composition and microbial processes remain to be determined.

Taphonomic experiments are critical to our understanding of organic preservation because they can test the effects of clay minerals on the decay of modern soft-bodied organisms and provide information on the preservation of soft tissues in past environments. Previous studies such as Naimark et al. (2016) and Wilson and Butterfield (2014) reported better preservation of polychaetes and crustaceans in the presence of kaolinite relative to montmorillionite, calcite or quartz. They suggested that kaolinite, an aluminum-rich clay, suppresses bacterial decay enzymes in a process similar to tanning which polymerizes organic material (Wilson and Butterfield, 2014). Additionally, experiments with microbial mats have demonstrated the formation of extensive, clay-rich veneers around cyanobacterial filaments by processes of trapping/binding and biomineral precipitation (Newman et al., 2016, 2017). Similarly, Martin et

al. (2004) experimentally demonstrated the adhesion of fine particles from the sediment to invertebrate eggs. However, organomineral interactions involved in the early decay and preservation of soft tissues remain to be characterized.

This study uses experimental taphonomy to probe the role of kaolinite and microbial processes in the preservation of soft tissues. Our experiments with kaolinite reconstruct soft tissue preservation in mm- to cm-thick claystone strata (e.g., the Chengjiang and Burgess Shale, Zhu and Li, 2001; Gabbott et al., 2008), but can also inform mechanistic models for mixed fine-grained/coarse-grained siliciclastic layers (e.g., Gehling, 1999). Scallop adductor muscles were selected as model tissues because they are readily available and are similar to Ediacaran organisms in size (~5 cm), morphology (discoidal) and likely composition (muscle fibers). We demonstrate that kaolinite particles from the sediment attach to the tissue surfaces and that authigenic clay minerals form between these trapped/agglutinated particles within 45 days. This combination of trapping and precipitation facilitates the formation of <0.5 mm-thick mineral veneers around soft tissues, delays organic decay and preserves the shape of the degrading tissues, with some loss of height due to decay and sediment compaction.

4.3 Results and Discussion

4.3.1 Visual observations after 45 days

To identify factors that lead to the delayed decay of soft tissues in fine-grained environments, we incubated scallop tissues for 45 days in kaolinite (purchased from Santa Cruz Biotechnology, Inc., Dallas, TX, USA). Control conditions tested decay in silica sand (purchased from the Ottawa Silica Company, Ottawa, IL, USA). All experiments were conducted in triplicate. Before incubation, scallop tissues were surficially sterilized by soaking specimens in 100% 200 proof

ethanol for 20 minutes. This sterilization procedure eliminated surficial bacterial contaminants but did not sterilize bacteria that were endogenous to the scallop. Soft tissues were incubated in the presence of an artificial seawater medium characterized by high concentrations of silica (0.1 mM) and low concentrations of sulfate (7.94 mM) relative to modern seawater (Fig. 4.1, Supplementary Fig. 4.1, see Newman et al. 2016, 2017 for medium composition). Sand, clay minerals and the artificial seawater medium were sterilized before experimentation by autoclaving at 121˚C for 20 minutes. The surface of the medium was in contact with the atmosphere and the culture jars were continuously agitated to facilitate fluid motion. However, the appearance of dark patches in the sand/clay (Supplementary Fig. 4.2) pointed to the establishment of anaerobic areas around the soft tissues due to microbial activity. We compared and contrasted tissues incubated in kaolinite with those incubated in silica sand (control experiments) over the same interval of time (Supplementary Fig. 4.1). The samples became increasingly malodorous after about 5 days and remained such until the end of the experiment.

After 45 days of incubation, we recovered two out of three scallops from kaolinite, only one out of three from silica sand (Fig. 4.2) and the remaining samples completely disintegrated during incubation. By the end of the experiment, all scallops lost between 60.8 to 100% of weight when incubated in kaolinite and between 29.7 to 100% when incubated in silica sand. Only scallops exhumed from kaolinite had a dark coating (Fig. 4.2) and attempts to separate this veneer from the tissues with tweezers were unsuccessful. In rare instances when we were able to remove pieces of the coatings, the soft interiors of the samples immediately liquefied. In contrast, coated scallops maintained their discoidal/ovoid shape throughout exhumation and later treatments.

4.3.2 Characterization of mineral veneers around soft tissues

To determine the composition of the dark coatings around soft tissues (Fig. 4.2b), we analyzed scallops by scanning electron microscopy, X-ray spectroscopy (SEM-EDS) and selected area electron diffraction (TEM-SAED). All fresh scallops were composed of carbon, oxygen and trace amounts of nitrogen (Fig. 4.3), with spots of magnesium, chlorine, sodium and calcium (Fig 4.3). In contrast, the dark coatings contained aluminum, silica, potassium, calcium, magnesium and iron indicating that clay minerals coated scallop surfaces that had been in contact with kaolinite (Fig. 4.3b, c). Minerals which comprised the coatings were either morphologically indistinguishable from tissue surfaces (Fig. 4.3b) or occurred as discrete, platy grains (Fig. 4.3c). The presence of both kaolinite grains and fine-grained particles which differed in composition from the sterile kaolinite (iron, potassium-rich smectites, Fig. 4.4) in the coatings suggested that some kaolinite grains adhered to the tissues and that new minerals, formed either as new phases or as transformed materials from the original kaolinite, precipitated on the surfaces of the decaying soft tissues. The coatings on the tissue surfaces were not covered by microbial biofilms and contained only sporadic microbial cells; these microorganisms likely proliferated from bacteria that were endogenous to the scallop tissues before incubation (Fig 4.3c, see methods).

Chemical assays demonstrated changes in the porewater chemistry due to the reduction of iron and the dissolution of silica associated with the decay of soft tissues. In the sterile medium and sediments, iron(II) was not detectable and dissolved iron(III) was present at micromolar concentrations. However, the concentrations of iron(II) in the porewaters of some replicates rose to 1.17 mM and those of iron(III) rose to 0.17 mM during the first 15 days of incubation, while soft tissues were still visible in the replicate incubation jars. Concentrations of silica were two to three times higher in sand/clay that contained soft tissues relative to the sterile sand/clay and

more than an order of magnitude higher than those in the sterile medium (Supplementary Table 4.1). These observations demonstrated active reduction of iron associated with heterotrophic degradation and the concomitant release of silica due to the dissolution of quartz and clay minerals. The lower concentrations of iron(II) and silica in samples that did not decay completely were consistent with the drawdown of iron and silica due to the formation of iron and silica-rich veneers.

To identify iron-rich mineral phases coating tissue surfaces, we used micro-X-ray diffraction (μXRD, beamline 12.3.2), X-ray fluorescence (XRF, beamline 10.3.2) mapping and iron K-edge X-ray absorption near edge spectroscopy (XANES, beamline 10.3.2) at the Advanced Light Source (Berkeley, CA, USA). μ-XRD analyses revealed that iron-, calcium- and sodium-rich clays coated soft tissues incubated in both kaolinite and silica sand (Supplementary Fig. 4.3). XRF mapping showed the accumulation of iron on all scallop tissues during burial (Fig. 4.5, compare 4.5a with 4.5b). XANES spectra of the samples exhumed from kaolinite best matched the following iron standard spectra (from the 10.3.2 iron standards database, ALS, Berkeley, CA, USA): iron-rich basaltic glass and iron-rich clays. This best-fit match supported the neoformed (possibly amorphous) nature of these minerals (Figs. 4.3, 4.4, 4.5). These observations suggest that iron(II)-rich minerals were authigenic precipitates that incorporated iron(II) released due to organic decay in the anoxic zone around the decaying tissues. Taken together, this demonstrates that iron-rich mineral veneers, composed of precipitated and attached minerals can form on scallop tissues incubated in either sandy or clay-rich environments. However, only when soft tissues were incubated in kaolinite did visible, extensive veneers form around tissue surfaces (Fig. 4.2b).

4.3.3 Clay minerals facilitate the preservation of soft tissues

Our taphonomic experiments identify the formation of authigenic minerals under anoxic conditions and in the presence of microbial iron reduction as conditions that best delay the decay of scallop adductor muscles. Direct or indirect microbial iron reduction requires organic matter (or H_2) as the source of electrons, but does not require strict anoxia or the presence of sealing layers; our system did not rely upon a sealing layer which acted as a barrier to sediment permeability, as hypothesized by Gaines et al. (2012) and Gehling et al. (1999).

The formation of mineral veneers also requires sources of silica and aluminum. Because more silica and iron(II) are released into the solution when soft tissues are present than when they are absent (Fig. 4.5, Supplementary Table 4.1), organic decay seems to enable the dissolution of labile sources of silica, iron(III) and aluminum in both kaolinite and silica sand. These findings are consistent with Michalopoulos and Aller (2004), who reported the formation of authigenic iron(II)-rich clay minerals around diatom frustules in modern silty sediments of the Amazon delta and invoked microbial iron reduction in this process. Our experiments extend these observations from small siliceous organisms in modern clay-rich deltaic systems to larger organisms that lacked original mineral components and were preserved in Ediacaran sandstones and siltstones.

Factors that control the rates of organic degradation around soft-bodied organisms remain an open question. In fact, the mere presence of kaolinite did not delay the decay in all triplicate experiments and the one scallop recovered from silica sand without kaolinite had lost the least weight of all preserved samples (Fig. 4.2c). Thus, the overall availability of reactive iron(III) and

the activity of heterotrophic microorganisms in the sediment is likely of paramount importance to the decay delay of soft tissues.

Based on observations from our study and assuming no bioturbation during the Ediacaran/early Cambrian (Seilacher and Pflüger, 1994), we propose the following model of preservation: (1) organisms are buried under a layer of sediment; (2) during the early stages of decay (days, see Newman et al. 2016) kaolinite grains adhere to the organic surfaces and form a discontinuous veneer; (3) over time, organic decay under anaerobic conditions facilitates the release of silica, iron and aluminum and enables the formation of authigenic, cation-rich clay mineral veneers on the surfaces of the decaying tissues; (4) this physical barrier slows down microbially-catalyzed decay and preserves the shape of the organism; (5) the organic material in the interior eventually decays, leading to compaction and a decrease in height, but preserves the width and the length of the original tissue.

4.4 Conclusions

Our experiments demonstrate that muscle tissues can be protected by clay coatings in shallow marine siliciclastic environments characterized by abundant clay mineral horizons. Similar mechanisms can explain the preservation of two-dimensional compression fossils observed in Burgess Shale-type deposits (Orr et al., 1998) or part-counterpart impressions (Gehling et al. 1999). Veneers composed of an authigenic component (see Orr et al., 1998 for similar mechanisms in deep water settings) and sedimentary clay minerals that initially adhered onto the organic surfaces may have facilitated the preservation of these fossils in clay-rich sediments. Thin mineral veneers protected soft tissues from microbial decay by (1) inhibiting physical contact between tissues and heterotrophic microorganisms and (2) providing support for

the decaying soft tissues. Thin mineral veneers (<0.5 mm thick) may have facilitated the preservation of two-dimensional compression fossils, whereas thicker, more extensive mineral coatings would have inhibited soft tissue compression during diagenesis and facilitated the formation of molds and three-dimensional casts in some Ediacaran and early Cambrian coarse-grained siliciclastic sediments (Gehling, 1999; Narbonne, 2005; Mapstone and McIlroy, 2006; Callow and Brasier, 2009; Meyer et al., 2014). Future experiments should determine the optimal thickness and extent of mineral coverage required to form two- and three-dimensional fossils and investigate the evolution of veneer formation at various time points throughout the burial process.

4.5 References

Anderson, E.P., Schiffbauer, J.D., Xiao, S., 2011. Taphonomic study of Ediacaran organic-walled fossils confirms the importance of clay minerals and pyrite in Burgess Shale-type preservation. Geology 39, 643–646. doi:10.1130/G31969.1.

Butterfield, N.J., 1990. Organic preservation of non-mineralizing organisms and the taphonomy of the Burgess Shale. Paleobiol. 16, 272–286.

Cai, Y., Schiffbauer, J.D., Hua, H., Xiao, S., 2012. Preservational modes in the Ediacaran Gaojiashan Lagerstätte: Pyritization, aluminosilicification, and carbonaceous compression. Palaeogeogr. Palaeoclimatol. Palaeoecol. 326, 109–117. doi:10.1016/j.palaeo.2012.02.009.

Callow, R.H.T., Brasier, M.D., 2009. Remarkable preservation of microbial mats in Neoproterozoic siliciclastic settings: Implications for Ediacaran taphonomic models. Earth-Science Rev. 96, 207–219. doi:10.1016/j.earscirev.2009.07.002.

Darroch, S.A.F., Laflamme, M., Schiffbauer, J.D., Briggs, D.E.G., 2012. Experimental formation of a microbial death mask. Palaios 27, 293–303. doi:10.2110/palo.2011.p11-059r.

Gabbott, S.E., Zalasiewicz, J., Collins, D., 2008. Sedimentation of the Phyllopod Bed within the Cambrian Burgess Shale Formation of British Columbia. J. Geol. Soc. London. 165, 307–318. doi:10.1144/0016-76492007-023.

Gaines, R.R., Briggs, D.E.G., Yuanlong, Z., 2008. Cambrian Burgess Shale-type deposits share a common mode of fossilization. Geology 36, 755–758. doi:10.1130/G24961A.1.

Gaines, R.R., Hammarlund, E.U., Hou, X., Qi, C., Gabbott, S.E., Zhao, Y., Peng, J., Canfield, D.E., 2012. Mechanism for Burgess Shale-type preservation. Proc. Natl. Acad. Sci. 109, 5180–5184. doi:10.1073/pnas.1.

Gehling, J.G., 1999. Microbial mats in terminal Proterozoic siliciclastics: Ediacaran death masks. Palaios 14, 40–57. doi:10.2307/3515360.

Gehling, J.G., Droser, M.L., 2009. Textured organic surfaces associated with the Ediacara biota in South Australia. Earth-Science Rev. 96, 196–206. doi:10.1016/j.earscirev.2009.03.002.

Laflamme, M., Schiffbauer, J.D., Narbonne, G.M., Briggs, D.E.G., 2011. Microbial biofilms and the preservation of the Ediacara biota. Lethaia 44, 203–213. doi:10.1111/j.1502-3931.2010.00235.x.

Liu, A.G., 2016. Framboidal pyrite shroud confirms the "death mask" model for moldic preservation of Ediacaran soft-bodied organisms. Palaios 31, 259–274.

Mapstone, N.B., McIlroy, D., 2006. Ediacaran fossil preservation: Taphonomy and diagenesis of a discoid biota from the Amadeus Basin, central Australia. Precambrian Res. 149, 126–148. doi:10.1016/j.precamres.2006.05.007.

Martin, D., Briggs, D.E.G., Parkes, R.J., 2004. Experimental attachment of sediment particles to invertebrate eggs and the preservation of soft-bodied fossils. J. Geol. Soc. London. 161, 735–738. doi:10.1144/0016-764903-164.

McMahon, S., Anderson, R.P., Saupe, E.E., Briggs, D.E.G., 2016. Experimental evidence that clay inhibits bacterial decomposers: Implications for preservation of organic fossils. Geology 44, 867–870. doi:10.1130/G38454.1.

Meyer, M., Elliott, D., Schiffbauer, J.D., Hall, M., Hoffman, K.H., Schneider, G., Vickers-Rich, P., Xiao, S., 2014. Taphonomy of the Ediacaran fossil *Pteridinium simplex* preserved three-dimensionally in mass flow deposits, Nama Group, Namibia. J. Paleontol. 88, 240–252. doi:10.1666/13-047.

Michalopoulos, P., Aller, R.C., 2004. Early diagenesis of biogenic silica in the Amazon delta: Alteration, authigenic clay formation, and storage. Geochim. Cosmochim. Acta 68, 1061–1085. doi:10.1016/j.gca.2003.07.018.

Naimark, E., Kalinina, M., Shokurov, A., Boeva, N., Markov, A., Zaytseva, L., 2016. Decaying in different clays: Implications for soft-tissue preservation. Palaeontology 59, 583–595. doi:10.1111/pala.12246.

Narbonne, G.M., 2005. The Ediacara biota: Neoproterozoic origin of animals and their ecosystems. Annu. Rev. Earth Planet. Sci. 33, 421–442. doi:10.1146/annurev.earth.33.092203.122519.

Newman, S.A., Klepac-Ceraj, V., Mariotti, G., Pruss, S.B., Watson, N., Bosak, T., 2017. Experimental fossilization of mat-forming cyanobacteria in coarse-grained siliciclastic sediments. Geobiology 15, 484–498. doi:10.1111/gbi.12229.

Newman, S.A., Mariotti, G., Pruss, S., Bosak, T., 2016. Insights into cyanobacterial fossilization in Ediacaran siliciclastic environments. Geology 44, 579–582. doi: 10.1130/G37791.1.

Orr, P.J., Briggs, D.E., Kearns, S.L., 1998. Cambrian Burgess Shale animals replicated in clay minerals. Science 281, 1173–1175. doi:10.1126/science.281.5380.1173.

Petrovich, R., 2001. Mechanisms of fossilization of the soft-bodied and lightly armored faunas of the Burgess Shale and of some other classical localities. Am. J. Sci. 301, 683–726. doi:10.2475/ajs.301.8.683.

Seilacher, A., Pflüger, F., 1994. From biomats to benthic agriculture: A biohistoric revolution, in: Krumbein, W.E., Paterson, D.M., Stal, L.J. (Eds.), Biostabalization of Sediments. Bibliotheks - und Informationssystem der Universitat Oldenburg, Oldenburg, Germany, pp. 97–105.

Wilson, L.A., Butterfield, N.J., 2014. Sediment effects on the preservation of Burgess Shale-type compression fossils. Palaios 29, 145–154. doi:10.2110/palo.2013.075.

Zhu, M.-Y., Zhang, J.-M., Li, G.-X., 2001. Sedimentary environments of the early Cambrian Chengjiang biota: Sedimentology of the Yu'anshan Formation in Chengjiang County, Eastern Yunnan. Acta Palaeontol. Sin. 40, 80–105.

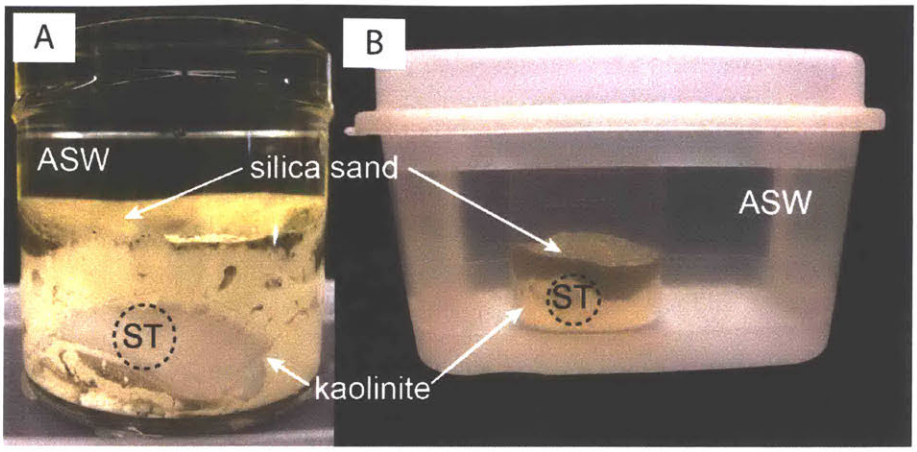

Fig. 4.1. Setup for taphonomic experiments. A) Scallop (ST) incubated in a 68 mm tall and wide plastic jar with 30 g of kaolinite powder and covered by a ~1.5 cm-thick layer of silica sand. ASW marks the artificial seawater medium. B) Experimental jar in a larger container filled with ASW.

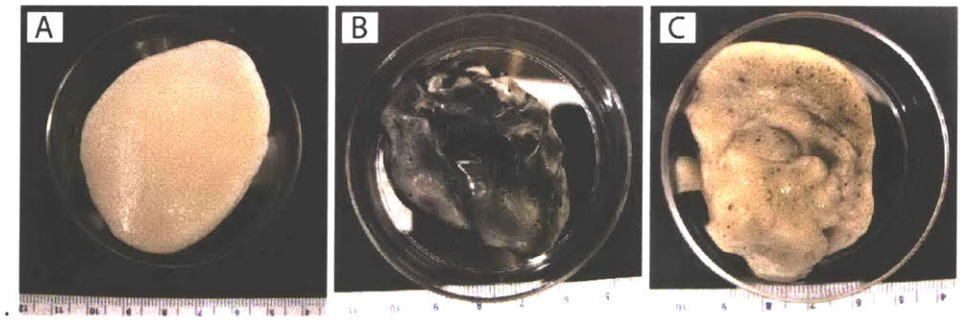

Fig. 4.2. Photographs of the decaying soft tissues after 45 days. A) Representative photograph of scallop tissue before experiment on day 0. B) Scallop exhumed from kaolinite substrate. The scallop surface is coated in dark, clay minerals. C) Scallop exhumed from a silica sand substrate without kaolinite.

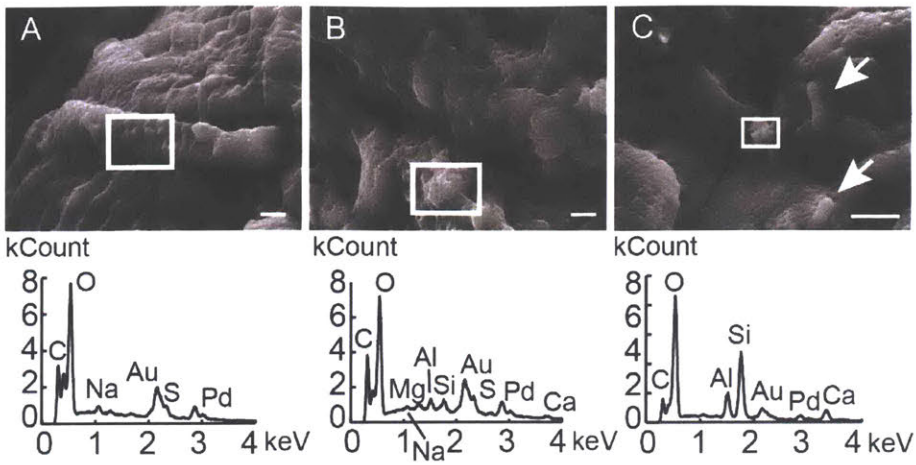

Fig. 4.3. Representative scanning electron micrographs and energy dispersive X-ray spectra of scallop tissues. All scallops were exhumed on day 45, unless otherwise stated. A) Scallop on day 0 (before incubation), B) scallop incubated in kaolinite; minerals coating soft tissues are morphologically indistinguishable from the background organic material and C) scallop incubated in kaolinite; mineral is bulky and platy. Arrows denote microbial cells. Samples were coated with gold and palladium. Scale bar in all micrographs is 1μm. White boxes denote areas analyzed by SEM-EDS; the spectra of these areas are found below the corresponding SEM images.

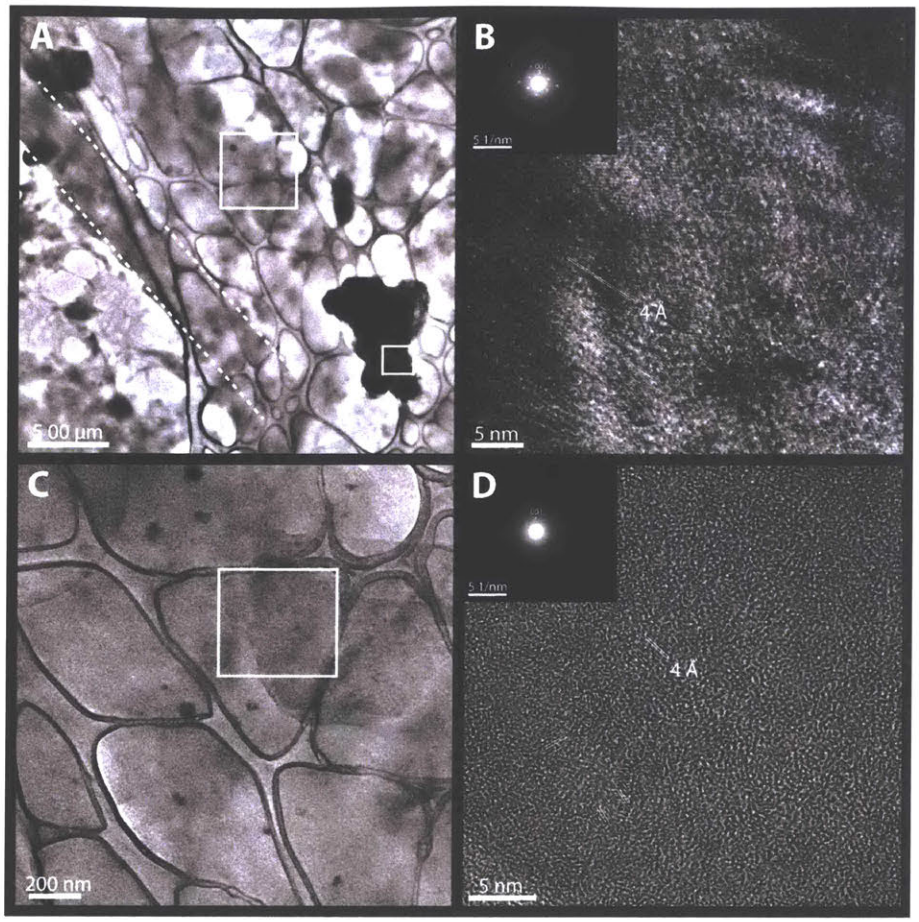

Fig. 4.4. Scallop tissue incubated in kaolinite for 45 days. A) Bright-field transmission electron microscopy (TEM) image of scallop tissue exhumed after 45 days. Crystalline minerals adhere to tissue. The white small square on the crystalline mineral shows the area targeted for selected area electron diffraction (SAED) shown in B. B) High resolution transmission electron microscopy (HRTEM) showing interplanar d-spacing of 4 Å. The SAED pattern from the mineral area marked in A shows ring patterns of authigenic euhedral crystallite exhibiting monoclinic net pattern characteristics of clay minerals (potassium and iron-rich illite/smectite). C) Represents the area marked by the larger white square in panel A. The scallop tissue is characterized by dark patches due to permineralization. The white square shows the area targeted for SAED. D) SAED of the area marked in panel C. HRTEM images show microcrystalline minerals embedded in the tissue with a uniform lattice fringe that corresponded to (001) plane with interplanar spacing of 4 Å. This is characteristic of potassium and iron-rich illite/smectite.

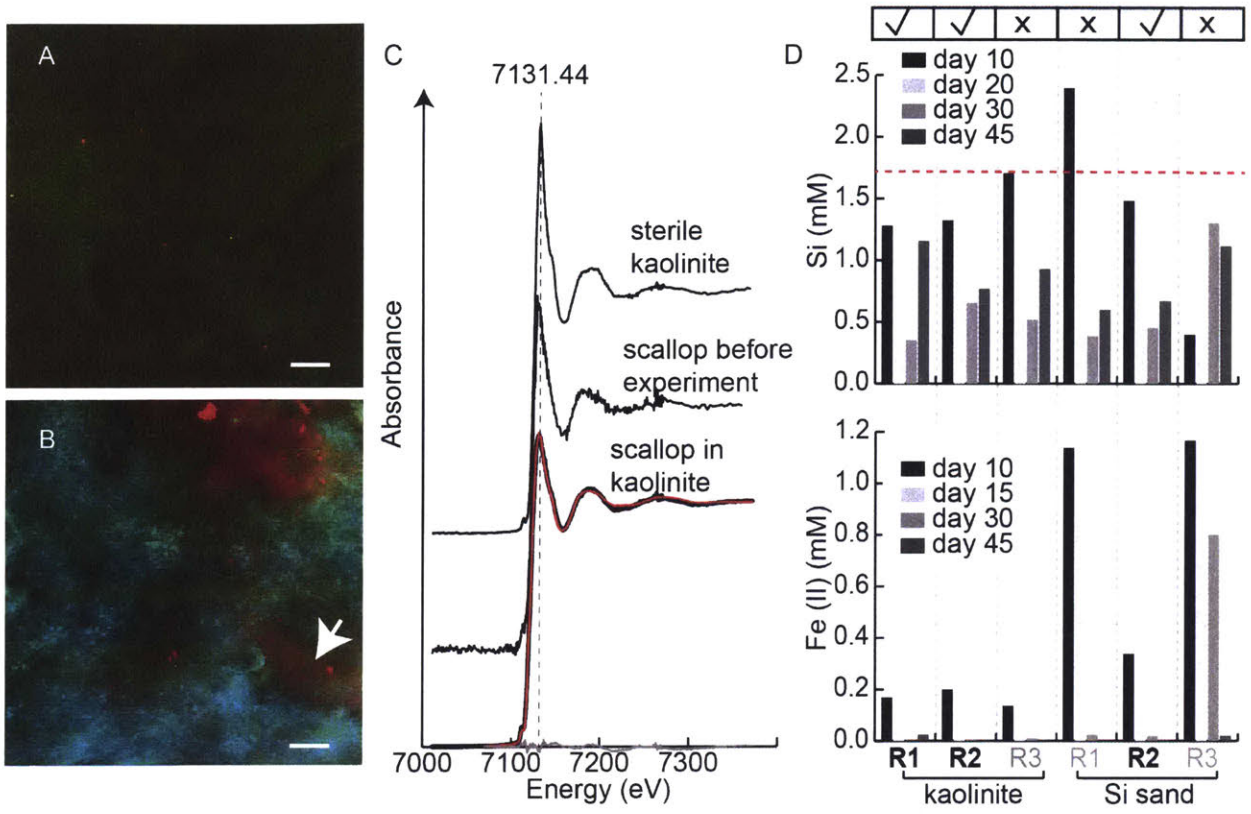

Fig. 4.5. Chemical changes. X-ray fluorescence maps of calcium (green) and iron (red) on soft tissue surfaces: A) Scallop before experiment (day 0) and B) scallop incubated in kaolinite for 45 days. Arrow denotes area of interest on scallop analyzed by XANES. C) Representative iron K-edge XANES spectra for sterile kaolinite grains, scallop before experimentation (average of 5 spots) and scallop buried in kaolinite for 45 days. Best fit standard (iron-rich basaltic glass, 57.5%, ferrosmectite, 22.0% and kaolinite, 20.2%, sum sq: 9.9×10^{-5}; 10.3.2 iron standard database at 10.3.2 ALS, Berkeley, CA, USA) is plotted in red and residuals are plotted in grey. D) Concentrations of dissolved silica (mM) and iron(II) (mM) in porewaters. X denotes replicates that underwent complete degradation; check mark denote replicates with recovered scallops after 45 days. R1-3 denotes replicates 1-3. Dashed red line denotes saturation with respect to amorphous silica. Scale bar for A and B is 200 μm.

4.6 Supplementary Information

Supplementary Methods

Tissue preparation

To identify factors that determine the preservation of soft tissues by clay minerals, we incubated scallop adductor muscles in kaolinite (Fig. 4.1, Supplementary Fig. 4.1); our experiments tested soft tissue preservation in cm-thick layers of fine-grained material and reconstructed fossilization in the clay-rich strata of the Ediacaran and early Cambrian (e.g., Zhu and Li, 2001; Gabbott et al., 2008). Although many fossiliferous siliciclastic sediments of the Ediacaran and early Cambrian included mixed substrate types (both fine-grained and coarse-grained particles, e.g. Gehling, 1999), we buried soft tissues in kaolinite to specifically determine the role of clay minerals in preservation. Fresh, untreated scallops were purchased from the New Deal Fish Market (Cambridge, MA, USA) and the adductor muscles were cut from the shell on the same day to kill the scallops. The adductor muscles were frozen at -20°C (for one to two days) until the first day of the experiment to prevent soft tissue decay before incubation. Scallops were thawed at room temperature on the first day of incubation. Scallops were rinsed with double distilled water to remove dirt, sand and other impurities and sterilized by soaking in 100% 200 proof ethanol for 20 minutes; this procedure surficially sterilized the scallop tissues, but did not sterilize endogenous bacteria. The ethanol was decanted by pouring and the scallop tissues were left in the fume hood for one hour to evaporate excess ethanol. Any remaining ethanol was removed by rinsing the scallops with filter-sterilized double distilled water (0.2 μm Nalgene Rapid Flow Sterile Top Filters, VWR, Radnor, PA, USA). All excess water was removed by pipetting and scallops were weighed. Previous experiments had shown no observable difference

in tissue decay between scallops frozen and sterilized with ethanol and those that were incubated in silica sand immediately after their removal from the shell. However, the freezing and sterilizing process removed surficial bacterial contaminants and allowed for us to determine the role of endogenous bacteria in soft tissue decay.

Experimental setup

Scallops were incubated in sterile culture jars (diameter: 68 mm, height: 68 mm; Grenier Bio-One, Kremsmünster, Austria) in the presence of 30 g of kaolinite powder (Santa Cruz Biotechnology, Inc., Dallas, TX, USA). The kaolinite powder was sterilized before experimentation by autoclaving at 121°C for 20 min. Scallops were buried a few cm below the kaolinite surface (Fig. 4.1a) and a ~1.5 cm thick layer of sterile silica sand (autoclaved; purchased from the Ottawa Silica Company, Ottawa, IL, USA) was added to the surface of kaolinite to prevent the suspension of kaolinite into solution (Fig. 4.1a). The culture jar with a single scallop was placed in a larger plastic container with a closeable lid (18.7 x 16.5 x 11.4 cm [l x w x h], Sterilite Flip Top, Sterilite Corporation, Townsend, MA, USA); each container was pre-filled with 1.5 L of sterile artificial seawater characterized by high concentrations of silica (0.1 mM, see Newman et al. 2016, 2017 for the medium composition) (Fig. 4.1b). Control conditions investigated the decay of scallop tissues buried in sterile silica sand (130 g, purchased from the Ottawa Silica Company, Ottawa, IL, USA) without added kaolinite under identical conditions to those described above (Supplementary Fig. 4.1a, b). All experiments (kaolinite and control experiments) were conducted in triplicate.

All undecayed tissues were exhumed on day 45 with a plastic serological pipette. Exhumed scallops were rinsed with filter-sterilized double distilled water (0.2 µm Nalgene Rapid

Flow Sterile Top Filters, VWR, Radnor, PA, USA) and placed in a sonicating bath for 10 min to facilitate the removal of fine grains that were not tightly bound to the scallop surface. The samples were weighed after rinsing and the weight loss was determined by calculating the difference in weight (in g) of the samples before and after incubation. This number was divided by the initial scallop weight and expressed as a percentage. This underestimated the weight of the actual tissues incubated in kaolinite because of the presence of clay veneers, but it did not affect comparisons between experiments because mineral veneers were thinner than 1 mm.

Throughout all experiments, the surface of the artificial seawater medium was in contact with the atmosphere because the plastic containers were not air tight (Fig. 4.1b, Supplementary Fig. 4.1b). Culture jars were continuously agitated on VWR Minishakers (VWR International, Radnor, PA, USA) to facilitate fluid motion. The medium was replaced every 5 to 10 days to remove dissolved organic matter and to maintain a semi-constant pH (~7.5) in the water column.

Water chemistry

To measure changes in porewater chemistry associated with decay, iron(II), iron(III), dissolved silica and sulfide were measured colorimetrically using a Biotek multiplate reader at the following wavelengths: 562 (iron), 810 (silica) and 670 nm (sulfide). See Stookey (1970), Newman et al. (2017) and Cline (1969) for methods describing iron, silica and sulfide determination, respectively. Experiments were sampled 5 days after each replacement of the medium. Porewater samples (<4 mL) were collected using 5 mL plastic syringes with 18 gauge needles (VWR International, Radnor, PA, USA) ~6.5 cm below the substrate surface. All porewater and water column samples were centrifuged aerobically for 10 minutes at 10,000 rotations per minute to separate particulate matter from the liquid medium. The supernatant was

decanted and filtered aerobically through 0.2 μm sterile syringe filters with a polyethersulfone membrane (Acrodisc®, Pall Laboratory, Westborough, MA, USA).

Electron microscopy

To identify the composition and distribution of minerals coating soft tissues, scallops were imaged by scanning electron and transmission electron microscopy with electron dispersive spectroscopy (SEM- and TEM-EDS). For all exhumed scallops, a small piece (~2 cm in width) was isolated using a 1 mL plastic pipette tip to separate the tissue. Samples were imaged by TEM using a JEOL 2010F transmission electron microscope (TEM, JOEL 2010F, JOEL, CA, USA) and an energy dispersive spectrometer (EDS, Bruker silicon drift detector SDD, Bruker, MA, USA). Samples for SEM were fixed in 2.5% glutaraldehyde in 0.1 M sodium cacodylate buffer with 0.1% $CaCl_2$ (pH = 7.4). Samples were stored for 3 to 7 days at 4°C to ensure the complete fixation of soft tissues. After this time, samples were rinsed twice for 10 min with a 0.1 mM sodium cacodylate buffer solution (stored at 4°C), followed by 6 rinses with double distilled water. Samples were dehydrated using an ethanol-water drying series (30%, 50%, 70%, 80%, 90%, 100%, 100%, 100%), with 20 min steps and left overnight in the fume hood to dry. Dehydrated scallop tissues were transferred to carbon tape and coated with gold and palladium to reduce SEM image charging (Keck Facility, Whitehead Institute, MIT, Cambridge, MA, USA). All samples were imaged on a Zeiss Supra Scanning Electron Microscope with a secondary electron detector (Center for Nanoscale Systems, Harvard University, Cambridge, MA, USA). Elemental composition in regions of interest was determined using an electron-dispersive X-ray spectrometer operating at 10 kV.

4.6.5 μXRD

The composition of minerals coating scallop tissues was determined at the Advanced Light Source (beamline 12.3.2, Berkeley, CA, USA) with a combination of micro-X-ray fluorescence (μXRD) mapping and micro-X-ray diffraction (μXRD) at 10 keV. Previously frozen samples were thawed, but not dried, and placed on the sticky side of Kapton® polyimide tape (DuPont, Hayward CA, USA) for analysis. A 3 x 3 μm XRF map was first generated and points with high iron intensity were selected for diffraction. XRD data was processed using the program available at the beamline and minerals were identified using the program HighScore Plus.

4.6.6 X-ray microprobe

We determined the spatial distribution and speciation of iron coating scallop tissues at the Advanced Light Source (beamline 10.3.2, Berkeley, CA, USA) using micro-focused X-ray fluorescence (μXRF) mapping and iron K-edge X-ray adsorption near edge structure (μXANES) spectroscopy, respectively. Pre-frozen samples (-80°C) were first thawed, air dried and then mounted on the non-sticky side of Kapton® polyimide tape (DuPont, Hayward CA, USA) for analysis. μXRF maps were first generated using an incident beam at 100eV above the iron K-edge and spots of interest were selected for XANES measurements. Fluorescence data were recorded using a germanium (Ge) solid state detector (Canberra, ON, Canada). Fluorescence emission counts were recorded for sulfur, iron, calcium, potassium, chlorine, silica and phosphorous. XANES spectra were calibrated with an iron foil (first derivative maximum set at 7110.75 eV). Maps were recorded with a beam spot size of 6 x 6 μm. Spectra were recorded with a beam spot size of 12 x 3 μm. Spectra were least-square fitted using a large database of iron bearing standard compounds (included in the 10.3.2 database). All spectra were deadtime-

corrected, calibrated, pre-edge background subtracted and post-edge normalized using a suite of LabVIEW based programs available at the beamline.

References

Cline, J.D., 1969. Spectrophotometric determination of hydrogen sulfide in natural waters. Limnol. Oceanogr. 454–458. doi:10.4319/lo.1969.14.3.0454.

Gabbott, S.E., Zalasiewicz, J., Collins, D., 2008. Sedimentation of the Phyllopod Bed within the Cambrian Burgess Shale Formation of British Columbia. J. Geol. Soc. London. 165, 307–318. doi:10.1144/0016-76492007-023.

Newman, S.A., Klepac-Ceraj, V., Mariotti, G., Pruss, S.B., Watson, N., Bosak, T., 2017. Experimental fossilization of mat-forming cyanobacteria in coarse-grained siliciclastic sediments. Geobiology 15, 484–498. doi:10.1111/gbi.12229.

Stookey, L.L., 1970. Ferrozine - A new spectrophotometric reagent for iron. Anal. Chem. 42, 779–781. doi:10.1021/ac60289a016.

Zhu, M.-Y., Zhang, J.-M., Li, G.-X., 2001. Sedimentary environments of the early Cambrian Chengjiang biota: Sedimentology of the Yu'anshan Formation in Chengjiang County, Eastern Yunnan. Acta Palaeontol. Sin. 40, 80–105.

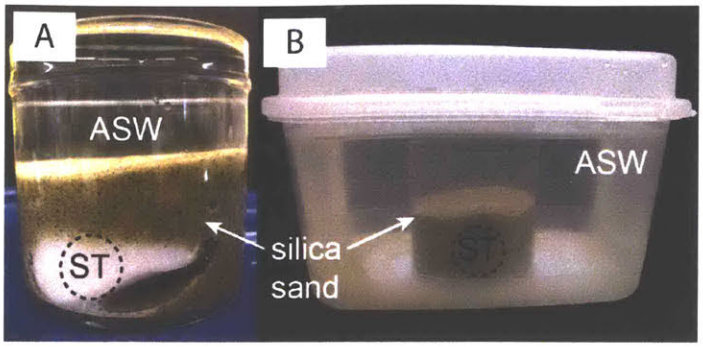

Supplementary Fig. 4.1. Setup for control experiment. A) Scallop (ST) incubated in a 68 mm tall and wide plastic jar with 30 g of silica sand. ASW marks the artificial seawater medium. B) Experimental jar in a larger container filled with ASW.

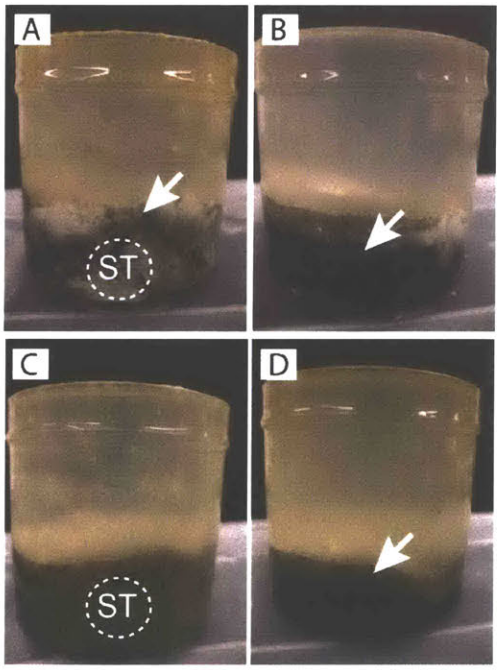

Supplementary Fig. 4.2. Photographs of culture jars on day 45 before soft tissue exhumation. Scallops (ST) buried in kaolinite: A) scallop remains intact and B) scallop has completely decayed. Scallops buried in silica sand without kaolinite: C) scallop remains intact and D) scallop has completely decayed. Arrows denote black patches, indicative of microbial activity.

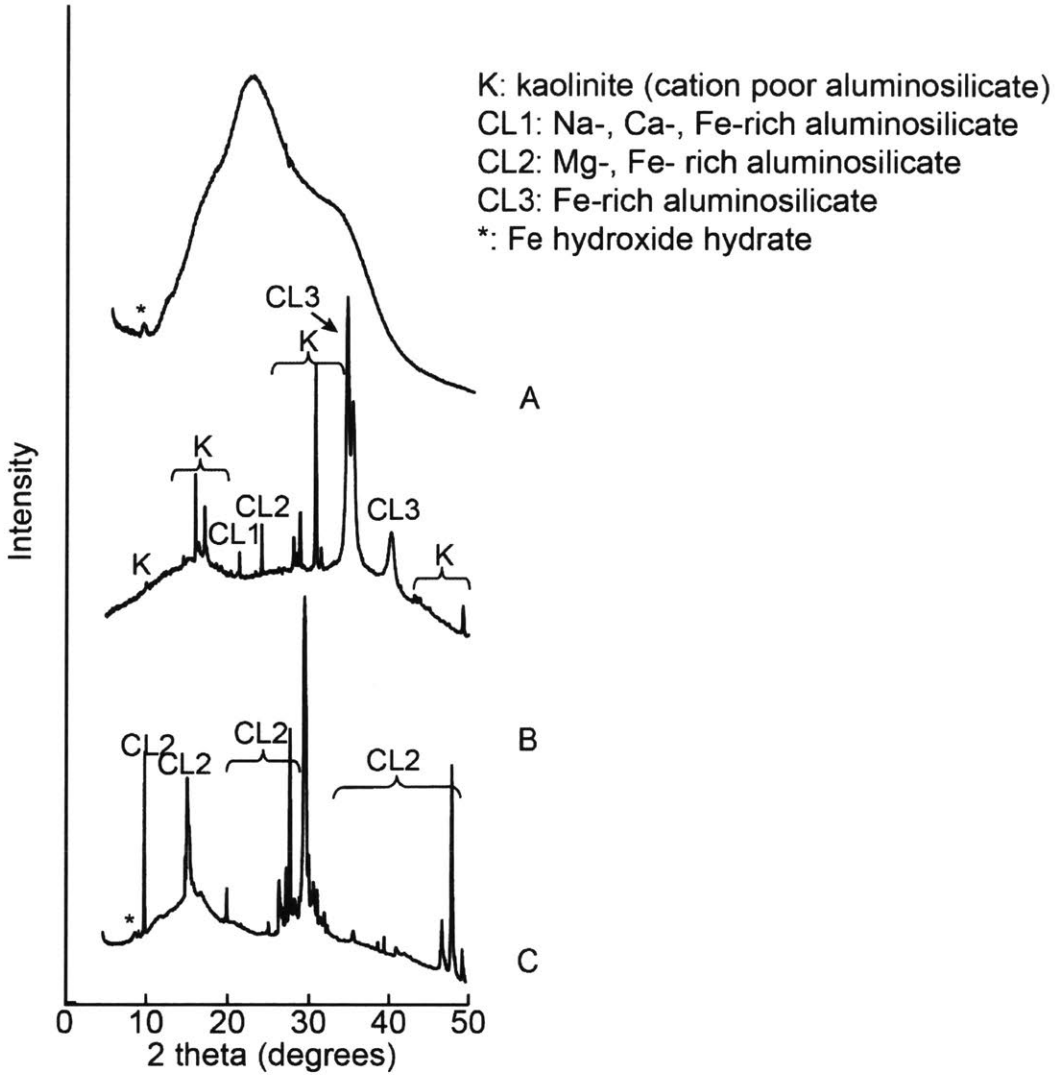

Supplementary Fig. 4.3. uXRD spectra of A) scallop before experiment, day 0, B) scallop incubated in kaolinite for 45 days and C) scallop incubated in silica sand without kaolinite for 45 days. For B) and C) the scallop background (A) was subtracted from the original spectra.

Supplementary Table 4.1. Concentrations of silica, iron(II), iron(III) and sulfide in porewaters

		Scallops incubated in clay/sand						Sterile experiments, no scallops			
Day	Ions/dissolved silica	Kaolinite			Silica sand			Kaolinite		Silica sand	
		R1[t]	R2[t]	R3	R1	R2[t]	R3	R1	R2	R1	R2
10	silica (mM)	1.28	1.32	1.71	2.39	1.48	0.40	0.46	0.62	0.45	0.39
	Fe^{2+} (mM)	0.17	0.20	0.14	>1.14*	0.34	>1.17*	<0.01	<0.01	<0.01	<0.01
	Fe^{3+} (mM)	0.10	0.09	0.14	>0.00*	>0.06*	>0.01*	<0.01	<0.01	<0.01	<0.01
	sulfide (μM)	0.02	n.d.	n.d.	1.22	6.53	37.99	--	--	--	--
15	silica (mM)	--	--	--	--	--	--	0.65	0.64	0.48	0.41
	Fe^{2+} (mM)	0.05	0.11	0.15	>0.97*	0.13	>1.04*	<0.01	<0.01	<0.01	<0.01
	Fe^{3+} (mM)	0.10	>0.00*	0.08	>0.00*	>0.17*	>0.00*	<0.01	<0.01	<0.01	<0.01
	sulfide (μM)	1.05	2.59	n.d.	1.82	3.92	10.34	--	--	--	--
20	silica (mM)	1.45	1.10	0.96	2.01	0.72	1.70	0.36	0.38	0.27	0.29
30	silica (mM)	0.35	0.65	0.52	0.39	0.45	1.30	0.30	0.51	0.23	0.42
	Fe^{2+} (mM)	<0.01	0.01	0.01	0.03	0.02	0.8	n.d.	<0.01	<0.01	<0.01
	Fe^{3+} (mM)	0.01	0.05	0.04	0.06	0.12	0.11	<0.01	<0.01	<0.01	<0.01
	sulfide (μM)	n.d.	n.d.	0.06	n.d.	1.39	1.61	--	--	--	--
45	silica (mM)	1.16	0.77	0.93	0.60	0.67	1.12	0.45	0.45	0.28	0.35
	Fe^{2+} (mM)	0.02	<0.01	<0.01	0.01	<0.01	0.02	n.d	n.d	<0.01	<0.01
	Fe^{3+} (mM)	0.04	0.03	0.02	0.12	0.13	0.29	<0.01	<0.01	<0.01	<0.01
	sulfide (μM)	n.d.	n.d.	n.d.	n.d.	n.d.	1.95	--	--	--	--

*Sample diluted 20x in 0.1 M NaCl water after the addition of ferrozine.

[t]Sample was successfully recovered on day 45.

R1-R3 denotes replicates one through three.

n.d. denotes below the limit of detection.

Chapter 5. Microbially mediated cycling of iron controls the decay and preservation of soft tissues in siliciclastic environments

5.1 Abstract

Fossils of Ediacaran and early Cambrian soft-bodied organisms were commonly preserved on the bedding soles of sandstones and siltstones as positive or negative impressions. The rarity of similarly preserved organisms in siliciclastic sediments of the later Phanerozoic suggests that temporally unique environmental conditions may have facilitated this type of preservation. Here we used experimental taphonomy to test the roles of photosynthetic microbial mats, clay minerals (kaolinite/illite) and porewater chemistries (concentrations of iron(II), iron(III), sulfide, silica and oxygen) in the preservation of soft tissues. Specifically, we monitored the decay of the scallop adductor muscle over 45 days. The presence of millimolar concentrations of iron(II) and micromolar concentrations of sulfide in the porewaters provided evidence for organic decay under anoxic conditions. The most extensive decay occurred in the presence of greater than 0.9 mM of iron(II) in porewaters that were saturated with respect to amorphous silica (≥1.7 mM). This indicated a strong coupling between organic decay, microbial iron reduction and the dissolution of silicate minerals. Newly formed iron(II) and iron(III)-rich minerals and clay minerals from the surrounding substrates also coated the surfaces of well-preserved soft tissues, forming veneers around these tissues. Thus, we propose a role for iron redox cycling in the formation of mineral veneers on soft tissue surfaces and the preservation of soft tissues in siliciclastic sediments.

5.2 Introduction

Soft-bodied organisms were frequently preserved on the beddings soles of Proterozoic and early Cambrian siliciclastic sediments as external molds, positive casts and/or composite impressions. This type of preservation rarely occurred at other times throughout geologic history. Thus, it is likely that a taphonomic window facilitated the exceptional preservation of early macrofauna in sandy and silty sediments. However, the mechanisms which preserved soft tissues remain to be identified.

The absence of external polymers during the Ediacaran complicates questions of how and why Ediacaran organisms were preserved. Because the siliciclastic rock record of the Ediacaran Period contains abundant microbial fossils and textures (e.g., MISS, Noffke et al., 2001) that are also commonly associated with the casts and molds of Ediacaran macrofauna (Hagadorn and Bottjer, 1997; Mapstone and McIlroy, 2006), Gehling (1999) proposed a 'death mask' model of macrofaunal preservation. This model invokes the formation of a sole veneer composed of iron sulfide due to the presence of overlying microbial mats and the bacterial reduction of sulfate.

Other hypotheses consider the role of dissolved iron in macrofaunal preservation, mostly by suggesting the release of iron(II) by iron(III)-reducing bacteria and the nucleation of iron-rich clay minerals on soft tissue surfaces (Petrovich, 2001). Cations such as iron(II) are toxic to at least some aerobic heterotrophic microorganisms and may contribute to the inhibition of soft tissue decay (McMahon et al., 2016). The occurrence of laminae enriched in iron between some part and counterpart reliefs (Gehling, 1999; Liu, 2016) may support these models of preservation in a few, but not most, fossil localities. Aluminum has been shown to have negative effects on bacterial growth (Pettersson et al., 1986, 1988), although some experiments have shown

aluminum tolerance in heterotrophic bacteria (Fischer et al., 2002). Overall, microbial processes involved in the preservation of these macroscopic organisms remain poorly constrained.

Ediacaran oceans are thought to have had higher concentrations of silica (estimates range up to 2.2 mM, Siever, 1992; Konhauser et al., 2007) due to the effective absence of silica-secreting organisms such as radiolarians, diatoms and sponges. However, the formation of cherts primarily in peritidal environments suggests that most surface waters may not have been supersaturated with respect to the formation of amorphous silica (Maliva et al., 1989). In spite of this, some authors have proposed that the precipitation of opaline veneers around soft tissues facilitated the preservation of casts and molds in Ediacaran/early Cambrian siliciclastic sediments (Callow and Brasier, 2009; Tarhan et al., 2016). Tarhan et al. (2016) investigated fossils in a single unit in the Ediacara Member of South Australia and determined that three-dimensional casts and molds were preserved by silica-rich cements and were rarely found in association with iron sulfide or clay-rich laminae. Although this study proposed an important role for early silicification in fossilization, this mode of preservation may not be applicable to other fossil localities and the conditions that enabled early silicification in sandstones remain poorly understood.

The current study aims to identify environmental and biological factors that inhibit the decay of soft tissues buried in sandy substrates for 45 days. We selected scallop adductor muscles for taphonomic experiments because they are morphologically similar to Ediacaran discoidal fauna and lack a chitinous layer. The experiments determined the influence of various factors (such as the presence of clay minerals and cyanobacterial mats) on soft tissue decay, characterized the evolution of the porewater chemistry and identified conditions that are the best predictors of decay/decay delay. Clay-rich and/or iron-rich veneers coated soft tissues that experienced the least decay within 30 days. This suggested that the mineral veneers formed immediately around

the decaying tissues and protected the labile, organic material from microbial degradation. These results inform a mechanistic model for soft tissue preservation in coarse-grained siliciclastic environments.

5.3 Methods

5.3.1 Experimental setup

To determine the preservation potential of molluscan muscle tissues in siliciclastic environments, we incubated the adductor muscles of fresh Atlantic sea scallops (*Placopecten magellanicus*, purchased from the New Deal Fish Market, Cambridge, MA, USA) in 130 g of silica sand (purchased from the Ottawa Silica Company, Ottawa, Illinois, USA) for 45 days, unless otherwise stated (Table 5.1). The sand was composed of quartz, mica and 0.03% clay minerals, with grains that had an average diameter of ~250 μm. Before incubation, the adductor muscles, hereafter referred to as soft tissues or simply, scallops, were cut from their shell to kill the organism and immediately frozen at -20˚C for one to two days to inhibit decay before incubation. Scallops were thawed at room temperature on the first day of the experiment and rinsed in double distilled water to remove dirt and additional impurities. Specimens were then sterilized by immersion in 100% 200 proof ethanol for 20 minutes to remove surficial bacterial contaminants; this procedure did not sterilize endogenous bacteria. The ethanol was decanted by pipetting and the scallops were air-dried in the fume hood for one hour to facilitate the evaporation of the remaining ethanol. Any trace ethanol that remained after this procedure was removed by rinsing scallops with filter-sterilized double distilled water (0.2 μm Nalgene Rapid Flow Sterile Top Filters, VWR, Radnor, PA, USA). Wet scallops were weighed before incubation. All surficially sterilized and air-dried scallops were then buried ~2 cm below the surface of the pre-sterilized

silica sand/clay substrate (see below, Fig. 5.1a-d) and incubated in the presence of an artificial seawater medium characterized by high concentrations of dissolved silica (0.1 mM) and low concentrations of sulfate (7.9 mM) (see Newman et al. 2016, 2017 for a complete list of medium ingredients). The medium was replaced every 5 to 10 days.

A preliminary experiment in which we incubated soft tissues in the presence of photosynthetic microbial mats and illite seemed to delay the decay of soft tissues. Thus, to determine the effects of microbial mats and illite on soft tissue preservation, scallop tissues were incubated (1) in the presence of cyanobacteria, (2) in the presence of 100 mg of illite powder (Time Laboratories, Pocatello, ID, USA) or (3) in the absence of cyanobacteria or added clay minerals (control experiments) (Fig. 5.1a-b, d, Table 5.1). In the first case, cyanobacterial mats were inoculated onto the sand surface in 10 mL of artificial seawater using a plastic, serological pipette. In the second case, a layer of clay powder was placed above the sand surface and was in physical contact with the soft tissues and covered by a ~1.5 cm-thick layer of sand to hinder the suspension of illite particles into solution. Two culture jars, each containing a single scallop and silica sand, were placed in a larger plastic container (26.5 x 15.5 x 14.0 cm [l x w x h], Sterilite Medium Clip Box, Sterilite Corporation, Townsend, MA, USA) that had been pre-filled with 2 L of artificial seawater (Fig. 5.1e, Table 5.1). Cyanobacteria were inoculated onto the substrate surface several times throughout the experiments to facilitate the formation of cyanobacterial mats (see Newman et al. 2017 for their description of the mat-forming cyanobacteria). Samples for chemical assays were collected from the water column (~3 cm above the substrate surface) on days 15, 30 and 45 (see details below). Soft tissues were recovered on days 30 or 45 with a sterile plastic serological pipette. A gentle lifting motion from underneath the scallop removed the undecayed tissue from the substrate without damaging it.

Scallops buried in the presence of illite decayed as much as did scallops incubated under other experimental conditions. Therefore, we decided to test the role of kaolinite in the delay of organic decay. This clay has been previously shown to inhibit soft tissue decay (Chapter 4 of this Thesis, Wilson and Butterfield, 2014; Naimark et al., 2016) and reduce the activity of aerobic heterotrophic bacteria (McMahon et al., 2016). In the current experiment, soft tissues were completely buried in 30 g of kaolinite (Santa Cruz Biotechnology, Inc., Dallas, TX, USA) and covered with an additional 1.5 cm-thick layer of silica sand to hinder the suspension of kaolinite particles into solution (Fig. 5.1c, Table 5.1). Control experiments investigated the decay of scallop tissues buried in silica sand in the absence of kaolinite (Fig 5.1d, Table 5.1). One culture jar with a single buried scallop was placed in an 18.7 x 16.5 x 11.4 cm (length x width x height) external container (Sterilite Flip Top, Sterilite Corporation, Townsend, MA, USA) that was pre-filled with 1.5 mL of artificial seawater (Fig. 5.1f, Table 5.1). Samples for chemical assays were collected on days 1, 5, 10, 15, 30 and 45 (see details below). Soft tissues were recovered from their containers on day 45 using a sterile serological pipette.

Sterile control experiments in duplicate jars with clay/sand that lacked soft tissues showed the evolution of water chemistry in the absence of organic decay. Water sampled from the water column and porewaters were collected on days 1, 5, 10, 15, 30 and 45 for silica, iron (iron (II), total iron) and sulfide assays. Additional samples were collected on day 20 to determine the concentration of dissolved silica.

5.3.2 Water chemistry

Water samples for chemical analyses were sampled 5 days after each replacement of the medium. To collect samples from the water column, 45 mL of the medium was sampled ~3 cm

above the clay/sand surface using a plastic serological pipette and the samples were stored in 50 mL conical centrifuge tubes (VWR International, Radnor, PA, USA). Porewater samples were collected using 5 mL plastic syringes with 18 gauge needles (VWR International, Radnor, PA, USA) ~1.5 cm below the substrate surface (upper substrate) and ~6.5 cm below the substrate surface (lower substrate), unless otherwise stated. All porewater and water column samples were centrifuged aerobically for 10 minutes at 10,000 rotations per minute to separate the particulate matter from the liquid medium. The supernatant was decanted and filtered aerobically through 0.2 μm sterile syringe filters with a polyethersulfone membrane (Acrodisc®, Pall Laboratory, Westborough, MA, USA). A Biotek multiplate reader (Synergy 2, Winooski, VT, USA) was used for colorimetric assays at the following wavelengths: 562 nm (iron), 670 nm (sulfide) and 810 nm (silica). All colorimetric measurements were conducted in triplicate.

Iron - Following the methods of Stookey (1970) for iron(II) and iron(III) determination, 100 μL of ferrozine reagent (3-(2-pyridyl)-5,6-bis(4-phenylsulfonic acid)-1,2,4-triazine, Aldrich #160601, prepared in 1.0 M ammonium acetate solution, CH_3COONH_4, Aldrich #372331) was added to 1 mL of experimental sample and stored at -20°C until analyzed. Standards were prepared from stock solutions of 2.02 mM $FeCl_2$ and 6.16 mM $FeCl_3$ and were diluted with 0.1 M solutions of NaCl; stock solutions were diluted with double distilled water and acidified with 2% HCl by volume. Total iron was determined by reducing iron(III) in samples and standards to iron(II) by adding 150 μL of 1.4 M hydroxalamine hydrochloride ($H_2NOH.HCl$, Aldrich # 379921) and 50 μL of 10 M ammonium acetate to 800 μL of sample/standard. The concentration of iron(III) was calculated by subtracting the previously determined concentration of iron(II) from the total iron concentration in the same sample. The following standard dilution series were

analyzed in tandem with experimental samples: 0, 0.01, 0.03, 0.04, 0.05, 0.10 mM of iron(II) and 0, 0.001, 0.003, 0.005, 0.025, 0.050 mM of iron(III)/total iron.

Several porewater samples exceeded the saturation limit for measurement and were diluted 20x with 0.1 M NaCl water after the addition of ferrozine (Supplementary Table 5.1 and 5.2). The effect of sample dilution on the measurements was determined by assaying the following standard dilution series, diluted 20x with a 0.1 M NaCl solution after the addition of ferrozine: 0.0, 0.10, 0.25, 0.50, 1.01, 1.51 and 2.01 mM of iron(II). The results of undiluted and diluted samples from the same experiments and time points were compared when possible. Dilution had little to no effect on the measured concentration of iron(II) if the original sample/standard contained less than 0.75 mM of iron(II) (Supplementary Fig. 5.1). However, this concentration was underestimated in samples/standards that contained greater than 0.75 mM of iron(II) (Supplementary Fig. 5.1). In contrast, assays consistently underestimated the concentrations of total iron/iron(III) when samples were diluted after the addition of ferrozine. Therefore, all measurements of iron(III) concentrations from samples that were diluted after the addition of ferrozine are lower bounds.

Silica - Silica concentrations were determined following the methods described in Newman et al. (2017). To determine the concentrations of dissolved silica, filtered and frozen samples that had been stored at -20°C in tightly capped 15 mL conical centrifuge tubes were left at room temperature until the liquid had completely thawed. Samples were diluted 10x (unless otherwise specified) in a silica-free, sterile medium. Two standard dilution series were prepared using a concentrated silica standard (J.T. Baker "Dilut-IT" silica standard, 16.64 mM) and added to the silica-free medium: (1) 0, 0.02, 0.04, 0.08, 0.10, 0.21, 0.42 and (2) 0, 0.21, 0.42, 0.83, 1.04, 2.08,

4.16 mM. Silica standards were also diluted 10 times. Potential contamination by silica from the syringe filters (0.2 μm, Acrodisc®, Pall Laboratory, Westborough, MA, USA) and needles (VWR International, Radnor, PA, USA) was determined to be negligible. Only the concentrations of dissolved silica in the water column (~3 cm above the substrate surface) and lower substrate (~6.5 cm below the substrate surface) were measured because of limited sample volume.

Sulfide – Dissolved sulfide concentrations (H_2S, HS^- and S^{2-}) were determined by adding 1 mL of 0.05 M zinc acetate ($Zn(CH_3COO)_2 \cdot 2H_2O$, Aldrich #383058, prepared in double distilled water) to 200 μL of sample, using the modified method of Cline (1969). Samples were stored at 4°C until measurement. The 0.1 M stock solution of Na_2S was prepared by adding 0.1 M of sodium sulfide nonahydrate ($Na_2S \cdot 9H_2O$, Aldrich #431648) to anaerobic double distilled water that had been allowed to boil at 100°C. The solution was transferred to a hermetically sealed container and the headspace of this bottle was flushed with CO_2:N_2 (20:80, v/v) using standard anaerobic techniques. Standards were prepared by diluting 100 mM Na_2S with 0.05 M zinc acetate (to 0.005, 0.01, 0.02, 0.05 and 0.1 mM concentrations). Before the colorimetric assay, 40 μL of diamine reagent was added to all samples and standards. This reagent included 1.6 g N,N dimethyl-p-phenyldiamine sulfate salt ($(CH_3)_2NC_6H_4NH_2 \cdot H_2SO_4$], Aldrich #186384) and 4 g of anhydrous ferric chloride ($FeCl_3$, Aldrich #157740) dissolved in 100 ml of 6 N hydrochloric acid.

pH - The pH of the water column and porewater was measured every 5 to 10 days using a portable pH meter (WTW 3A30110 pH 1970i, Wilhelm, Germany) and/or pH test strips

(ColorpHast pH Test Strips 0-14, Millipore). The pH meter was used for all water column samples and the pH of all porewater samples was measured using pH test strips. When possible, pH values derived from the pH test strips and pH meter were compared for consistency.

5.3.3 Scanning electron and transmission electron microscopy

To identify the composition and distribution of minerals coating scallops, we used scanning electron and transmission electron microscopy. Samples were prepared for SEM by fixing them in 2.5% glutaraldehyde in a 0.1 M sodium cacodylate buffer with 0.1% $CaCl_2$ (pH = 7.4). After 3 to 5 days, samples were removed from this buffer and rinsed with a 0.1 mM sodium cacodylate buffer solution. Following this, samples were rinsed 6 times with double distilled water and then dehydrated using the following ethanol-water drying series: 30%, 50%, 70%, 80%, 90%, 100%, 100%, 100%, with 20 min steps. Samples were allowed to air dry (for one day) and dehydrated tissues were placed on carbon tape and coated with gold and palladium at the Keck Facility (Whitehead Institute, MIT, Cambridge, MA, USA). Samples were imaged on a Zeiss Supra scanning electron microscope with a secondary electron detector at the Center for Nanoscale Systems (Harvard University, Cambridge, MA, USA). We determined elemental composition in regions of interest using an electron-dispersive X-ray spectrometer operating at 10 kV.

To prepare samples for TEM analyses, pre-frozen scallop tissues (-80°C) were partially thawed at room temperature for 5 to 10 min and a small piece of tissue (~2 mm) was removed from the scallop with a sterile, plastic pipette tip. This tissue was then placed in a 1.7 mL microcentrifuge tube (VWR International, Radnor, PA, USA), suspended in filter-sterilized double distilled water (Arodisc® Syringe Filters with Supor® Membrane, Pall Laboratory, Port Washington, NY, USA) and shaken by hand for 1 min. Two µL of the suspended solution was

placed on a LC-200 grid (Electron Microscopy Sciences, Cat # LC-200-Cu, PA, USA) for analysis. Scallop tissues were imaged with a JEOL 2010F transmission electron microscope (TEM, JOEL 2010F, JOEL, CA, USA). Gold standard was used as a reference for SAED determination of the sample. The high-angle annular dark field detector (HAADF, Gatan, CA, USA) for atomic resolution scanning electron transmission microscopy in free-lens control mode (STEM) and energy dispersive spectrometer (EDS, Bruker silicon drift detector SDD, Bruker, MA, USA) enabled elemental analysis at nanoscale resolution. Images were taken using a digital camera (Gatan Orius, Gatan, CA, USA) for TEM and STEM mode. SAED patterns were imaged using Gatan digiscan unit (Gatan, CA, USA). TEM, STEM and SAED images were recorded and treated using Gatan digital micrograph software (Gatan, CA, USA). EDS spectra were recorded and treated using INCA program (Oxford instruments, UK).

5.3.4 X-ray microprobe

To identify the spatial distributions and oxidation states of elements coating scallop surfaces, we analyzed soft tissues at the Advanced Light Source (beamline 10.3.2, Berkeley, CA, USA) using micro-focused X-ray fluorescence (μXRF) mapping and iron and sulfur K-edge X-ray adsorption near edge structure (μXANES) spectroscopy, respectively. We analyzed scallops incubated for 45 days in the presence and absence of kaolinite or cyanobacteria. To identify changes in mineral chemistry that preceded the final time point, samples incubated for 30 days with and without cyanobacteria were also analyzed and compared with tissues incubated for 45 days under identical conditions. Frozen samples (-80˚C) were thawed and air-dried for ~1 h before analysis. These samples were attached to the non-sticky side of Kapton® polyimide tape (DuPont, Hayward CA, USA). XRF elemental maps were generated using a 6 x 6 μm beam spot size and

XANES spectra were generated using a beam spot size of 12 x 3 μm. Fluorescence data were recorded using a germanium (Ge) solid state detector (Canberra, ON, Canada). For sulfur calibration, a gypsum standard was used using the maximum of the main peak at 2482.75. XRF counts were collected for sulfur, iron, calcium, potassium, chlorine, silica and phosphorous. Sulfur and iron K-edge XANES spectra were acquired on spots of interest. The 10.3.2 iron standard database was used to identify iron-bearing minerals.

5.4 Results

5.4.1 Visual observations

Soft tissues were buried in clay or sand for up to 45 days to identify factors that facilitate or inhibit decay. The surface of the artificial seawater medium was in constant contact with the atmosphere, but during the first two weeks of incubation, the degradation of soft tissues led to a decrease in oxygen concentrations in the porewaters which remained anoxic for the remainder of the experiment (Supplementary Fig. 5.2). The overlying solution became cloudy (Fig. 5.2) and malodorous due to the release of degraded organic matter into the water column. Dark grey to black patches formed around soft tissues during the first 15 to 30 days of incubation. The extent of these patches increased with time in samples that underwent complete decay. These dark patches were rarely present in jars with scallops that underwent the least amount of decay (Fig. 5.2, Supplementary Fig. 5.3). Thus, the formation of dark patches was an indicator of extensive anaerobic heterotrophic activity and conditions that were less conducive to preservation. When scallops were buried in kaolinite, 1 to 2 mm-thick grey patches appeared in the clay/sand around all tissues during the first 15 days of incubation (Fig. 5.2). However, these patches were not indicative of extensive decay. The substrates in sterile control experiments that lacked soft

tissues did not change color, indicating that these environments remained sterile and aerobic (see supplementary methods, results and figures for oxygen measurements).

In experiments with cyanobacteria, microbial mats began to form after the inoculation of cyanobacteria. However, by day 15, the cells had detached from the surface of the substrate and lost much of their green pigment. This indicated suboptimal conditions for cyanobacterial growth. In fact, full microbial mats never formed on the substrate surface in spite of repeated inoculations.

Wet scallops were weighed before burial and after removal from the substrate to quantify decay during incubation. Between 16.3 to 100% of the initial weight was lost by day 30 and 29.7 to 100% by day 45 (Table 5.2). Containers in which scallops lost less than 50% of their initial weight after 30 days consistently yielded well-preserved scallops on day 45 (Table 5.2). In contrast, when samples lost more than 90% of the weight by day 30, the tissues decayed completely by day 45 (Table 5.2). Only one out of three specimens were successfully exhumed by the end of the experiment when scallops were buried in sand in the presence or absence of cyanobacteria and illite. In contrast, when scallops were buried in kaolinite, two out of three specimens were recovered (see Chapter 4 of this Thesis, Table 5.2). The measured weight loss was consistent with the chemical evolution of the solution (see below) as well as with the continued release of organic material into the overlying solution in spite of the weekly medium replacements.

All soft tissues decayed during burial (Fig. 5.3). Scanning electron micrographs (SEMs) of soft tissues before inoculation revealed intact muscle fibers that were distributed as parallel bands and surrounded by connective tissues (Fig. 5.3a). In contrast, scallops exhumed on day 45

had lost this banding, indicating extensive decay (Fig. 5.3b). We did not notice differences in muscle morphologies between samples collected on days 30 and 45.

5.4.2 Chemical changes on the surface of the scallop tissues

We analyzed the elemental composition of soft tissues by SEM-EDS and TEM-SAED to identify chemical changes occurring at the tissue surface during decay. Scallop tissues before incubation were composed of carbon, oxygen, nitrogen, chlorine, magnesium, phosphorus, sodium and sulfur (Fig. 5.3a, Fig. 5.4a, b). The surfaces of samples that had been incubated in the presence of kaolinite or illite powder also accumulated silica, aluminum and potassium in the form of micron-sized clay minerals (Fig. 5.3c, 5.4, Chapter 4 of this Thesis). Scallops incubated in kaolinite were coated by authigenic and trapped minerals (see Chapter 4 of this Thesis) that were visible by SEM. These samples also contained iron-rich organic sulfur groups that were not found in the scallop before incubation. Scallops incubated in the presence of illite included calcium-, iron-, magnesium-, potassium- and/or sodium-rich aluminosilicates (Fig. 5.3c). These minerals were similar in composition to the sterile illite powder (Fig. 5.3d). Thus, a sediment-derived component could not be excluded. Scallops incubated in silica sand contained both iron (II) and iron (III)-rich minerals (Fig. 5.4).

5.4.3 Concentrations of ions and dissolved silica in solution

Changes in the concentrations of dissolved iron(II), iron(III), silica and sulfide documented major chemical patterns during soft tissue decay and tracked heterotrophic activity in the substrates. When concentrations of ions and dissolved silica in the porewater were detectable, they were typically the highest in the lower substrate (~6.5 cm below the surface of the

substrate), reached intermediate values in the upper substrate (~1.5 cm below the surface of the substrate) and were the lowest in the water column (~3 cm above the surface of the substrate) (Supplementary Tables 5.1-5.4). Sterile control experiments provided baseline values for understanding water chemistry in the absence of soft tissues. The concentrations of porewater ions and silica in the absence of soft tissues were much lower (Supplementary Tables 5.1-5.4). Thus, scallops were used as the organic electron donor and the resulting vertical gradient in ion and silica concentrations was driven by the decay of buried tissues.

Microbial reduction of iron released abundant iron(II) into the porewaters (Supplementary Table 5.1); in the presence of soft tissues, concentrations of iron(II) ranged from below the limit of detection to 14.11 μM in the water column, 0.93 to >1102.82 μM in the upper substrate and 1.81 to >1167.35 μM in the lower substrate (Fig. 5.5, Supplementary Table 5.1). In the absence of scallop tissues, iron(II) values were orders of magnitude lower, ranging from below the limit of detection to 0.02 μM in the water column, below the limit of detection to 0.27 μM in the upper substrate and below the limit of detection to 0.27 μM in the lower substrate (Supplementary Table 5.1). The concentration of iron(II) in all cultures was the highest during the first 30 days of incubation and declined during the last 15 days, suggesting a decline in microbial iron reduction or the removal of reduced iron by mineral adsorption/precipitation (Supplementary Table 5.1). Soft tissues in cultures with the highest concentrations of porewater iron(II) (>1000 μM) experienced the greatest amount of decay (Fig. 5.5, Supplementary Table 5.1). This would be expected for conditions most conducive to anaerobic organic decay resulting from iron(II) or sulfate reduction.

The oxidative recycling of iron also increased concentrations of dissolved iron(III) to at least an order of magnitude above those measured in substrates that lacked soft tissues

(Supplementary Table 5.2). In experiments with scallop tissues, concentrations of iron(III) ranged up to 8.8 μM in the water column, 188.50 μM in the upper substrate and 292.54 μM in the lower substrate (Supplementary Table 5.2). Concentrations of iron(III) in sterile control experiments ranged from 0.10 to 0.79 μM in all samples. This indicates that iron(III) was released in the presence of soft tissues.

Concentrations of dissolved silica in the initial (sterile) medium ranged from 0.06 to 0.19 mM; those in the water column ranged from 0.05 to 0.97 and those in the porewater ranged from 0.35 to 2.39 mM (Fig. 5.5, Supplementary Table 5.3). Only in the presence of soft tissues did concentrations of dissolved silica rise above 0.7 mM in the porewater (Supplementary Table 5.3). The water column was undersaturated with respect to the precipitation of amorphous silica (<1.7 mM) in all experiments. However, porewaters in three experiments were close to or above the saturation with respect to amorphous silica during the first 20 days of incubation (Supplementary Table 5.3). The porewater samples in other experiments were undersaturated with respect to silica. When dissolved silica concentrations in the porewater were lower than 1.7 mM, the scallop tissues experienced the least amount of decay. Those in culture jars where we measured the highest concentrations of dissolved silica were completely degraded.

The water column did not contain detectable dissolved sulfide, but micromolar concentrations of sulfide in the porewaters indicated active microbial sulfate reduction in the presence of soft tissues (Supplementary Table 5.4). Sulfide concentrations in jars that contained kaolinite were lower during the first 30 days than those in silica sand. With the exception of a single replicate in the silica sand experiment (1.95 μM sulfide; Supplementary Table 5.4), sulfide became undetectable by day 45 in all porewaters. The initial, sterile medium contained 7.9 mM of sulfate. Thus, concentrations of sulfide less than 7.9 mM in most experimental media

(Supplementary Table 5.4) indicated that microbial sulfate reduction did not consume all available sulfate.

5.4.4 pH

The pH of the water column was higher than that in the clay/sand substrates. In sterile control experiments that lacked soft tissues, pH ranged from 8.0 to 8.2 in the water column and 6.5 to 7.5 in the upper and lower substrates (Supplementary Table 5.5) for both kaolinite and sand substrates. pH values generally were lower when scallops were present and ranged from 6.98 to 8.14 in the water column, 4.5 to 7.3 in the upper substrate and 4.5 to 7.5 in the lower substrate (Supplementary Table 5.5). However, pH values in replicate experiments that yielded recoverable samples after 45 days were similar to those in which soft tissues had undergone complete decay by that time point.

5.4.5 X-ray microprobe

Chemical changes occurred on the surfaces of soft tissues during the 45-day incubation interval. X-ray fluorescence elemental mapping showed that sulfur was present in soft tissues before and after burial (Fig. 5.6). Some iron was present on the tissue surfaces before burial, but the abundance of this element increased with incubation time in all experiments (Fig. 5.6), suggesting the accumulation of iron during decay. Iron K-edge XANES spectra acquired from select spots on the tissue surfaces at the Advanced Light Source (Beamline 10.3.2, Berkeley, CA, USA) offered information about the redox states of iron coating soft tissues. Samples incubated in kaolinite contained reduced iron that best matched the following standards in the 10.3.2 iron standard database: basalt glass, iron sulfate and iron-rich clay (Chapter 4 of this Thesis). Samples

exhumed from silica sand matched with the following standards, revealing a potential for the presence of both reduced and oxidized iron: iron sulfates, iron oxides and iron sulfides (10.3.2 iron standard database, Fig 5.6). Sulfur K-edge XANES suggested the presence of metal-bound sulfates coating soft tissues as well as organic-bound sulfur (Fig. 5.6). Additional investigations of the iron K-edge energies will be necessary to definitively classify the oxidation states of minerals coating soft tissues.

5.5 Discussion

5.5.1 Iron promotes soft tissue preservation in silica-rich environments

Hypotheses regarding the formation of exceptionally preserved fossils in siliciclastic environments often focus on the role of silica- and/or iron-rich minerals in fossilization processes (e.g., Callow and Brasier, 2009; Petrovich, 2001; Tarhan et al. 2016; Gehling et al. 1999; McMahon et al. 2016). Recent taphonomic investigations have advanced our understanding of decay inhibition in modern soft tissues by hypothesizing the role of low pH and aluminum in the cross-linking of organic compounds (Wilson and Butterfield, 2014) as well as the role of iron(II) and aluminum (III) in the inhibition of aerobic microbial growth (McMahon et al., 2016). However, the effects of microbial processes that control the cycling of dissolved iron and silica around soft tissues remain unclear.

Our experiments show that the early decay of soft tissues under anaerobic and mixed aerobic-anaerobic conditions stimulates the release of silica from sedimentary minerals into the solution. Decay processes have been shown to increase the solubility of quartz minerals in seawater, due to the mobilization of silica by dissolved organic compounds (Bennet and Siegel, 1987) and active redox cycling of iron in the presence of oxygenated surface waters (Morris and

Fletcher, 1987). However, it is unclear how and if the latter process applies to fine-grained sediments because iron cycling in the current experiment did not have a clear effect on the release of silica when kaolinite was present. Taken together, these processes may explain why we detected the highest concentrations of dissolved silica and iron in experiments associated with the most decay, moderate concentrations in those associated with the least decay and the lowest concentrations in the absence of soft tissues (Fig. 5.5, Supplementary Tables 5.1, 5.3).

Our observations do not support some previously proposed models of fossilization which suggest that seawaters saturated with respect to amorphous silica led to Ediacaran-style preservation of macrofossils (e.g., Callow and Brasier, 2009; Tarhan et al., 2016). For example, Tarhan et al. (2016) identify the formation of silica-rich cements around macrofossils in a single locality, the Ediacara Member of South Australia. They suggest that the formation of these siliceous veneers facilitated the preservation of soft-bodied organisms, but the universality of their proposed mechanism remains to be determined. Our experiments show that although high concentrations of dissolved silica may have accumulated within weeks around decaying soft tissues buried in clay or sand, neither saturated waters nor the precipitation of amorphous silica around soft tissues were key to preservation. Instead, our findings are in line with those of Michalopolous and Aller (2004), who document the precipitation of iron-rich, smectite-type minerals on siliceous surfaces in clay- and iron-rich environments. Our study expands these observations from siliceous diatoms and deltaic muds (Michalopoulos and Aller, 2004) to animal soft tissues and kaolinite-rich sandy environments. Thus, we suggest that in environments where dissolved silica is not a limiting factor (i.e., the Ediacaran/early Cambrian seafloor), iron-rich veneers will likely play a critical role in preservation processes.

The link between metal-based microbial metabolisms and the preservation of organic material has been widely explored in the literature (e.g., Konhauser et al., 2001; Michalopoulos and Aller, 2004; Lützow et al., 2006; Lalonde et al., 2012). For example, Petrovich (2001) hypothesized a multi-step process in soft tissue preservation involving (1) the adsorption of iron(II) (or other metals) from solution onto the surfaces of soft tissues, (2) the inhibition of heterotrophic enzymatic activities through the preferential binding of iron(II) to reactive sites on the soft tissues and (3) the formation of iron(II)-rich biominerals which promote the fossilization of organic material. Our μXANES analyses support Petrovich (2001) by demonstrating the formation of minerals that contain iron(II) and iron(III) on soft tissues recovered after 30 and 45 days (Fig. 5.6). These findings are largely consistent with the results of Michalopolous and Aller (2004), which highlight the role of bacterial iron(III) reduction in the rapid formation (months to years) of iron(II)-rich aluminosilicate minerals. Our findings show that even faster formation of authigenic mineral veneers is possible in the presence of active microbial reduction of iron, possibly through tanning processes which polymerize organic matter in the presence of metals. The presence of iron-bound organic sulfur in the interior of tissue samples (Fig. 5.4) may have served this role. However, the highest concentrations of porewater iron(II) (>1000 μM) are indicative of extensive decay that outpaced preservation.

5.5.2 The effect of clay minerals on preservation

We observed the delayed decay of soft tissues in the presence of kaolinite, but not in the presence of illite, although clay particles adhered to all scallops that were buried in clay minerals (Fig. 5.3c, Chapter 4 of this Thesis). Kaolinite binds to scallop surfaces, facilitates the precipitation of authigenic minerals and forms <0.5 mm-thick protective veneers around tissues

(Chapter 4 of this Thesis). However, when scallops were buried in the presence of a thin layer of illite, we did not observe similar veneers on the tissue surfaces (Supplementary Fig. 5.3). This likely occurred because only one side of the scallop was in physical contact with the illite grains. Therefore, a continuous veneer composed of clay particles could not form around the entire scallop, leaving large areas of tissue exposed to microorganisms. Secondly, illite is a cation-rich clay and may not have the same preservative properties as kaolinite (Wilson and Butterfield, 2014; McMahon et al., 2016; Naimark et al., 2016). Although illite is commonly associated with well-preserved soft-bodied fossils in the rock record, it is often attributed to the secondary replacement of authigenic minerals during diagenesis (e.g., Gabbott et al., 2001). Thus, the role of illite in preservation remains to be elucidated. Additional experiments should test the ratio of tissue to clay minerals that is required to preserve soft tissues and determine if visible veneers form around scallops buried in more illite than what was tested by the current study.

5.5.3 The balance between microbial activity and decay delay

Heterotrophic microbial activity plays an important, if not paramount role in determining the fate of soft tissues during early diagenesis. Decay is thought to be facilitated by heterotrophic microorganisms both endogenous to the soft tissues (e.g., Briggs et al., 1993; Eagan et al., 2017) and from external sources (Briggs et al., 1993). In the current experiment, we attempted to sterilize scallops by soaking them in ethanol before incubation. However, the rapid growth of microbial communities in the clay and sand grains around the soft tissues (within 10 to 15 days) across multiple experiments suggests that such sterilization methods were not effective and that microbial communities grew. In natural environments, macroscopic organisms become fossilized in sediments that are teeming with bacteria and organisms which undergo processes of

preservation host microbial consortia even before death. Thus, taphonomic experiments must at least consider the activity of endogenous microorganisms if natural conditions are to be replicated in the laboratory.

The release of iron(II) and sulfide into porewaters demonstrated the presence of microbial iron and sulfate reduction. At the same time, concentrations of dissolved iron(III) in the presence of soft tissues were greater than those found in the sterile medium and clay or sand substrates without buried tissues. This suggests that the microbial oxidation of iron(II) and the reduction of iron(III)/sulfate were simultaneously occurring in our system. It is likely that oxidation occurred near the surface of the substrate, where oxygen was present and iron and sulfate reduction took place around the soft tissues that acted as localized sources of organic electron donors. Many previous studies have focused on the role of sulfate reduction in the formation of Burgess Shale-type fossils (Gabbott et al., 2004; Gaines et al., 2008, 2012). Gaines et al. (2012) suggested that a permeability barrier limited sulfate diffusion into early Cambrian porewaters, thereby decreasing sulfate reduction around carcasses and inhibiting decay. However, in the current experiments, sulfate reduction had no observable effect on soft tissue preservation. Instead, we show that microbial metabolisms and abiotic processes involved in the redox cycling of iron had the greatest immediate effect on soft tissue decay/decay delay. Flocculation and sludge studies have similarly demonstrated the importance of iron in the preservation of organic matter (Park et al., 2006; Park and Novak, 2007).

The presence of active iron redox cycling provides another parallel between modern clay-forming environments such as the actively mobilized layers of mud in river deltas (Michalopoulos and Aller, 1995, 2004) and our experiments. Oxidative recycling of reduced iron may ensure a continuous supply of the electron acceptor for organic decay. The presence of

iron(III) coating sand grains in the original, sterile substrate and the release of millimolar concentrations of iron(II) within the first two weeks after burial suggest that the availability of iron did not limit microbial iron reduction in quartz-rich sand, regardless of whether clay minerals were added or not. However, the importance of the recycling of iron(II) released by microbial processes for the preservation of soft tissues remains to be tested by comparing tissue preservation in the presence and absence of an oxic water column. In any case, the proximity of the oxygenated water column to the reduced iron in the sediments and the wave- or current-driven exchange between the water column and porewaters (Bosak et al., 2013) is consistent with the physical and redox conditions at the sediment-water interface during the Ediacaran/early Cambrian (Callow and Brasier, 2009), and the presence of oxygen-consuming macroscopic organisms at the sediment surface during the Ediacaran Period (e.g., Runnegar, 1982).

The current study could not directly evaluate the effect of "microbial death masks" composed of cyanobacterial mats that seal the soft tissues (Gehling, 1999), but does not support the hypothesis of subsequent precipitation of iron sulfide phases within such masks (Gehling, 1999). Our experimental conditions instead revealed that cyanobacteria were not able to form extensive mats over the buried scallops. Instead, cyanobacteria grew as clumps and their mass decreased in time despite repeated inoculations throughout the incubation process (Supplementary Fig. 5.3a). We attribute this to the unfavorable conditions for cyanobacterial growth associated with extensive organic decay, including low porewater pH (4 to 6, Supplementary Table 5.5) and an organic-rich and opaque water column (Fig. 5.2). These experiments provide a realistic model for cyanobacterial growth in the presence of decomposing tissues and suggest that the local environments around decaying soft tissues are hostile to the establishment and extensive growth of photosynthetic microbial mats. However, scenarios in

which more than a cm of sediment separates the decaying soft tissues from the cyanobacteria could reduce the negative effects of decay on microbial mat growth. Future work should explore the presence of thicker and/or less porous sediments which would protect microorganisms from the negative effects of decay.

5.5.4 Importance of the extent and timing of soft tissue decay

Preliminary stages of fossilization require some decay (Briggs, 2003), while excessive decay is of course disadvantageous for preservation (Briggs et al., 1993; Briggs and Kear, 1994; Briggs, 2003). Thus, a window of time must exist within which initial decay enables the replication of soft tissues by minerals, but extensive decay is delayed to prevent the complete deterioration of the macroscopic organism. The samples in our experiments lost between less than 20 to 100% of their initial weight, and in no experiment was decay completely inhibited. The organic decay provided the electron donors for iron and sulfate reduction. This released iron(II) that was subsequently incorporated into mineral veneers. The timing of decay was critical to preservation; experiments in which the decay of soft tissues was delayed during the first 30 days of incubation consistently yielded the best preserved scallops on day 45 (Supplementary Fig. 5.3, Table 5.2). In contrast, partially preserved or completely decayed scallops on day 30 had undergone complete decay by day 45 (Supplementary Fig. 5.3, Table 5.2). Environmental variables that track organic decay include high concentrations of iron(II)/dissolved silica and the formation of black patches in the clay/sand surrounding soft tissues during the first two weeks after burial (Fig. 2, Supplementary Fig. 5.3, Supplementary Tables 5.1-5.4). Taken together, this suggests that environmental and biological conditions during the first month of burial are most important in fossilization processes.

5.5.5 A model for decay delay and implications for the fossil record

The siliciclastic fossil record of the Ediacaran and early Cambrian contains abundant and well-preserved fossil impressions. Our study explored the delicate balance between microbial decay and preservation and its findings establish the following model for soft tissue preservation:

(1) Soft-bodied organisms with endogenous communities of microorganisms are buried in silica sand. Burial is important for preservation and endogenous bacteria facilitate the initial decay of soft tissues. Within the first 10 to 15 days of burial, heterotrophic activity contributes to the development of porewater anoxia, an increase in the concentrations of iron(II)/sulfide/dissolved silica and a reduction in pH. These hostile conditions hinder the establishment of photosynthetic mats at the sediment-water interface. In the absence of sealing microbial mats, the sediment, porewater and tissues remain in contact with the water column. This enables iron reduction, the formation of anoxic zones around soft tissues and iron redox cycling closer to the sediment/water interface.

(2) High concentrations of porewater iron(II) and dissolved silica are indicative of the complete decay of soft tissues. However, moderate concentrations of these ions in the sediments are necessary for the formation of protective aluminosilicate veneers around soft tissues. A continuous supply of iron(III) is also necessary to facilitate the dissimilatory reduction of iron(III) to iron(II) and the formation of iron(II)-rich minerals on tissue surfaces.

(3) During the first month of burial, fine particles from the sediment attach to the surfaces of soft tissues. Extensive mineral veneers form around tissues only when specimens are completely buried by clay. In this case, authigenic minerals can form between

sedimentary fine particles within months. This creates a protective layer around the tissues and reduces microbial access to tissue surfaces. Other environmental factors (e.g., the presence/absence of heterotrophic microorganisms, the availability of iron, the availability of aluminum and silica) are of paramount importance to preservation.

(4) The first 15 to 30 days after the burial are critical for the preservation of soft tissues in siliciclastic settings. Organisms and tissues that decay minimally (<40% loss of original mass) during this interval are more likely to become incorporated into the fossil record because it is during this window of time that protective minerals form on soft tissues through processes of precipitation (see Newman et al., 2016). Tissues that are stabilized by iron (likely through tanning processes) during the 30-day window of decay delay are more likely to become replicated by minerals at a later point during diagenesis; this would facilitate the formation of three-dimensional fossil impressions.

5.6 Conclusions

Soft-bodied organisms were commonly preserved in Ediacaran and early Cambrian sandstones and siltstones. A number of factors enabled the preservation of soft tissues in taphonomic experiments including, (1) the presence of clay minerals such as kaolinite that act as physical barriers to heterotrophic microorganisms and provide nucleation sites for the precipitation of authigenic aluminosilicates, (2) the activity of anaerobic heterotrophic microorganisms including iron(III)-reducing microorganisms that release iron(II) and silica into porewaters around the soft tissues and (3) the formation of protective iron-rich mineral veneers (e.g., clay minerals) around soft tissues. The decay of soft tissues has to be delayed within the first month of burial. Soft tissues that undergo minimal decay (<40% loss of mass) during this timeframe are most likely to

be incorporated into the siliciclastic fossil record. Similar factors likely facilitated the formation of soft tissue impressions in coarse-grained siliciclastic sediments during the Ediacaran and contributed to the exceptional preservation of soft-bodied organisms in clay-rich sediments at other times during Earth's history.

5.7 References

Bennet, P., Siegel, D.I., 1987. Increased solubility of quartz in water due to complexing by organic compounds. Nature 326, 684–686. doi:10.1038/326684a0.

Bosak, T., Knoll, A.H., Petroff, A.P., 2013. The meaning of stromatolites. Annu. Rev. Earth Planet. Sci. 41, 21–44. doi:10.1146/annurev-earth-042711-105327.

Briggs, D.E.G., 2003. The role of decay and mineralization in the preservation of soft-bodied fossils. Annu. Rev. Earth Planet. Sci. 31, 275–301. doi:10.1146/annurev.earth.31.100901.144746.

Briggs, D.E.G., Kear, A.J., 1994. Decay and mineralization of shrimps. Palaios 9, 431-456. doi:10.2307/3515135.

Briggs, D.E.G., Kear, A.J., Briggs, D.E.G., Kear, A.J., 1993. Decay and preservation of polychaetes: Taphonomic thresholds in soft-bodied organisms. Paleobiol. 19, 107–135.

Callow, R.H.T., Brasier, M.D., 2009. Remarkable preservation of microbial mats in Neoproterozoic siliciclastic settings: Implications for Ediacaran taphonomic models. Earth-Science Rev. 96, 207–219. doi:10.1016/j.earscirev.2009.07.002.

Cline, J.D., 1969. Spectrophotometric determination of hydrogen sulfide in natural waters. Limnol. Oceanogr. 14, 454–458. doi:10.4319/lo.1969.14.3.0454.

Eagan, J.L., Andrews, M.E., Pearson, R.L., Turner, F.R., Raff, E.C., Raff, R.A., 2017. Identification and modes of action of endogenous bacteria in taphonomy of embryos and larvae. Palaios 32, 206–217. doi:10.2110/palo.2016.071.

Fischer, J., Quentmeier, A., Gansel, S., Sabados, V., Friedrich, C.G., 2002. Inducible aluminum resistance of *Acidiphilium cryptum* and aluminum tolerance of other acidophilic bacteria. Arch. Microbiol. 178, 554–558. doi:10.1007/s00203-002-0482-7.

Gabbott, S.E., Hou, X.-G., Norry, M.J., Siveter, D.J., 2004. Preservation of early Cambrian animals of the Chengjiang biota. Geology 32, 901–904. doi:10.1130/G20640.1.

Gabbott, S.E., Norry, M.J., Aldridge, R.J., Theron, J.N., 2001. Preservation of fossils in clay minerals; a unique example from the Upper Ordovician Soom Shale, South Africa. Proc. Yorksh. Geol. Soc. 53, 237–244. doi:10.1144/pygs.53.3.237.

Gaines, R.R., Briggs, D.E.G., Yuanlong, Z., 2008. Cambrian Burgess Shale-type deposits share a common mode of fossilization. Geology 36, 755–758. doi:10.1130/G24961A.1.

Gaines, R.R., Hammarlund, E.U., Hou, X., Qi, C., Gabbott, S.E., Zhao, Y., Peng, J., Canfield, D.E., 2012. Mechanisms for Burgess Shale-type preservation. Proc. Natl. Acad. Sci. U. S. A. 109, 5180–5184. doi:10.1073/pnas.1.

Gehling, J.G., 1999. Microbial mats in terminal Proterozoic siliciclastics: Ediacaran death masks. Palaios 14, 40–57. doi:10.2307/3515360.

Hagadorn, J.W., Bottjer, D.J., 1997. Wrinkle structures: Microbially mediated sedimentary structures common in subtidal siliciclastic settings at the Proterozoic-Phanerozoic transition. Geology 25, 1047–1050.

Konhauser, K.O., Lalonde, S. V, Amskold, L., Holland, H.D., 2007. Was there really an Archean phosphate crisis? Science 315, 1234. doi:10.1126/science.1136328.

Konhauser, K.O., Phoenix, V.R., Bottrell, S.H., Adams, D.G., Head, I.M., 2001. Microbial-silica interactions in Icelandic hot spring sinter: Possible analogues for some Precambrian siliceous stromatolites. Sedimentology 48, 415–433.

Lalonde, K., Mucci, A., Ouellet, A., Gélinas, Y., 2012. Preservation of organic matter in sediments promoted by iron. Nature 483, 198–200. doi:10.1038/nature10855.

Liu, A.G., 2016. Framboidal pyrite shroud confirms the "death mask" model for moldic preservation of Ediacaran soft-bodied organisms. Palaios 31, 259–274.

Lützow, M. v., Kögel-Knabner, I., Ekschmitt, K., Matzner, E., Guggenberger, G., Marschner, B., Flessa, H., 2006. Stabilization of organic matter in temperate soils: Mechanisms and their relevance under different soil conditions – a review. Eur. J. Soil Sci. 57, 426–445.

Maliva, R.G., Knoll, A.H., Siever, R., 1989. Secular change in chert distribution: A reflection of evolving biological participation in the silica cycle. Palaios 4, 519–532. doi:10.2307/3514743.

Mapstone, N.B., McIlroy, D., 2006. Ediacaran fossil preservation: Taphonomy and diagenesis of a discoid biota from the Amadeus Basin, central Australia. Precambrian Res. 149, 126–148. doi:10.1016/j.precamres.2006.05.007.

McMahon, S., Anderson, R.P., Saupe, E.E., Briggs, D.E.G., 2016. Experimental evidence that clay inhibits bacterial decomposers: Implications for preservation of organic fossils. Geology 44, 867–870. doi:10.1130/G38454.1.

Michalopoulos, P., Aller, R.C., 2004. Early diagenesis of biogenic silica in the Amazon delta: Alteration, authigenic clay formation, and storage. Geochim. Cosmochim. Acta 68, 1061–1085. doi:10.1016/j.gca.2003.07.018.

Michalopoulos, P., Aller, R.C., 1995. Rapid clay mineral formation in Amazon Delta sediments: Reverse weathering and oceanic elemental cycles. Science 270, 614–617. doi: 10.1126/Science.270.5236.614.

Morris, R.C., Fletcher, A.B., 1987. Increased solubility of quartz following ferrous-ferric iron reactions. Nature 330, 558–561. doi:10.1038/330558a0.

Naimark, E., Kalinina, M., Shokurov, A., Boeva, N., Markov, A., Zaytseva, L., 2016. Decaying in different clays: Implications for soft-tissue preservation. Palaeontology 59, 583–595. doi:10.1111/pala.12246.

Newman, S.A., Klepac-Ceraj, V., Mariotti, G., Pruss, S.B., Watson, N., Bosak, T., 2017. Experimental fossilization of mat-forming cyanobacteria in coarse-grained siliciclastic sediments. Geobiology 15, 484–498. doi:10.1111/gbi.12229.

Newman, S.A., Mariotti, G., Pruss, S., Bosak, T., 2016. Insights into cyanobacterial fossilization in Ediacaran siliciclastic environments. Geology 44, 579–582. doi: 10.1130/G37791.1.

Noffke, N., Gerdes, G., Klenke, T., Krumbein, W., 2001. Microbially induced sedimentary structures — A new category within the classification of primary sedimentary structures. J. Sediment. Res. 71, 649–656.

Park, C., Muller, C.D., Abu-Orf, M.M., Novak, J.T., 2006. The effect of wastewater cations on activated sludge characteristics: Effects of aluminum and iron in floc. Water Environ. Res. 78, 31–40. doi:10.2175/106143005X84495.

Park, C., Novak, J.T., 2007. Characterization of activated sludge exocellular polymers using several cation-associated extraction methods. Water Res. 41, 1679–1688. doi:10.1016/j.watres.2007.01.031.

Petrovich, R., 2001. Mechanisms of fossilization of the soft-bodied and lightly armored faunas of the Burgess Shale and of some other classical localities. Am. J. Sci. 301, 683–726. doi:10.2475/ajs.301.8.683.

Pettersson, A., Hällbom, L., Bergman, B., 1986. Aluminium uptake by *Anabaena cylindrica*. J. Gen. Microbiol. 132, 1771–1774.

Pettersson, A., Hällbom, L., Bergman, B., 1988. Aluminum effects on uptake and metabolism of phosphorus by the cyanobacterium *Anabaena cylindrica*. Physiol. Plant. 86, 112–116.

Runnegar, B., 1982. Oxygen requirements, biology and phylogenetic significance of the late Precambrian worm Dickinsonia, and the evolution of the burrowing habit. Alcheringa An Australas. J. Palaeontol. 6, 223–239.

Siever, R., 1992. The silica cycle in the Precambrian. Geochim. Cosmochim. Acta 56, 3265–3272. doi:10.1016/0016-7037(92)90303-Z.

Stookey, L.L., 1970. Ferrozine - A new spectrophotometric reagent for iron. Anal. Chem. 42, 779–781. doi:10.1021/ac60289a016.

Tarhan, L.G., Hood, A.v.S., Droser, M.L., Gehling, J.G., Briggs, D.E.G., 2016. Exceptional preservation of soft-bodied Ediacara Biota promoted by silica-rich oceans. Geology 44, 951–954. doi:10.1130/G38542.1.

Wilson, L.A., Butterfield, N.J., 2014. Sediment effects on the preservation of Burgess Shale-type compression fossils. Palaios 29, 145–154. doi:10.2110/palo.2013.075.

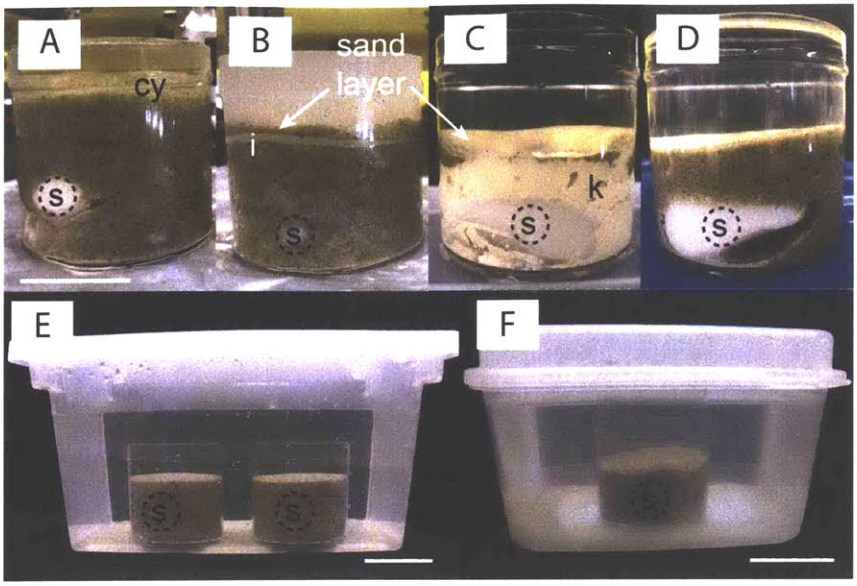

Fig. 5.1. Setup for taphonomy experiments. Scallops (s) buried ~2 cm beneath the surface of the sandy substrate in the presence of A) cyanobacteria in silica sand, B) silica sand covered by a layer of illite powder (100 g), C) kaolinite powder or D) silica sand without added cyanobacteria or clay minerals. Cy denotes cyanobacteria, i denotes illite and k denotes kaolinite. E and F) Culture jars were incubated in external containers filled with artificial seawater. Scale bars for A-D: 0.034 cm and E, F: 5 cm.

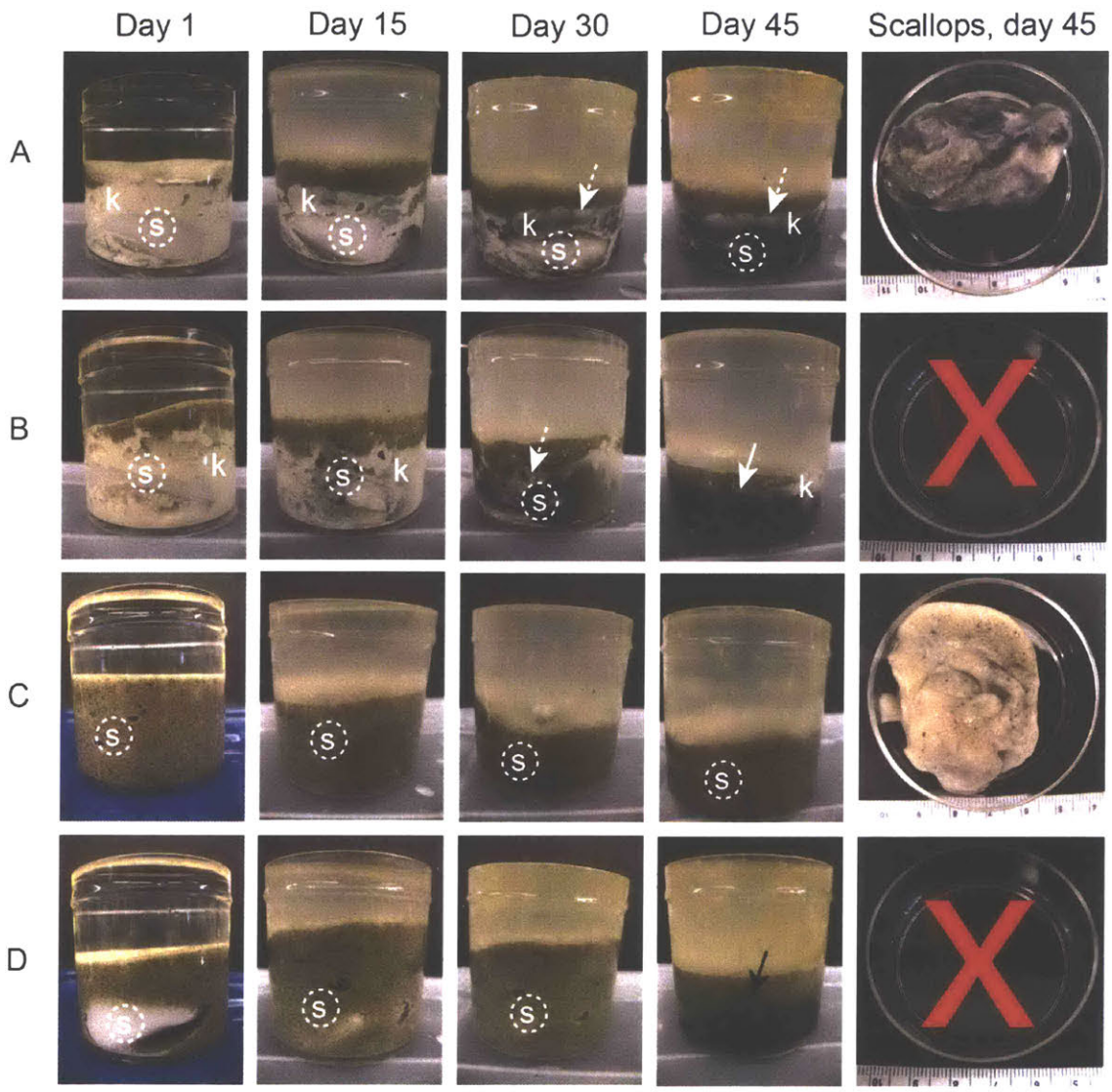

Fig. 5.2. Photographs of decaying soft tissues at 1, 5, 15, 30 and 45 days. The rows show different experimental conditions; the first four columns show progressively advanced time points. The rightmost column shows specimens exhumed from the clay/sand substrate on day 45. Scallop tissues incubated in kaolinite: A) a recovered scallop B) completely decayed tissues. Scallop tissues incubated in silica sand without added clays or cyanobacteria: C) a recovered scallop and D) completely decayed tissues. K denotes kaolinite and X denotes the complete decay of soft tissues by the end of the experiment. Solid arrows point to the extensive black patches in the clay/sand around the soft tissues that are indicative of heterotrophic microbial activity. Dashed arrows point to the less extensive, dark grey patches in kaolinite that did not result in the complete decay of soft tissues.

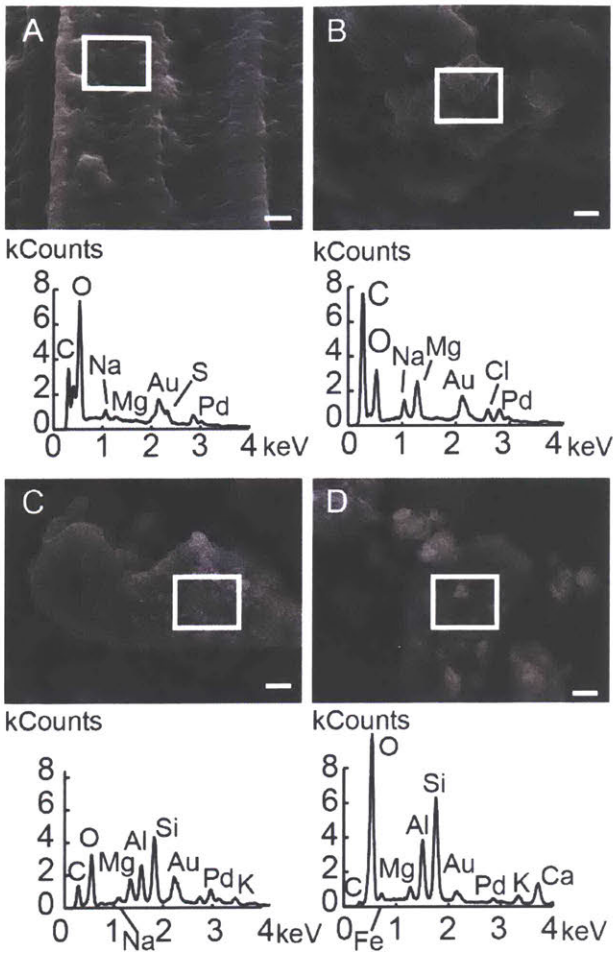

Fig. 5.3. Representative scanning electron micrographs of scallop tissues A) before experimentation (day 0) and B) incubated for 45 days in silica sand without added cyanobacteria or clays. C) Scallop incubated in illite powder and D) sterile illite grains. Samples were coated with gold and palladium. Scale bar in all micrographs is 1 μm. White boxes denote areas analyzed by EDS; the spectra of these areas are found below the corresponding SEM images.

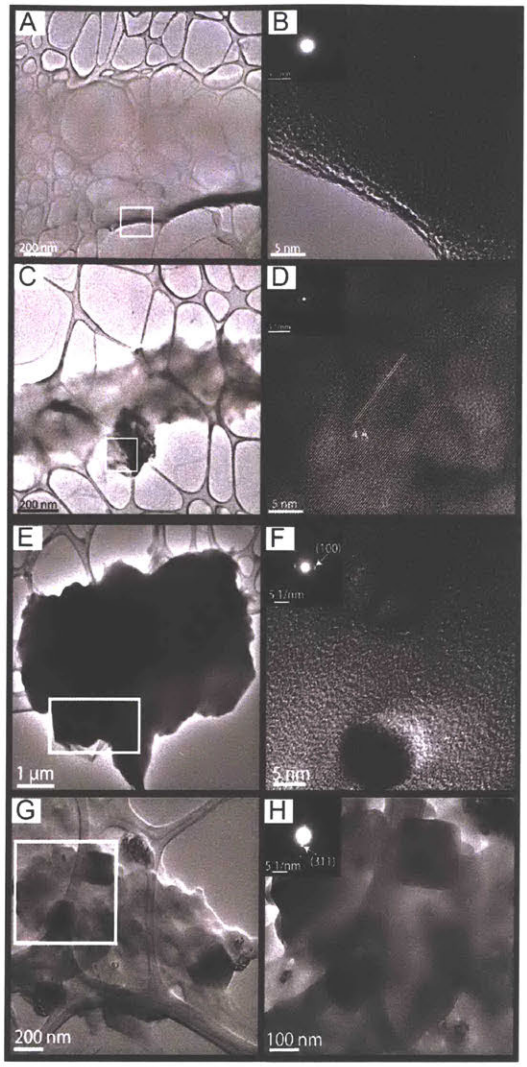

Fig. 5.4. TEM-SAED analysis of scallop tissues before and after incubation in kaolinite and silica sand. A) Bright-field transmission electron microscopy (TEM) image of scallop tissue before the experiment. The scallop tissue before incubation had no apparent dark patches and mineralized areas. B) HRTEM of the tissue area marked in A shows the absence of a diffraction pattern due to the presence of amorphous organic carbon and the absence of crystalline or microcrystalline minerals. C) Scallop tissue exhumed from kaolinite after 45 days. The scallop tissue is encrusted by minerals. D) HRTEM of the area selected in panel C, showing uniform lattice fringe of interplanar spacing of 4 Å. The SAED of the same material demonstrated a diffraction pattern of euhedral crystallite exhibiting monoclinic net pattern characteristics of clay minerals (K, Fe-rich illite/smectite). E) Scallop exhumed from silica sand after 45 days. The scallop is encrusted by dark minerals and F) HRTEM of the area selected in panel E, showing the presence of iron oxyhydroxides. F) Scallop tissue exhumed from silica sand after 45 days and H) close-up of mineral grains; diffraction patterns reveal the presence of iron (II, III) sulfides associated with the soft tissues.

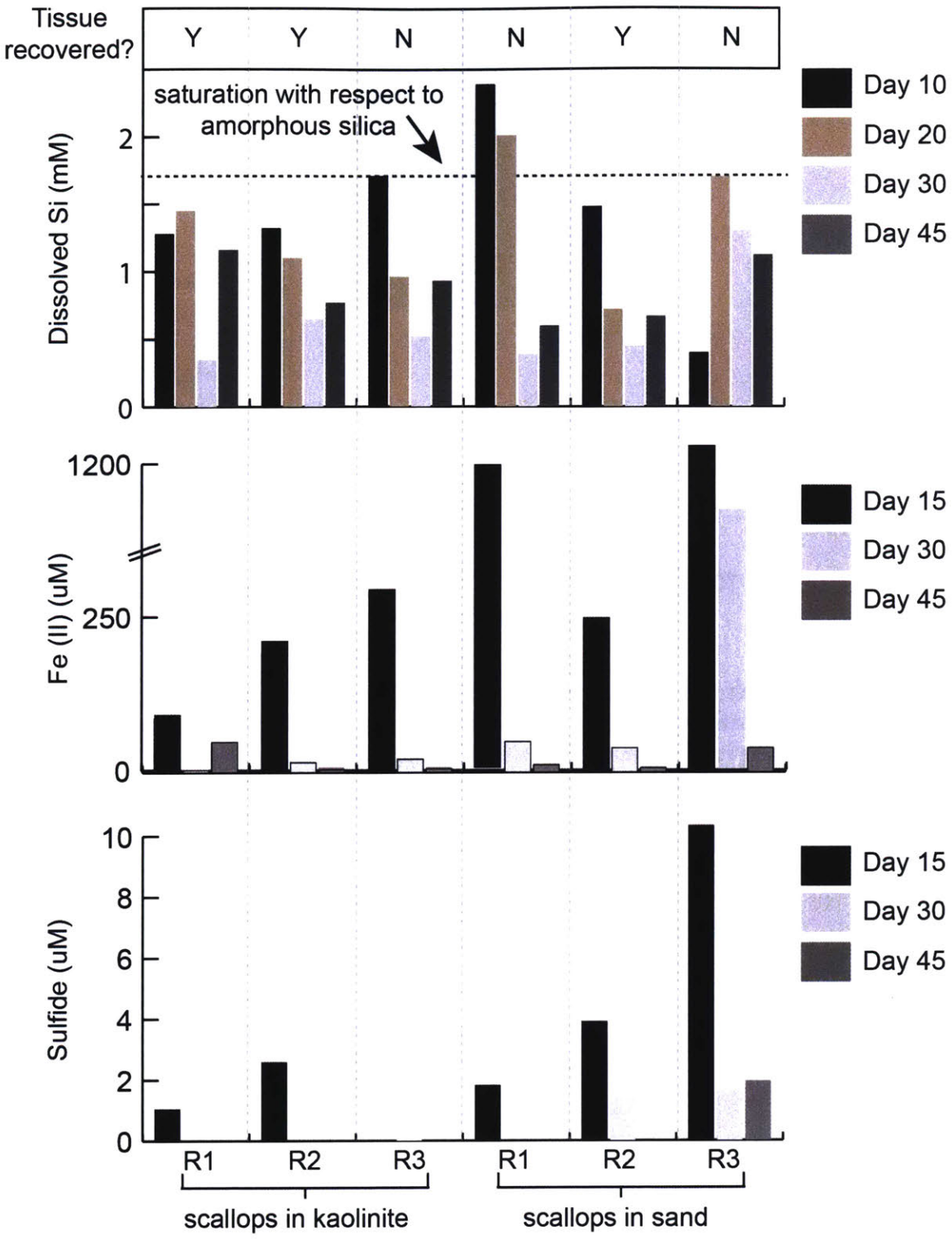

Fig. 5.5. Concentrations of dissolved silica (mM), iron(II) (μM) and sulfide (μM) in experimental porewaters. Saturation with respect to amorphous silica (~1.7 mM) is shown. Y indicates tissues were recovered on day 45; N marks complete tissue decay by the end of the experiment. R1-R3: experimental replicates one through three.

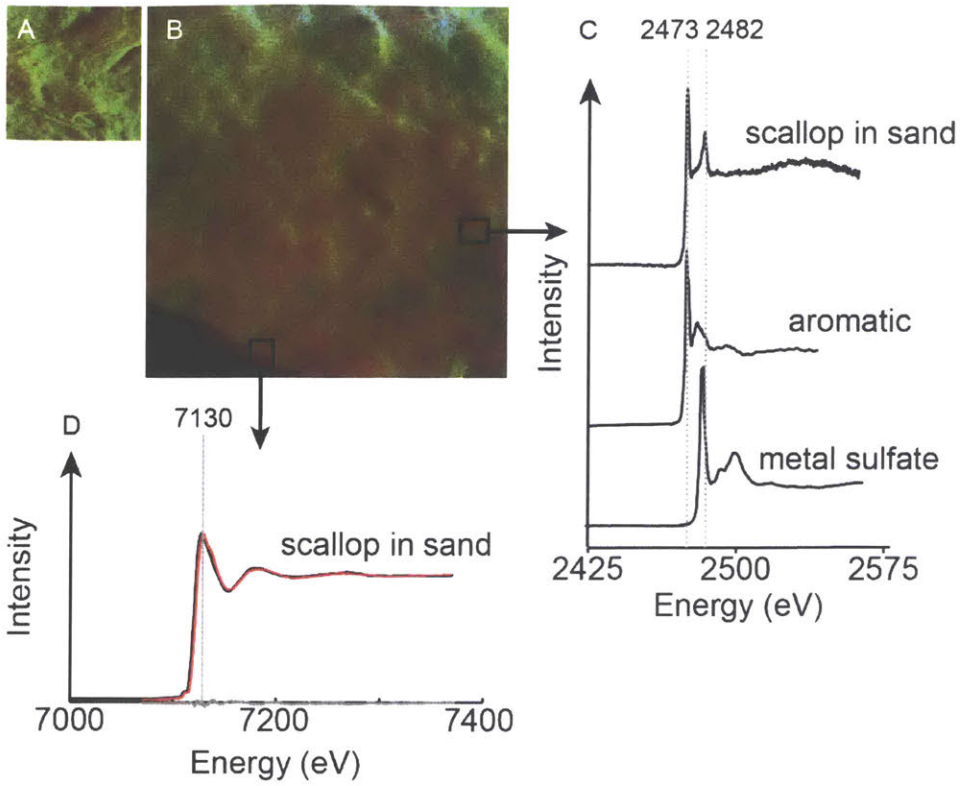

Fig. 5.6. XRF maps with iron and sulfur K-edge XANES spectra. Elemental distribution maps of A) scallop before incubation (day 0) and B) scallop after 45 days of incubation in silica sand. Iron is in red and sulfur is in green. C) Sulfur K-edge spectra of scallop exhumed from sand and standards from the 10.3.2 database. D) Iron K-edge spectra of scallop exhumed from sand. The best fit standard from the 10.3.2 database (iron sulfate, 59.5%, goethite, 27.8% and pyrite, 11.9%, sum sq.: 7.9×10^{-5}) is plotted in red. Residual is shown in grey.

Table 5.1. List of experimental conditions

Experiment no.	Variables tested*	Artificial seawater volume (L)	Substrate*	Number of scallops**	Scallops exhumed on day	Water column sampled?	Porewater sampled?
1	cyanobacteria	2	silica sand	2	30 and 45	Y	N
	illite powder	2	silica sand and illite	2	30 and 45	Y	N
	control	2	silica sand	2	30 and 45	Y	N
2	kaolinite powder	1.5	kaolinite and silica sand	1	45	Y	Y
	control	1.5	silica sand only	1	45	Y	Y
3	kaolinite powder	1.5	kaolinite and silica sand	0	n/a	Y	Y
	control	1.5	silica sand	0	n/a	Y	Y

* Illite powder was purchased from Time Laboratories (Pocatello, ID, USA) and kaolinite powder was purchased from Santa Cruz Biotechnology, Inc. (Dallas, TX, USA).

** Individual scallops were incubated in culture jars (190 mL, Grenier Bio-One, Kremsmünster, Austria) which were placed inside larger sterile containers with closeable lids (Sterilite Corporation, Townsend, MA, USA). Number of scallops indicates the total number of scallops incubated in the large sterile boxes.

Table 5.2. Weight loss of scallop tissues after 30 and 45 days of incubation

Experiment	Variable tested	Replicate	% Weight loss**	
			Day 30	Day 45
1*	cyanobacteria	1	100.0	99.0
		2	16.3	33.0
		3	95.3	99.5
	illite	1	21.6	50.0
		2	71.7	100.0
		3	100.0	100.0
	silica sand, no added clays/cyanobacteria	1	97.1	100.0
		2	17.6	36.1
		3	100.0	100.0
2*	kaolinite	1	n/a	72.5
		2	n/a	60.8
		3	n/a	100.0
	silica sand, no added clays/cyanobacteria	1	n/a	100.0
		2	n/a	29.7
		3	n/a	100.0

*See Table 5.1 for a list of experimental conditions.

** Percent weight loss for each scallop was calculated by determining the difference in weight between the exhumed and buried scallop tissues. This number was divided by the initial scallop weight and expressed as a percentage. Tissues exhumed on days 30 and 45 from the same experimental replicate were different specimens incubated in the same container.

5.8 Supplementary Information

Supplementary Methods

Dissolved oxygen concentrations were measured on days 10, 30 and 45 by injecting known volumes of samples collected either from the porewater or from the water column with a syringe into 60 mL serum bottles and measuring oxygen partial pressure change in the headspace. The bottles were previously flushed with oxygen free nitrogen and oxygen diffused out of the samples in less than 20 minutes. Oxygen partial pressure was measured by detecting changes in the fluorescence lifetime of palladium (II)-5,10,15,20-tetrakis-(2,3,4,5,6-pentafluorphenyl)-porphyrin (Pd-TFPP) (Lehner et al., 2015) using an in-house built fluorescence lifetime sensor (Pajusalu et al., in prep). Due to unexpectedly large oxygen absorption rates of the reductive compounds in the sample, the dissolved concentrations underestimate the actual oxygen concentrations.

References

Lehner, P., Larndorfer, C., Garcia-Robledo, E., Larsen, M., Borisov, S.M., Revsbech, N.P., Glud, R.N., Canfield, D.E., Klimant, I., 2015. LUMOS - A sensitive and reliable optode system for measuring dissolved oxygen in the nanomolar range. PLoS One 10, 1–15. doi:10.1371/journal.pone.0128125.

Pajusalu M., Borlina C., Seager S., Bosak T., Ono S. Open-source networked fluorescence lifetime sensor for sub part per million level oxygen measurements, in prep.

Supplementary Results

Dissolved oxygen values were determined for the porewater (~6.5 cm below the sand/clay surface) and water column (~3 cm above the sand/clay surface). Values for dissolved oxygen in the porewaters were less than 8.12 ± 2.8 μM. Dissolved oxygen values in the water column ranged from 20.39 ± 12.93 to 40.78 ± 10.9 μM on day 10, 19.12 ± 2.27 to 60.25 ± 6.03 μM on day 30 and 32.02 ± 5.66 to 63.76 ± 15.74 μM on day 45. Observed increases in dissolved oxygen concentrations as the experiments progressed likely resulted from the removal of decaying organic material by replacement of the medium.

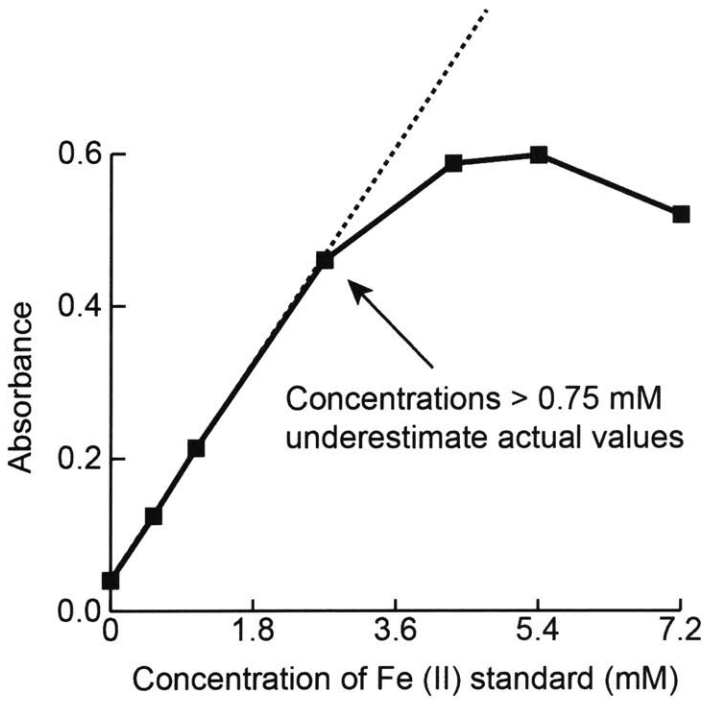

Supplementary Fig. 5.1. Dilution curve for concentrations of iron(II). Standards were diluted 20x after the addition of ferrozine and measured using colorimetric assays. Concentrations of diluted standards that were originally greater than 0.75 mM were underestimated. Solid line represents observed absorbance values for diluted standards; dashed line represents theoretical calculations for absorbance values.

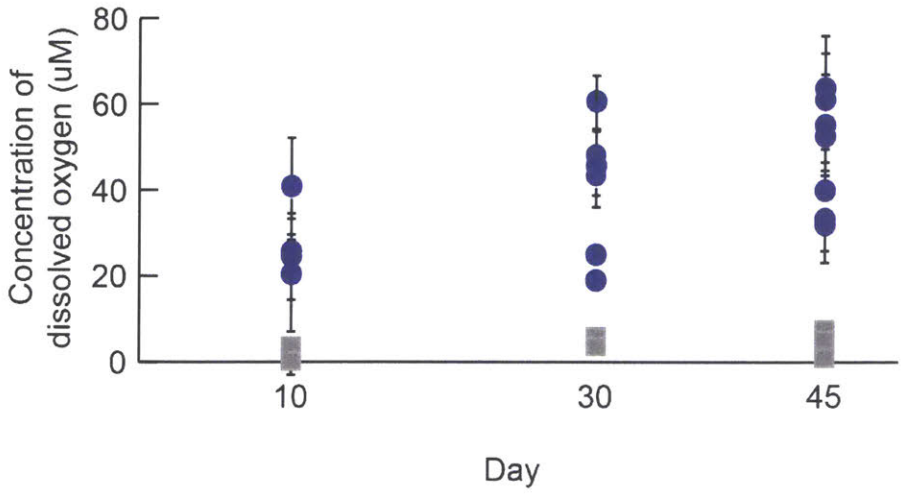

Supplementary Fig. 5.2. Concentrations of dissolved oxygen in water column (μM) and porewater samples from select experimental conditions on days 10, 30 and 45 of scallop incubation. Water column values are marked by purple circles and porewater samples are marked by grey squares. Error bars are shown for triplicate measurements.

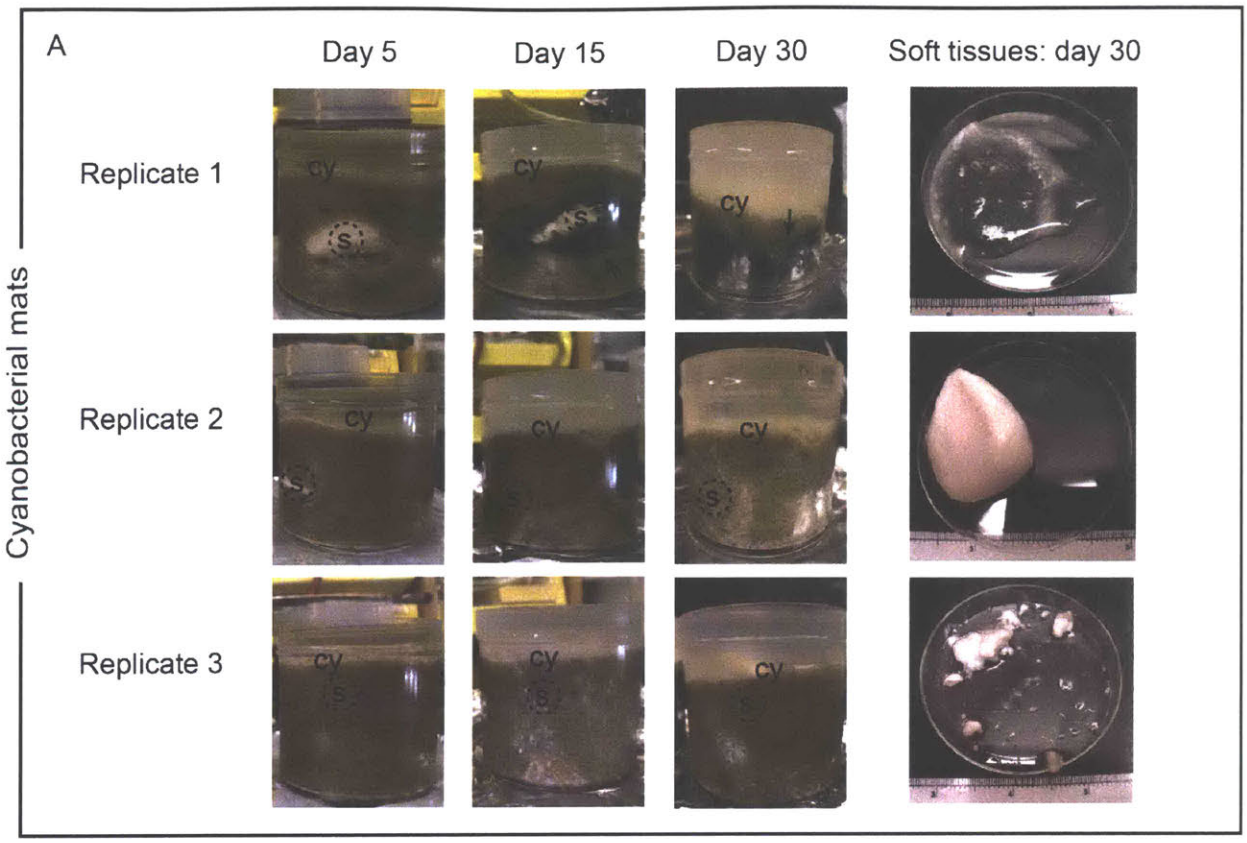
A
Day 5
Day 15
Day 30
Soft tissues: day 30
Cyanobacterial mats
Replicate 1
Replicate 2
Replicate 3
cy
s

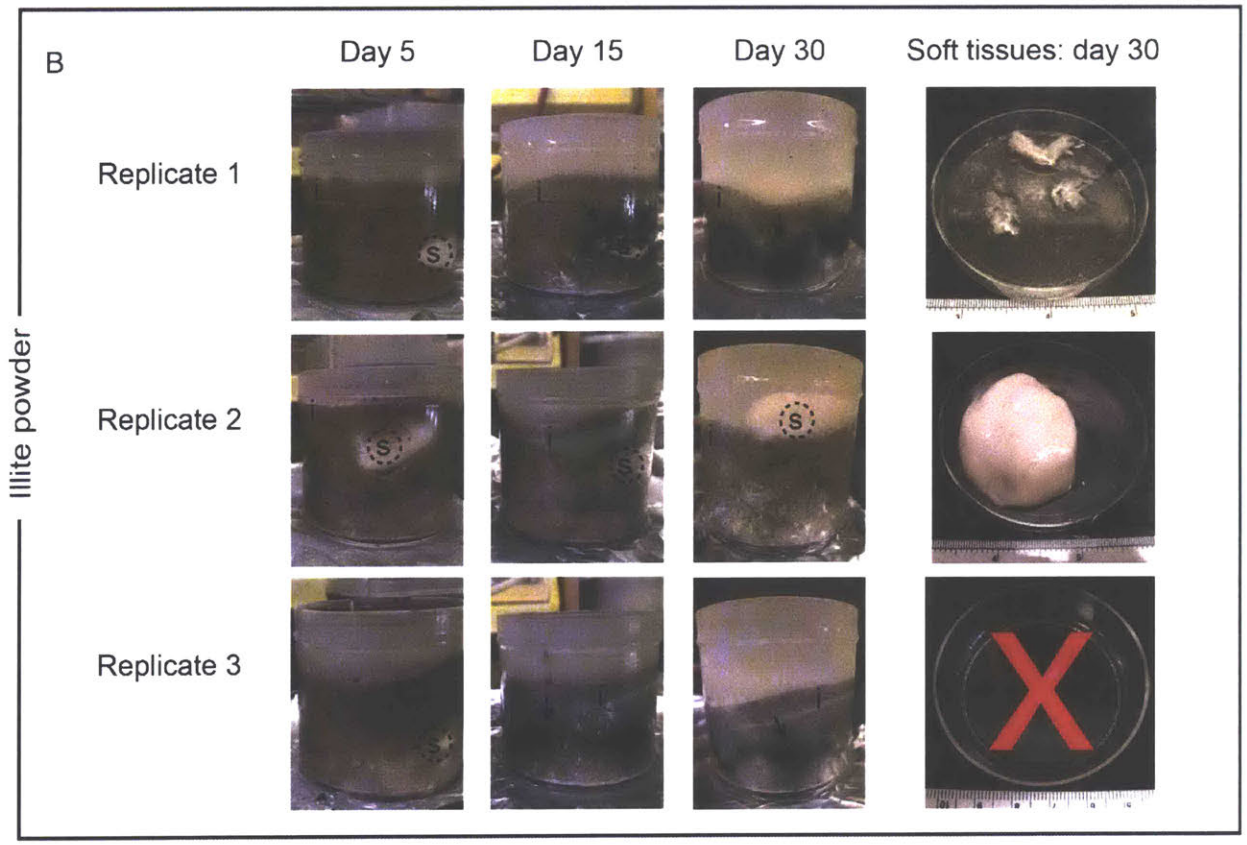
B
Day 5
Day 15
Day 30
Soft tissues: day 30
Illite powder
Replicate 1
Replicate 2
Replicate 3
s
X

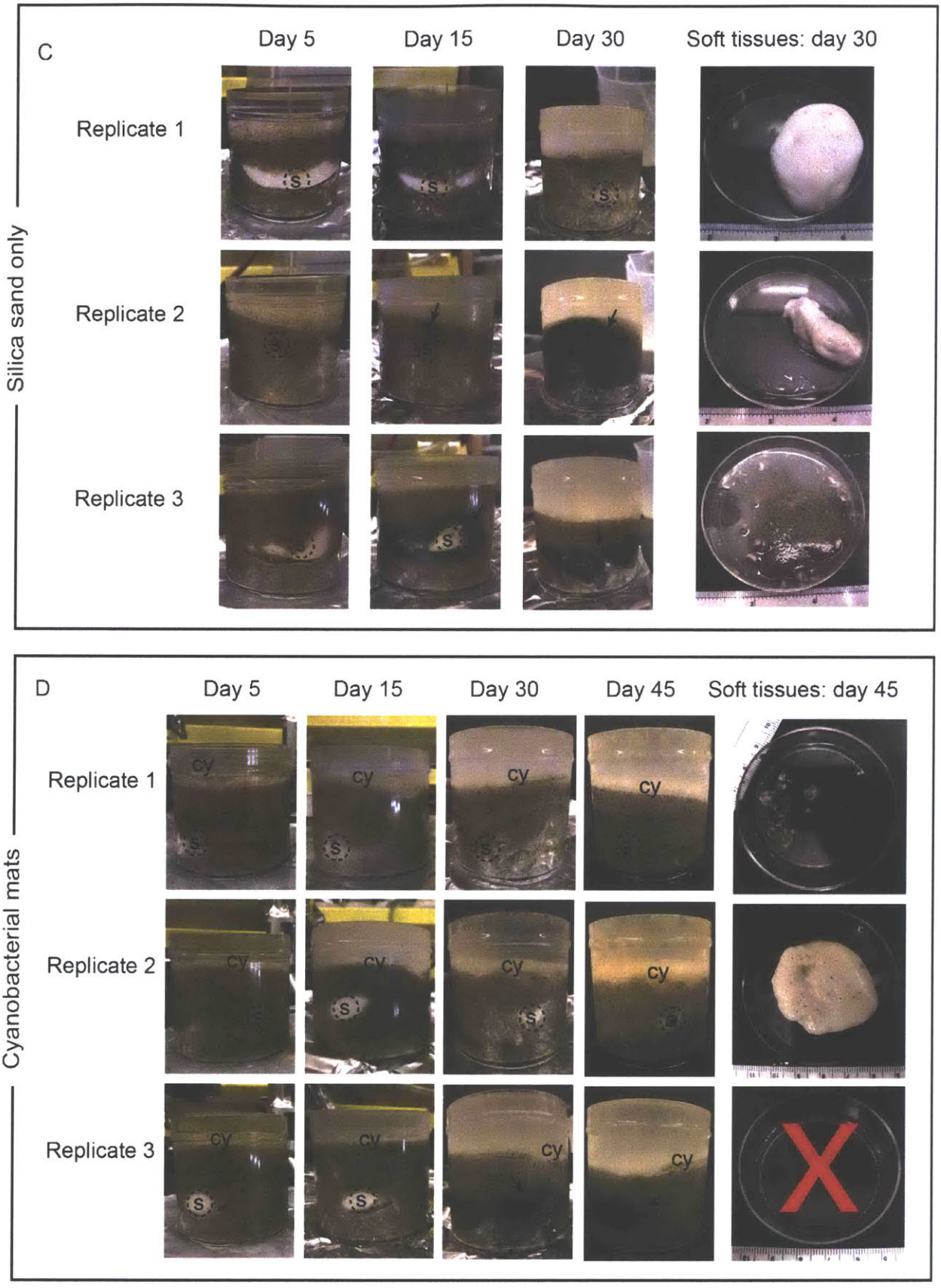
C
Day 5
Day 15
Day 30
Soft tissues: day 30
Replicate 1
Replicate 2
Replicate 3
Silica sand only
S
D
Day 5
Day 15
Day 30
Day 45
Soft tissues: day 45
Replicate 1
Replicate 2
Replicate 3
Cyanobacterial mats
cy
S
X

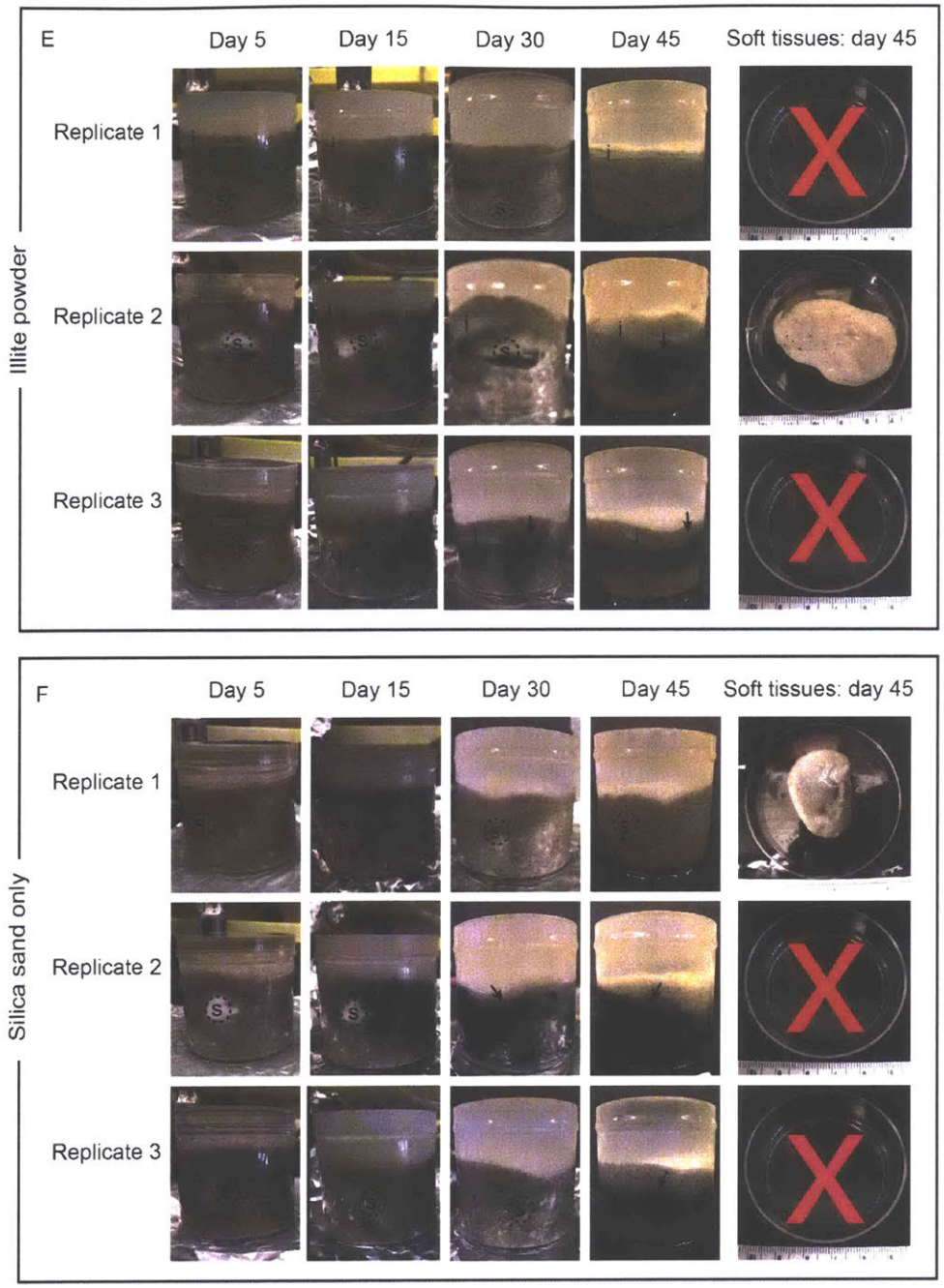

Supplementary Fig. 5.3. Photographs of soft tissues at different time points (1, 5, 15, 30 and 45 days) and specimens exhumed from the sand on day 30 or 45. Photographs of decayed scallops (s) or no scallop are to the right of corresponding time series photographs. Scallop tissues incubated for 30 days in the presence of A) cyanobacterial mats, B) illite and C) silica sand without added cyanobacteria/clay minerals. Scallops incubated for 45 days in the presence of D) cyanobacteria, E) illite and F) silica sand without added cyanobacteria/clay minerals. I denotes illite and X denotes the complete decay of soft tissues by the end of the experiment. Solid arrows point to the formation of extensive black patches in the sand around the soft tissues. Culture jar volume: 190 mL.

Supplementary Table 5.1a. Concentrations of iron(II) (μM) in experiments with kaolinite and silica sand.

		Scallops buried in kaolinite			Scallops buried in silica sand			Sterile kaolinite, no tissues		Sterile silica sand, no tissues	
Day	Sample*	**R1**	**R2**	R3	R1	**R2**	R3	R1	R2	R1	R2
1	WC	**n.d.**	**n.d.**	n.d.	n.d.	**n.d.**	n.d.	n.d.	0.02	n.d.	n.d.
5	WC	**0.05**	**0.07**	n.d.	0.64	**0.46**	1.68	n.d.	n.d.	n.d.	n.d.
10	WC	**n.d.**	**0.85**	0.01	n.d.	**0.01**	n.d.	0.02	n.d.	n.d.	n.d.
	PW1	**22.41**	**87.04**	21.00	>1074.22	**14.93**	92.81	0.11	n.d.	0.11	0.11
	PW2	**168.93**	**199.66**	135.97	>1138.28	**337.75**	>1167.35	n.d.	0.04	0.27	0.27
15	WC	**0.05**	**2.17**	2.08	0.05	**0.03**	n.d.	n.d.	n.d.	n.d.	n.d.
	PW1	**21.30**	**23.64**	111.95	>1102.82	**40.81**	>889.21	n.d.	n.d.	0.02	n.d.
	PW2	**47.14**	**107.69**	149.92	>966.27	**126.55**	>1041.53	0.07	0.02	0.09	0.09
30	WC	**n.d.**	**0.14**	4.33	2.58	**0.16**	<0.01	<0.01	n.d.	n.d.	n.d.
	PW1	**1.56**	**2.37**	8.19	86.42	**11.61**	25.54	0.02	n.d.	0.07	0.27
	PW2	**1.81**	**8.19**	10.81	25.07	**19.76**	803.05	n.d.	0.09	0.23	0.14
45	WC	**0.04**	**0.15**	0.35	0.33	**0.06**	0.15	n.d.	n.d.	n.d.	n.d.
	PW1	**1.34**	**1.65**	12.10	1.94	**0.93**	4.43	n.d.	n.d.	n.d.	n.d.
	PW2	**24.97**	**2.23**	2.86	5.84	**3.42**	19.81	n.d.	n.d.	0.14	0.05
Decay delay?[t]		Y	**Y**	N	N	**Y**	N	n/a	n/a	n/a	n/a

*WC: Water column (~3 cm above the surface of the substrate); PW1: Upper porewater (~1.5 cm below the surface of the substrate); PW2: Lower porewater (~6.5 cm below the surface of the substrate).
[t]N denotes complete decay after 45 days of incubation; Y denotes recovery of scallop after 45 days. Experiments in which scallops were successfully recovered on day 45 are bolded for emphasis.
R1-R3: Replicates one through three.
n.d. denotes below the limit of detection.
Iron(II) concentrations in the sterile medium were undetectable.

Supplementary Table 5.1b. Concentrations of iron(II) (μM) in the water columns of experiments with cyanobacteria, illite and sand.

	Scallops in the presence of cyanobacteria			Scallops in the presence of illite			Scallops incubated in silica sand (no added cyanobacteria or clay minerals)		
Day	R1	**R2**	R3	**R1**	R2	R3	R1	**R2**	R3
15	7.97	**5.84**	5.93	**6.03**	3.00	14.11	8.80	**0.90**	2.49
30	0.74	**n.d.**	8.11	**0.14**	n.d.	0.60	0.14	**0.02**	0.79
45	n.d.	**n.d.**	n.d.	**n.d.**	n.d.	n.d.	n.d.	**n.d.**	n.d.
Decay delay?[t]	N	**Y**	N	**Y**	N	N	N	**Y**	N

[t]N denotes complete decay after 45 days of incubation; Y denotes recovery of scallop after 45 days. Experiments in which scallops were successfully recovered on day 45 are bolded for emphasis.
R1-R3: Replicates one through three.
n.d. denotes below the limit of detection.
Iron(II) concentrations in the sterile medium were undetectable.

Supplementary Table 5.2a. Concentrations of iron(III) (μM) in experiments with kaolinite and sand.

		Scallops buried in kaolinite			Scallops buried in silica sand			Sterile kaolinite, no tissues		Sterile silica sand, no tissues	
Day	Sample*	**R1**	**R2**	R3	R1	**R2**	R3	R1	R2	R1	R2
1	WC	**0.41**	**0.55**	0.49	0.55	**0.46**	0.55	0.58	0.50	0.74	0.79
5	WC	**0.95**	**2.63**	0.55	6.00	**2.36**	6.51	0.25	0.30	0.60	0.47
10	WC	**3.97**	**5.95**	5.24	4.24	**5.57**	4.56	0.45	0.28	0.60	0.58
	PW1	**4.34**	**13.08**	6.01	>0.00	**17.66**	24.59	0.25	0.28	0.33	0.44
	PW2	**100.56**	**88.72**	144.95	>0.00	**64.32**	>0.69	0.17	0.18	0.63	0.60
15	WC	**5.21**	**8.80**	8.25	5.91	**4.11**	>0.22	0.41	0.36	0.47	0.44
	PW1	**29.32**	**10.64**	188.50	>0.00	**98.41**	>0.00	0.41	0.28	0.53	0.47
	PW2	**100.09**	**>0.00**	81.76	>0.00	**168.94**	>0.00	0.26	0.26	0.73	0.71
30	WC	**0.36**	**0.47**	2.11	4.74	**3.58**	0.44	0.27	0.35	0.35	0.40
	PW1	**11.45**	**12.42**	12.09	112.07	**44.86**	79.84	0.32	0.22	0.38	0.13
	PW2	**8.57**	**47.00**	36.68	61.25	**119.87**	113.39	0.22	0.10	0.38	0.49
45	WC	**0.25**	**0.27**	1.82	1.62	**0.25**	0.27	0.40	0.22	0.40	0.47
	PW1	**18.35**	**20.88**	14.12	21.96	**6.63**	94.27	0.53	0.24	0.45	0.79
	PW2	**37.20**	**34.00**	21.90	117.04	**126.85**	292.54	0.24	0.19	0.52	0.48
Decay delay?[f]		**Y**	**Y**	N	N	**Y**	N	n/a	n/a	n/a	n/a

*WC: Water column samples (~3 cm above the surface of the substrate); PW1: Upper porewater samples (~1.5 cm below the surface of the substrate); PW2: Lower porewater samples (~6.5 cm below the surface of the substrate)

[f]N denotes complete decay after 45 days of incubation; Y denotes recovery of scallop after 45 days. Experiments in which scallops were successfully recovered on day 45 are bolded for emphasis.

R1-R3: Replicates one through three.

n.d. denotes below the limit of detection.

Iron(III) concentrations in the sterile medium ranged from 0.2 to 0.9 μM.

Supplementary Table 5.2b. Concentrations of iron(III) (μM) in the water columns of experiments with cyanobacteria, illite and silica sand.

	Scallops in the presence of cyanobacteria			Scallops in the presence of illite			Scallops incubated in silica sand (no added cyanobacteria or clay)		
Day	R1	**R2**	R3	**R1**	R2	R3	R1	**R2**	R3
15	0.17	**5.74**	1.33	**n.d.**	1.25	n.d.	4.27	**3.92**	4.03
30	3.81	**1.66**	n.d.	**1.40**	1.51	1.36	4.25	**0.90**	2.24
45	1.35	**0.17**	1.38	**0.99**	0.89	0.73	1.75	**0.33**	1.11
Decay delay?[1]	N	**Y**	N	**Y**	N	N	N	**Y**	N

[1]N denotes complete decay after 45 days of incubation; Y denotes recovery of scallop after 45 days.
Experiments in which scallops were successfully recovered on day 45 are bolded for emphasis.
R1-R3: Replicates one through three.
n.d. denotes below the limit of detection.
Iron(III) concentrations in the sterile medium ranged from 0.2 to 0.9 μM.

Supplementary Table 5.3a. Concentrations of dissolved silica (mM) in experiments with kaolinite and sand.

		Scallops buried in kaolinite			Scallops buried in silica sand			Sterile kaolinite, no tissues		Sterile silica sand, no tissues	
Day	Sample*	**R1**	**R2**	R3	R1	**R2**	R3	R1	R2	R1	R3
1	WC	**0.17**	**0.10**	0.17	0.14	**0.17**	0.17	0.09	0.16	0.17	0.17
5	WC	**0.09**	**0.19**	0.26	0.18	**0.21**	0.97	0.26	0.33	0.11	0.37
10	WC	**0.09**	**0.09**	0.19	0.16	**0.22**	0.30	0.14	0.22	0.19	0.31
	PW2	**1.28**	**1.32**	1.71	2.39	**1.48**	0.40	0.46	0.62	0.45	0.39
15	WC	**0.27**	**0.16**	0.14	0.13	**0.14**	0.15	0.27	0.27	0.14	0.21
	PW2	--	--	--	--	--	--	0.65	0.64	0.48	0.41
20	WC	**0.34**	**0.28**	0.29	0.39	**0.27**	0.24	0.05	0.02	0.21	0.10
	PW2	**1.45**	**1.10**	0.96	2.01	**0.72**	1.70	0.36	0.38	0.27	0.29
30	WC	**0.13**	**0.07**	0.05	0.28	**0.15**	0.23	0.17	0.02	0.18	0.08
	PW2	**0.35**	**0.65**	0.52	0.39	**0.45**	1.30	0.30	0.51	0.23	0.42
40	WC	**0.47**	**0.43**	0.43	0.43	**0.40**	0.50	--	--	--	--
	PW2	**1.06**	**0.87**	0.63	0.85	**0.65**	1.03	--	--	--	--
45	WC	**0.16**	**0.21**	0.20	0.21	**0.16**	0.13	0.23	0.27	0.09	0.21
	PW2	**1.16**	**0.77**	0.93	0.60	**0.67**	1.12	0.45	0.45	0.28	0.35
Decay delay?[1]		**Y**	**Y**	N	N	**Y**	N	n/a	n/a	n/a	n/a

*WC: Water column (~3 cm above the surface of the substrate); PW2: Lower porewater (~6.5 cm below the surface of the substrate)

[1]N denotes complete decay after 45 days of incubation; Y denotes recovery of scallop after 45 days. Experiments in which scallops were successfully recovered on day 45 are bolded for emphasis.

R1-R3: Replicates one through three.

Concentrations of dissolved silica in the sterile medium ranged from 0.06 to 0.19 mM.

Supplementary Table 5.3b. Concentrations of dissolved silica (mM) in the water columns of experiments with cyanobacteria, illite and sand.

	Scallops in the presence of cyanobacteria			Scallops in the presence of illite			Scallops incubated in silica sand (no added cyanobacteria or clay)		
day	R1	**R2**	R3	**R1**	R2	R3	R1	R2	R3
15	0.18	**0.12**	0.16	**0.09**	0.09	0.12	0.13	0.19	0.17
30	0.05	**0.13**	0.06	**0.08**	0.06	0.12	0.18	0.10	0.08
45	0.14	**0.09**	0.17	**0.07**	0.15	0.07	0.13	0.09	0.08
Delay decay?[1]	N	**Y**	N	**Y**	N	N	N	Y	N

[1]N denotes complete decay after 45 days of incubation; Y denotes recovery of scallop after 45 days. Experiments in which scallops were successfully recovered on day 45 are bolded for emphasis.
R1-R3: Replicates one through three.
Concentrations of dissolved silica in the sterile medium ranged from 0.06 to 0.19 mM.

Supplementary Table 5.4. Concentrations of porewater sulfide (μM) in experiments with kaolinite and sand.

		Scallops buried in kaolinite			Scallops buried in silica sand		
Day	Sample*	**R1**	**R2**	R3	R1	**R2**	R3
10	PW1	**n.d.**	**n.d.**	n.d.	5.29	**2.85**	n.d.
	PW2	**0.02**	**n.d.**	n.d.	1.22	**6.53**	37.99
15	PW1	**n.d.**	**n.d.**	n.d.	5.20	**3.06**	n/a
	PW2	**1.05**	**2.59**	n.d.	1.82	**3.92**	10.34
30	PW1	**0.62**	**n.d.**	0.02	1.90	**n.d.**	n.d.
	PW2	**n.d.**	**n.d.**	0.06	n.d.	**1.39**	1.61
45	PW1	**n.d.**	**n.d.**	n.d.	n.d.	**n.d.**	n.d.
	PW2	**n.d.**	**n.d.**	n.d.	n.d.	**n.d.**	1.95
Decay delay?[1]		**Y**	**Y**	N	N	**Y**	N

*PW1: Upper porewater (~1.5 cm below the surface of the substrate); PW2: Lower porewater (~6.5 cm below surface of the substrate)

[1]N denotes complete decay after 45 days of incubation; Y denotes recovery of scallop after 45 days.

Experiments in which scallops were successfully recovered on day 45 are bolded for emphasis.

R1-R3: Replicates one through three.

n.d. denotes below the limit of detection.

Concentrations of sulfide in the sterile medium were undetectable.

Supplementary Table 5.5a. pH in experiments with kaolinite and sand.

		Scallops buried in kaolinite			Scallops buried in silica sand			Sterile kaolinite, no tissues		Sterile silica sand, no tissues	
Day	Sample*	R1	R2	R3	R1	R2	R3	R1	R2	R1	R2
5	WC	7.5	7.5	7.4	7.6	7.4	7.4	8.2	8.2	8.2	8.2
	PW1	--	--	--	--	--	--	7.0	7.0	7.0	7.0
	PW2	5.5	5.8	5.8	4.8	6.2	5.6	6.5	6.5	7.0	7.0
10	WC	7.7	7.6	7.6	7.7	7.7	7.7	8.2	8.3	8.2	8.2
	PW1	--	--	--	--	--	--	7.5	7.5	7.5	7.5
	PW2	--	--	--	--	--	--	7.0	7.0	7.0	7.0
15	WC	7.8	7.6	7.6	7.8	7.8	7.8	8.2	8.2	8.2	8.2
	PW1	6.5	6.5	6.0	4.5	7	5.5	7.5	7.5	7.5	7.5
	PW2	6.5	6.5	6.0	4.5	6.5	5.5	7.0	7.0	7.0	7.0
30	WC	7.8	7.8	7.8	7.7	7.8	7.8	8.4	8.3	8.3	8.3
	PW1	7.0	6.5	6.5	6.5	6.5	7.0	7.5	7.5	7.5	7.5
	PW2	7.0	6.5	6.5	6.5	7.0	6	7.0	7.0	7.0	7.0
45	WC	7.8	7.8	7.9	7.9	8.0	7.7	8.3	8.3	8.2	8.3
	PW1	7.0	6.5	6.8	6.8	6.8	7.0	7.5	7.5	7.5	7.5
	PW2	7.5	7.5	7.0	7.0	7.5	7.5	7.0	7.0	7.0	7.0

*WC: Water column samples (~3 cm above the surface of the substrate); PW1: Upper porewater (~1.5 cm below the surface of the substrate); PW2: Lower porewater (~6.5 cm below the surface of the substrate)

**The sterile medium had a pH of 7.6.

R1-R3: Replicates one through three.

Supplementary Table 5.5b pH in experiments with cyanobacteria, illite and sand.

		Scallops in the presence of cyanobacteria**			Scallops in the presence of illite**			Scallops incubated in silica sand (no added cyanobacteria or clay)**		
Day	Sample*	R1	R2	R3	R1	R2	R3	R1	R2	R3
5	WC	7.3	7.0	7.0	7.4	7.0	7.1	7.5	7.6	7.5
10	WC	7.5	7.5	7.5	7.5	7.6	7.6	7.6	7.6	7.5
	PW1	6.0	6.2	5.9	6.1	6.0	6.2	6.1	6.1	6.0
	PW2	6.0	6.0	5.7	5.7	6.3	6.0	5.9	6.2	6.0
15	WC	7.6	7.8	7.8	7.7	7.9	7.7	7.7	7.8	7.7
	PW1	5.5	5.8	5.4	6.0	6.4	6.5	6.4	5.9	6.2
	PW2	6.1	6.8	5.4	5.2	6.2	6.2	6.3	6.1	6.4
20	WC	7.3	7.7	7.4	7.9	7.6	7.5	7.6	7.7	7.5
	PW1	5.4	7.0	5.4	6.2	6.9	6.7	6.5	6.2	6.7
	PW2	6.4	5.7	5.6	5.0	6.9	6.5	6.8	6.6	6.6
25	WC	7.6	7.7	7.2	7.7	7.8	7.6	7.7	7.6	7.9
	PW1	5.9	6.0	5.6	6.4	7.0	6.8	7.0	6.2	6.8
	PW2	6.5	6.4	6.0	4.9	7.2	6.6	6.7	6.7	6.9
30	WC	7.8	8.0	7.8	7.9	8.0	7.9	7.9	7.9	7.9
	PW1	6.2	6.9	6.4	6.7	n/a	7.0	7.0	6.5	6.9
	PW2	6.7	6.4	6.6	5.1	7.3	6.7	6.6	6.9	6.8
45	WC	7.9	8.0	7.9	7.9	8.1	8.0	8.0	8.0	8.0
	PW1	6.6	6.8	6.4	6.7	7.3	6.6	6.9	6.7	6.9
	PW2	6.8	6.6	6.5	6.8	7.2	7.0	7.0	6.9	7.1

*WC: Water column samples (~3 cm above the surface of the substrate); PW1: Upper porewater (~1.5 cm below the surface of the substrate); PW2: Lower porewater (~6.5 cm below the surface of the substrate)

**The sterile medium had a pH of 7.6.

R1-R3: Replicates one through three.

Chapter 6. Conclusions and Future Work

Fossiliferous sandy sediments containing the remains of non-skeletonized organisms are commonly found in the Ediacaran/early Cambrian, but rarely occur outside of this interval of time. This suggests that unique environmental and biological conditions facilitated the exceptional preservation of organic material in subtidal and intertidal settings, but the specific factors that play a role in preservation remain to be elucidated. Hypotheses invoking the roles of high concentrations of oceanic silica, widespread microbial mats and/or the presence of clays in the preservation of soft tissues abound, but empirical tests of these hypotheses are few. To bridge this gap, this Thesis employs an experimental taphonomy approach. We use modern cyanobacteria and soft tissues to identify biological, chemical and physical processes that lead to the preservation of microbial and animal shapes in siliciclastic settings. Additionally, we develop mechanistic models of preservation that focus on the roles of authigenic mineral precipitation and the trapping of fine particles from the sediment. Experimental findings are then compared to observations from the siliciclastic fossil record.

In the preceding chapters, we showed that the initial preservation of microorganisms and soft tissues incubated in silica sand and kaolinite occurs within 30 to 45 days, during which time authigenic and trapped minerals formed continuous veneers on organic surfaces. We tested the role of dissolved silica in fossilization and showed that high concentrations ($\geq$0.1 mM) facilitated the preservation of microbial filaments in oxic environments (Chapters 2 and 3). However, solutions that were supersaturated with respect to amorphous silica indicated extensive decay and reduced preservation of soft tissues in locally anaerobic sediments (Chapters 4 and 5). Thus, our findings suggest a beneficial impact of moderate concentrations of dissolved silica (0.1 to 0.4 mM) on fossil preservation, but other factors such as the availability of iron and the presence and

activity of sedimentary microorganisms have a more profound effect on preservation than silica alone. Future experiments should evaluate the preservation of soft tissues in the presence of different initial concentrations of dissolved silica in solution.

Microbial iron reduction was critical for the preservation of soft-bodied organisms that were buried in siliciclastic sediments (Chapters 4 and 5). Both the microbial reduction of iron(III) and the oxidation of iron(II) occurred in these experiments. These processes controlled the amount of dissolved iron(II) that was directly incorporated into iron-rich minerals that formed veneers around soft tissues (Chapters 4 and 5). However, as demonstrated in Chapters 2 and 3, iron was not an essential factor in microbial preservation in oxic environments. Thus, the role of iron in fossilization requires further consideration. Iron is a cation that is frequently found in natural settings and it is hypothesized to bind to organic substrates and facilitate the nucleation of clays and other minerals. However, other cations such as aluminum may play an equal if not more important role in the formation of authigenic minerals. In this Thesis, we did not measure concentrations of aluminum in our solution during incubation. Therefore, it will be critical for future experiments to test the effects of aluminum on the preservation of organic material and the inhibition of heterotrophic microbial activities.

Both the composition of microbial surfaces and microbial metabolisms may play a role in fossilization. In Chapter 2, we showed that microorganisms with thick sheaths ($\geq$1 μm) were more likely to be coated in mineral veneers than those with thinner sheaths (<1 μm) or sheathless cyanobacteria. Thus, organisms with thick, sticky sheaths are more likely to be preserved in siliciclastic strata. To increase our understanding of how microbial sheaths may facilitate preservation, it will be necessary to directly compare aerobic and anaerobic microorganisms with and without sheaths. In doing so, we will not only be able to characterize the preservation

potential of various bacteria, but also identify the specific mechanisms by which sheaths facilitate the formation of mineral veneers.

All four chapters provide evidence for the role of clay minerals in the preservation of organic material. Clay minerals readily form veneers around microbial filaments (Chapters 2 and 3) and the presence of kaolinite in the substrate facilitated veneer formation around soft tissues (Chapters 4 and 5). However, our understanding of the role of clays in organic preservation is far from complete. Future studies should test how different clay minerals promote or inhibit the decay of soft tissues, the amount of clay required to facilitate preservation (i.e., the ratio of clays:tissue) and the processes by which authigenic clay minerals form on organic surfaces in predominantly sandy sediments. Longer studies should also investigate the decay of tissues within organic veneers and the potential for these tissues to be preserved as two-dimensional compressions or three-dimensional casts.

Future studies should also test the preservation potential of other soft-bodied organisms (such as jellyfish, worms and shrimp). Scallop adductor muscles were selected for the previously described experiments because they were readily available and are similar in size and morphology (cm in size, discoidal) to Ediacaran megafauna. However, it will be important to better constrain processes of decay/decay delay across a range of soft tissue types and sizes.

Overall, the experiments presented in this Thesis test various mechanisms for the preservation of organic material in siliciclastic environments. Our results help to confirm or disprove previous hypotheses regarding the preservation of fossils in Ediacaran and early Cambrian sandy and silty environments by demonstrating that minerals precipitated and adhered to organic material under moderate concentrations of dissolved silica (<1.7 mM) and porewater iron (<1.0 mM). We propose that the most exceptionally preserved fossils are likely to be found

in coarse-grained environments containing mm to cm-thick layers of clay minerals and that these fossils will be physically associated with iron-rich aluminosilicate laminae that preserve fine features. We suggest that this process likely facilitated the preservation of casts, molds and sedimentary patterns in the coarse-grained siliciclastic rock record as well as the preservation of two-dimensional carbonaceous compressions in shales.